1. REPORT INFORMATION

Project Title:	Next Generation Bipolar Plates for Automotive PEM Fuel Cells
Project Period:	March 1, 2007 to August 31, 2009
Report Period:	July 1. 2009 to September 30, 2009
Report Date:	December 31, 2009
Recipient:	GrafTech International Ltd.
Award Number:	DE-FG36-07GO17012

Working/Cost-Sharing Partners

GrafTech International Ltd. (GTI), Parma Ohio
Orest Adrianowycz, Ph.D., Principle Investigator and Team Leader
Julian Norley Ph. D., Director Advanced Energy R&D
David J. Stuart, Staff Scientist, Team Member
David Flaherty, Staff Scientist, Team Member
Ryan Wayne, Staff Scientist, Team Member
Larry Jones, Research Technologist, Team Member
Tom Weber, Research Technologist, Team Member

Ballard Power Systems (BPS), Vancouver Canada
Warren Williams, Team Leader

Huntsman Advanced Materials (HAM), Woodlands, Texas
Roger Tietze, Team Leader
Yen-Loan H. Nguyen, Senior Scientist, Team Member

Case Western Reserve University (CWRU), Cleveland, Ohio
Professor Tom Zawodzinski, Team Leader
Patrick Pietrasz, Graduate Student

Contact
Project Director: Orest Adrianowycz, Ph.D.
Phone: 216-676-2381
E-mail address: orest.adrianowycz@graftech.com

U. S. Department of Energy (DoE) Managers
DoE HQ Technology Manager: Jason Marcinkoski
DoE Field Project Officer: Reginald W. Tyler

2. EXECUTIVE SUMMARY

The results of a successful U.S. Department of Energy (DoE) funded two-year $2.9 MM program lead by GrafTech International Inc. (GrafTech) are reported and summarized. The program goal was to develop the next generation of high temperature proton exchange membrane (PEM) fuel cell bipolar plates for use in transportation fuel cell applications operating at temperatures up to 120 °C. The bipolar plate composite developed during the program is based on GrafTech's GRAFCELL® resin impregnated flexible graphite technology and makes use of a high temperature Huntsman Advanced Materials resin system which extends the upper use temperature of the composite to the DoE target. High temperature performance of the new composite is achieved with the added benefit of improvements in strength, modulus, and dimensional stability over the incumbent resin systems. Other physical properties, including thermal and electrical conductivity of the new composite are identical to or not adversely affected by the new resin system.

Using the new bipolar plate composite system, machined plates were fabricated and tested in high temperature single-cell fuel cells operating at 120 °C for over 1100 hours by Case Western Reserve University. Final verification of performance was done on embossed full-size plates which were fabricated and glued into bipolar plates by GrafTech. Stack testing was done on a 10-cell full-sized stack under a simulated drive cycle protocol by Ballard Power Systems. Freeze-thaw performance was conducted by Ballard on a separate 5-cell stack and shown to be within specification. A third stack was assembled and shipped to Argonne National Laboratory for independent performance verification.

Manufacturing cost estimate for the production of the new bipolar plate composite at current and high volume production scenarios was performed by Directed Technologies Inc. (DTI). The production cost estimates were consistent with previous DoE cost estimates performed by DTI for the DoE on metal plates. The final result of DTI's analysis for the high volume manufacturing scenario ($6.85 /kW) came in slightly above the DoE target of $3 to $5/kW. This estimate was derived using a "Best Case Scenario" for many of the production process steps and raw material costs with projections to high volumes. Some of the process improvements assumed in this "Best Case Scenario" including high speed high impact forming and solvent-less resins, have not yet been implemented, but have a high probability of potential success.

® GRAFCELL is a registered trademark of GrafTech International Inc.

3. RESULTS AND CONCLUSIONS

- Critical processing parameters for benzoxazine based high temperature resin plate embossing have been identified, optimized and full size bipolar plates successfully embossed, sealed and glued.
- New expanded graphite-resin composite systems have been shown to have superior thermal stability and equivalent or improved dimensional stability and mechanical properties over previous GRAFCELL composites.
- Gas impermeability of the new composite system has been demonstrated to a single plate thickness of less then 0.8 mm and an embossed web thickness of 350 µm.
- High temperature single-cell testing of the new composite system demonstrated greater than 1100 hours of operation at 120 °C.
- Glycol compatibility and leachate analyses indicate that the new composite system is stable for use in high temperature PEM transportation fuel cells.
- Full size 10-cell stack testing using a standard duty cycle was performed and over 980 hours of time under test logged.
- Manufacturing cost analysis conducted by Directed Technologies, Inc. indicated a cost slightly higher then the target range of 3 to 5 $/kW. Obtaining the DoE target for bipolar plate cost is potentially within reach provided additional manufacturing cost reductions in plate forming and resin formulation can be implemented.

4. TABLE OF CONTENTS

5. PROJECT OBJECTIVE

To develop the next-generation automotive bipolar plate based on an engineered composite of expanded graphite and resin. The new plate composite is intended to meet U. S. Department of Energy plate cost and performance targets and enable PEM fuel cell operation at temperatures up to 120 ºC.

Specific program objectives were:

- Develop new graphite/resin composites that meet the 120 ºC cell operating temperature target
- Demonstrate mold processing of new materials to a reduced bipolar plate thickness of 1.6 mm
- Validate performance of new plates under automotive conditions using a short (10-cell) stack.
- Evaluate material and process cost relative to the Department of Energy transportation PEM fuel cell cost targets. The goal was to develop cost effective materials which are amenable to high volume manufacturing

5.1 Technical Barriers

This project addresses the following U. S. Department of Energy technical barriers from the 3.4 section of the Hydrogen, Fuel Cells and Infrastructure Technologies Program Multi-Year Research, Development and Demonstration Plan[1].

A - Durability

- Improved corrosion resistance
- Decrease weight and volume

B - Cost

- Lower material & production costs
- Increased power density due to decreased thickness

C - Performance

- Improved gas impermeability
- Improved electrical and thermal conductivity

6. BACKGROUND

The typical PEM fuel cell for automotive applications operates at 80 °C, which is a compromise between material limitations and thermodynamic efficiency. High temperature operation of PEM fuel cells is a desirable goal due to the benefits afforded to balance of plant components and thermodynamic considerations. A PEM fuel cell requires cooling as well as external humidification to keep the membrane humidified and the cell at temperature. For the cooling loop, the temperature delta between the fuel cell and exterior environment determines component sizing and cost. A higher temperature difference reduces the required size of the heat exchanger for the fuel cell, compared to operation at 80 °C resulting in a reduction of component weight and cost.

In response to the benefits available from higher temperature operation, the 2010 U. S. Department of Energy targets for membrane and balance-of-plant called for fuel cells that can operate at temperatures up to 120 °C. For comparison, a typical automobile engine operates at 170-195 °C. Published DoE targets for flow field plate performance at the start of the program are summarized in the following table[2].

Table 1: DoE Targets for Bipolar Plate Performance

Characteristic	Units	Status 2005[a]	2010 Target	2015 Target
Cost[b]	$/kW	10[c]	5	3
Weight	kg/kW	0.36	<0.4	<0.4
H_2 Permeation Flux @ 80 °C, 3 atm (equivalent to <0.1 mA/cm^2)	cm^3 sec^{-1} cm^{-2}	< 2 x 10^{-6}	< 2 x 10^{-6}	< 2 x 10^{-6}
Corrosion	µA/cm^2	<1[d]	<1[d]	<1[d]
Electrical Conductivity	S/cm	>600	>100	>100
Resistivity[e]	Ohm cm^2	<0.02	0.01	0.01
Flexural Strength[f]	MPa	>34	>25	>25
Flexibility	% deflection at mid-span	1.5 to 3.5	3 to 5	3 to 5

[a] This is the first year for which status is available. 2005 status is for carbon plates, except for corrosion status which is based on metal plates.
[b] Based on 2002 dollars and costs projected to high volume production (500,000 stacks per year).
[c] Status is from 2005 TIAX study and will be periodically updated.
[d] May have to be as low as 1 nA/cm if all corrosion product ions remain in ionomer.
[e] Includes contact resistance.
[f] Developers have used ASTM C-651-91 Standard Test Method for Flexural Strength of Manufactured Carbon and Graphite Articles Using Four Point Loading at Room Temperature.

Higher temperature operation increases CO tolerance on the anode, allowing lower grade hydrogen to be used in the case of a vehicle application[3]. The operation at 120 °C also has benefits for the cathode, improving the kinetics of the ordinarily slow oxygen reduction reaction (ORR), due to the temperature dependence of the exchange current[4]. An increase in the temperature on the cathode results in an increase of the exchange current density[5]. Operation at 120 °C also assists in the removal of water from the cathode at high current densities (when cathode flooding is most likely due to

the water production rate) due to evaporative transport of the water away from the cathode as water vapor instead of liquid water[6].

However, the change from 80 °C to 120 °C operation requires a number of materials considerations[7,8]. Flow field plates are the most significant component in a PEM fuel cell by mass and volume, comprising between 60-90% of the operating cell. Concurrent with the DoE 2010 increased temperature targets are increased targets for power densities of 650 W/L. This increase necessitates that bipolar plates be made thinner than those used previously. These plates also must maintain physical properties and performance at the higher operating temperatures.

Over the last ten years, expanded natural graphite has quietly displaced synthetic graphite as the major material for PEM flow field plates. Expanded graphite bipolar plates are unique in that they are made from a continuous matrix of natural graphite, thereby eliminating electrochemical corrosion issues inherent with metal plates while reaching higher thermal and electrical conductivities than filled, “conductive” polymers and synthetic graphite components. The following table is a comparison of the major bipolar plate technologies and their relative advantages and disadvantages.

Table 2: Bipolar Plate Technology Comparison

Technology	Advantages	Disadvantages
GRAFCELL Resin Impregnated Expanded Graphite	Chemically inert Electrical conductivity Low Contact resistance Improved toughness Thermal conductivity Thin, Cost effective Proven performance	Permeability Temperature Strength
Graphite-Filled Polymers	Known fabrication techniques Molded-in flow fields Density	Thermal conductivity Electrical conductivity Temperature (thermoplastics) Brittleness Molding with high filler content
Carbon/Carbon Composites	Electrical conductivity Strength Chemically inert Density	Unproven volume manufacturing Thermal conductivity Thickness
Metals	Electrical conductivity Strength Temperature Thin Known fabrication techniques	Corrosion Contact resistance Thermal conductivity Density Expensive alloys and coatings

During manufacture, expanded graphite is compressed to a porous mat structure that can be impregnated with resins to tailor properties for a given design. This results in a bipolar plate that is thinner, lighter weight, and less brittle than alternative materials.

Expanded graphite bipolar plate components can be embossed with intricate features, thereby eliminating machining operations and resulting in a very cost-effective, reliable manufacturing process.

In this project, a continuous expanded natural graphite structure was impregnated with a new thermoset resin system capable of operation at temperatures in excess of 120 °C. The resulting bipolar plate material did not require a sacrifice of performance or properties for PEM fuel cells. The chemistry of the resin system and graphite raw material was chosen to improve the interaction between the resin and graphite. Physical properties of the impregnated resin flexible graphite composite were measured, and flow field plates of the composites evaluated in high temperature single cell testing. Full-size automotive plates of the new composite were molded and tested in a 10-cell stack under automotive operating conditions. A materials and manufacturing cost estimate was conducted to show how the new bipolar plate composite compared relative to U. S. Department of Energy cost targets for bipolar plates and their contribution to overall system cost goals.

7. RESULTS

The program's major tasks, subtasks and milestones are listed in the following table.

Table 3: Project Major Tasks and Milestone Status

Task	Description	Target End Date
1	**Expanded Graphite Material Selection**	
1.1	Define key flow field plate specifications with collaborators	3/1/2007
1.2	Natural Graphite Selection	3/27/2007
1.2.7	**Milestone: Final Graphite Flake Sources Selected**	3/23/2007
1.3	Intercalation Chemistry and Exfoliation Methods	3/12/2008
1.3.2.9	**Milestone: Graphite for resin evaluation Identified**	5/29/2007
1.3.3.9	**Milestone: Experimental Graphite Resin Evaluation Completed**	1/2/2008
2	**Resin Identification and Selection**	
2.1	Confirm Key Fuel Cell Performance Characteristics	3/8/2007
2.2	Definition of New Resin Chemistries	3/15/2007
2.3	Design Part Release Chemistry	3/22/2007
2.4	Formulate Lab Scale Resin Samples	3/29/2007
2.5	Evaluate Neat Resin Properties	5/11/2007
2.6	Summarize Neat Resin Results and Down select	5/18/2007
2.7	**Milestone: Resin Formulations for Composite Studies Selected**	5/21/2007
3	**Small-Scale Composite Preparation and Evaluation**	
3.1	Prepare Graphite Mat for Preliminary Resin Impregnation	6/4/2007
3.2	Preliminary Composite Preparation and Evaluation	10/4/2007
3.2.10	**Milestone: Resins for Single Cell Testing Selected**	8/30/2007
3.2.12	**Contingency Point: Resins for Single Cell Testing Selected**	8/30/2007
3.3	Long-Term Testing of Selected Composite Samples	3/7/2008
3.5	Design Experiment and Execute Screening DoE	3/12/2008
4	**Machining and Embossment of Small-Scale Composites**	
4.1	Fabricate New Composite Materials	9/27/2007
4.2	Validate Properties of New Graphite Containing Composites	1/8/2008
4.3	Machined Plates for Single Cell Testing	11/28/2007
4.3.5	**Milestone: Machined Plates Completed**	10/12/2007
4.4	Design, Fabricate, and Evaluate Small Embossed Test Plates	1/8/2008
4.5	Summarize Embossability Studies & Review Status	3/17/2008
4.5.2	**Milestone: Composites Embossability Characterized**	1/16/2008
5	**Single Cell Testing**	
5.1	Select Fuel Cell Components Suitable for High Temperature Testing	9/13/2007
5.2	Develop Test Method for Analysis of Fuel Cell Leachates	10/11/2007
5.5	Set up and Start 1000 hr Single Cell Test	12/12/2007
5.6	Check Single Cell Station After Start Up	12/13/2007
5.7	Complete 1000 hr Single Cell Test	2/8/2008
5.8	Post Test Plate Analysis	3/7/2008
5.9	Summarize and Analyze Results of Single Cell Testing	3/12/2008
5.10	**Milestone: Single Cell Testing Completed**	3/13/2008
6	**Design and Manufacture Full-size Bipolar Plates**	
6.1	Develop Test Methods and Test Plate Coolant Durability	3/12/2008
6.2	Review of Existing Flow Field Plate Architectures	10/30/2008

Task	Description	Target End Date
6.4	Design Flow Field Plate Using Existing Architectures	7/1/2008
6.5	Fabricate Full Size Embossing Die Set	12/18/2008
6.5.7	**Milestone: Full Size Tool and Leak Check Device Ready**	9/3/2008
6.6	Emboss Full-size Bipolar Plates	1/21/2009
6.6.5	**Milestone: Final Graphite, Resin and Processing Parameters Selected**	3/17/2008
6.6.18	**Milestone: Full Size Plates Ready for Short Stack Testing**	10/1/2008
7	**Short Stack Test of Full-size Plates**	
7.1	Part and Test Station Preparation	3/4/2009
7.1.5	**Milestone: Short Stack Full Size Plates Ready for Testing**	11/5/2008
7.2	Test Cells in Short-Cell Stack	1/30/2009
7.3	Post-Test Analysis of Parts and Performance	7/13/2009
7.3.3	**Milestone: Final Review of Short Stack Test Results Completed**	2/20/2009
7.4	Deliver Full Size Plate Stack to DoE	7/29/2009
7.4.1	Fabricate Short Stack for DoE	3/5/2009
7.4.2	**Milestone: Stack Delivered to DoE**	3/6/2009
8	**Economic Assessment of New Technologies**	
8.1	Start Economic Assessment	12/15/2008
8.2	**Milestone: Economic Assessment Complete**	12/16/2008

The program's target end date was originally February 28, 2009 and a no-cost extension was granted to August 31, 2009. A summary of the activities and results for each major task are discussed in the following sections.

7.1 Task 1: Expanded Graphite Material Selection

7.1.1 Natural Graphite Selection

Natural graphite sources from a number of domestic and international suppliers were evaluated. Candidate flakes from these sources were selected based on data contained in a proprietary GrafTech database of raw material sources developed over the last 15 to 20 years. The starting graphites selected for screening are described in the following table.

Table 4: Natural Graphite Flake Candidates Selected for Evaluation

Graphite Code	Description	Sizing
G1S1P2	Current production flake	S1
G1S1P1	Current production Thermally Purified	S1
G1S2P1	Current production Thermally Purified	S2
G1S3P1	Current production Thermally Purified	S3
G2S1P2	Imported Current Production	S1
G2S2P2	Imported Current Production	S2
G3S1P1	Thermally Purified Domestic	S1
G4S1P1	Chemically Purified Imported	S1
G4S2P2	Chemically Purified Imported	S2
G5S1P2	Imported Intercalated	S1
G6S1P2	Alternative Imported	S1
G6S2P2	Alternative Imported	S2

The selected starting natural graphite materials include a variety of domestic and imported sources. Graphite flakes that are thermally and chemically purified were evaluated, as well as a commercially available intercalated flake. The selected samples were characterized using a standard regimen of raw material tests. Included in this analysis was an evaluation of the flakes for their suitability in expanded graphite production. Appendix A summarizes the elemental analysis testing data obtained on these materials. Data for the evaluation of the treat chemistries for the selected starting graphite materials are summarized in Appendix B.

7.1.2 Intercalation Chemistry and Exfoliation Methods

A design of experiments methodology was used to identify the working range of intercalation chemistries and exfoliation methods. An initial screening experiment was conducted to identify key graphite materials and processing variables that are specific to the requirements of a thinner, yet more robust bipolar plate. After completion of the screening experiment, a response surface experiment was conducted focused on the key variables to more clearly identify interactions, and a usable range of materials.

The independent variables selected for evaluation are shown in the following table along with the levels of each variable. Dependent variables selected for this study are mat tensile strength and Taber strength.

Table 5: Graphite Processing Designed Experiment Independent Variables

Treat Chemistry	**Sizing**
Current production process (T1)	Production sizing (S1)
Alternative routine process higher expansion (T2)	Experimental sizing (S2)
Experimental process (T3)	Experimental sizing (S3)
Expansion Method	**Thickness**
Current process (E1)	Current thickness (MT1)
Experimental process (E2)	Target thickness (MT2)
Alternative Experimental (E3)	

Statistical analysis of the testing data indicated that optimum properties are obtained for mat materials that are P1 in purity; S1 or S2 sizing; T1 acid treated; and E1 expanded. Based on the results a subset of graphite mats was selected for composite evaluation in Task 3. These materials and their processing conditions are shown in the following table.

Table 6: Selected Natural Graphite Intercalation, Expansion Processing Codes

Graphite	**Sizing**	**Purity**	**Treat**	**Expansion**
G1	S1	P2	T1	E1
G1	S3	P2	T1	E1
G3	S2	P1	T1	E1

7.2 Task 2: Resin Identification and Selection

7.2.1 Key Fuel Cell Performance Requirements and Resin Characteristics

GrafTech, Ballard Power Systems, and Huntsman Advanced Materials in collaboration agreed on the key fuel cell performance characteristics and developed detailed resin specifications based on these characteristics. The specifications are listed in the following table. Testing procedures and technical targets were identified and prioritized for every property. When available, universally accepted testing protocols for graphite and graphite composites were chosen.

Table 7: Resin Specifications

Property	Priority	Test	Technical Target
Processing			
Resin viscosity (in acetone)	1	Shear/Brookfield (25ºC)	0.8 cP (Max. 2.0 cP)
Curing conditions	1	DSC	205ºC, 1 h (Max. 230ºC, 2 h)
Polymerization volatiles	1	TGA	Not detectable
Resin latency			
Ambient	1	DSC/Thermosel	Indefinite
Thermal cycle	1	One cycle to 85ºC with 45-min. hold	Indefinite (Max. one month shelf life)
Resin softening point	1	DMA/TMA	50ºC (Max. 100ºC)
Shrinkage (linear, volumetric)	2	Huntsman internal	
Thermal			
Glass transition (T_g)	1	DMA/TMA	210ºC (Min. 150ºC)
Dimensional stability	1	TMA (*z*-axis)`	40 ppm $ºC^{-1}$ (Max. 70 ppm $ºC^{1}$)
Mechanical			
Flexural			
Strength	2	ASTM D790 (Method 1, Procedure A)	8700 psi (25ºC), 6100 psi (130ºC)
Modulus	2		2.1 Mpsi (25ºC), 1.4 Mpsi (130ºC)
Retention of flexural strength and modulus			
Thermal shock cycling	2	USCAR III (100 cycles, -40ºC to 130ºC)	No detectable change
Thermal cycling	2	USCAR III (10 cycles, -40ºC to 130ºC)	No detectable change
Freeze start up	2	30 d at -40ºC	No detectable change
Hot and humid conditions	1	48 h in air at 130ºC and 100% RH	50%
Tensile			
Strength	2	ASTM D638 (Type 1)	5500 psi (25ºC), 3900 psi (130ºC)
Modulus	2		5 Mpsi (25ºC), 7 Mpsi (130ºC)
Compressive			
Strength	2	ASTM F36 (Procedure J)	13,700 psi (25ºC), 10,800 psi (130ºC)
Modulus	2		
Toughness	2	ASTM D5045-99	
Creep	2	ASTM D2990 (modified)	0 at 200 psi, 130ºC
Chemical/Purity			

Property	Priority	Test	Technical Target
Amine, aromatic, and ionic leaching	1	HPLC (amines, aromatics) and solution conductance (ions) following treatment (50 h, 90ºC) with water, 1 mM H_2SO_4 (aq), 2 wt. % MeOH (aq), 60 wt. % MeOH (aq), or Glysantin® FC G 20	Not detectable
Maximum potential for specific elements	2	ICP (metals), FTIR (Br, Cl)	Not detectable
Fluid absorbance	2	Incorporated into leachables testing	No detectable fluid uptake
Flammability	2	UL94	V-0
Electrical	3	Huntsman internal	
Conformance with IMDS	3	International Material Data System	

7.2.2 Resin Formulation Chemistries

Based on the resin specifications, Huntsman Advanced Materials identified and formulated a number of benzoxazine and epoxy resin systems that were potentially capable of meeting the program goals. Resin reinforced expanded graphite composites are intended to be reciprocally embossed to a variety of complex net-shape flow field designs. Consequently, the part must release cleanly from the die surface to prevent damage and to reduce pressing time. Based on prior experience with similar system, Huntsman's formulations included internal part release additives that are known to be compatible with their recommended resin systems.

7.2.3 Preparation and Characterization of Lab Scale Resin Samples

From the selected resin formulations laboratory-scale neat resin samples were prepared. Differential scanning calorimetry (DSC) and dynamic mechanical analysis (DMA) were performed on the neat uncured resins to identify the cure onset and curing profile for each system. Thermal mechanical analysis (TMA) and DMA were used to measure the glass transition temperatures (T_g). In the case of DMA both the tan delta and storage modulus curves were used to obtain T_g. TMA glass transition temperatures were obtained from the extrapolated onset of the coefficient of thermal expansion (CTE) measurements. In addition, gel times, softening points and thermogravimetric analysis (TGA) weight loss and decomposition temperatures were measured. The thermal analysis results of the formulations are summarized in Appendix C. Examples of the DSC curves for one of the benzoxazine and one of the epoxy resin systems are shown in the following two figures.

Figure 1: DSC Curve for Benzoxazine Resin System 1

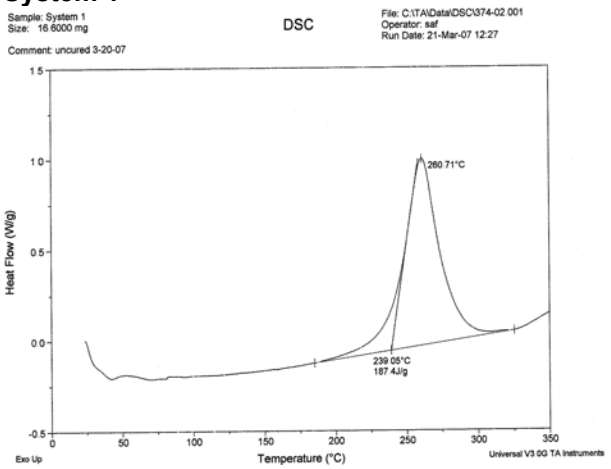

Figure 2: DSC Curve for Epoxy Resin System 1

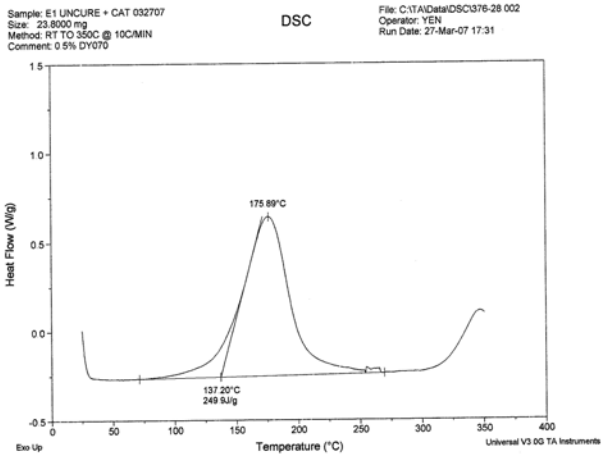

An example of a DMA curve for the benzoxazine resin system is shown in the following figure.

Figure 3: DMA Curve for Benzoxazine Resin System 1

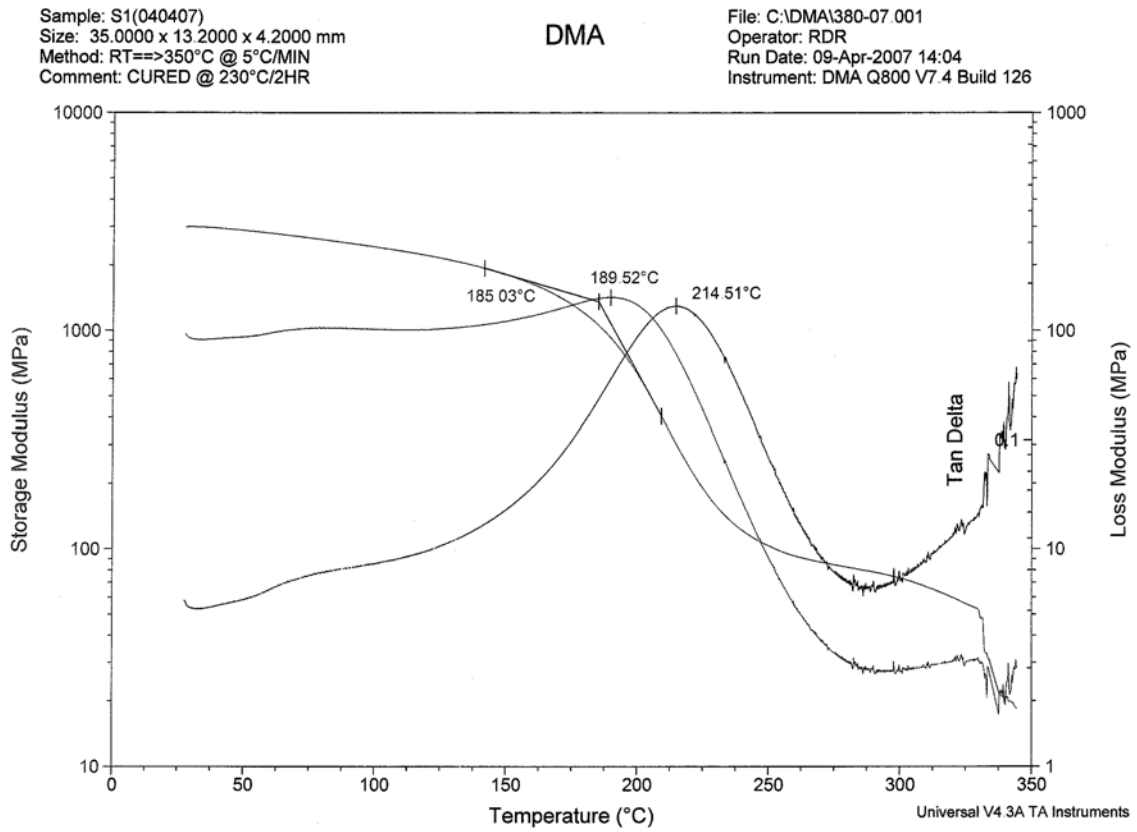

7.2.4 Resin System Down-Selection

Based on the results of the neat resins system analyses, three formulations were down selected for evaluation in resin flexible graphite composites. Selections were based on the key performance criteria in Table 7 and the measured thermal properties. The selected formulations are highlighted in the data tables in Appendix C and summarized in the following tables.

Table 8: Glass Transition Temperatures for Neat Resin Systems

System ID	Catalyst	DMA Tan Delta Tg, °C	DMA Storage Modulus Tg, °C	TMA Tg, °C	TMA CTE, µm/m °C
Benzoxazine Resins					
2G	No	282	252	247	61
2H	No	282	255	261	52
Epoxy Resins					
1	Yes	205.0	178.0	172.0	82

Table 9: Gel Time, Softening Point and TGA Results for Neat Resin Systems

System ID	Catalyst	Gel Time @ 200 °C, s	TGA Decomp Temp, °C	TGA Wt Loss, %	Softening Point, °C
Benzoxazine Resin					
2G	No	364.9	343	3.8	88.1
2H	No	440.9	347	3.8	74.6
Epoxy Resin					
1	Yes	30.3	336.0	3.8	Liquid

Table 10: Recommended Cure Conditions for Down Selected Resin Systems

System	Catalyst	Cure Condition, °C/hr
Benzoxazine Resin		
2G	No	200 °C/0.5 hr + 230 °C/2 hr
2H	No	200 °C/0.5 hr + 230 °C/2 hr
Epoxy Resin		
1	Yes	150 °C/2 hrs

7.3 Task 3: Small-Scale Composite Preparation and Evaluation

7.3.1 Composite Preparation and Evaluation

Resin impregnated expanded graphite composites from the three expanded graphite mats and three down selected resin systems were prepared. During the composite preparation process the decision was made to eliminate the epoxy resin due to a number of processing issues; but, primarily due to high reactivity. The cured resin expanded graphite composites were fabricated as blank stock with a target thickness of 0.60 mm. This base stock was used to prepare samples for physical testing, thermal testing, environmental cycle testing, leak testing, and single cell testing. Samples were also provided to CWRU for use in development of the leachate method and to Ballard Power Systems for use in their glycol compatibility evaluations.

7.3.2 Designed Experiments on Composite Forming Process Parameters

Statistically designed experiments were used to determine the effects of key process parameters on preparation of the flexible graphite resin composites. Independent variables included resin content, type of graphite flake and molding pressure. The dependent variables selected for the designed experiment are summarized in the following table with the testing method and target specification for each shown. Flat stock (blank plates) was used to determine most properties with the exceptions as noted in the table.

Table 11: Composite Fabrication Designed Experiment Dependent Variables

Variable	Test	Specification
Glass transition	DMA	150ºC
Permeability[a] (30 min, 0.9 bar)	Bubble	No detectable bubbles
Thermal conductivity	In-house	260 W m^{-1} K^{-1} (in-plane)
Electrical conductivity	In-house	7 µΩ m (in-plane) 300 µΩ m (through-plane)
Flexural strength (25ºC, 130ºC)	ASTM D790 (Method 1, Procedure A)	8700 psi (25ºC), 6100 psi (130ºC)
CTE (*x*, *y*, *z*)	TMA	40 ppm/ ºC (Max. 70 ppm /ºC)
Feature definition[2]	Visual (subjective)	Pass
Flexural modulus	ASTM D790 (Method 1, Procedure A)	2.1 Mpsi (25ºC), 1.4 Mpsi (130ºC)
Compressive strength	ASTM F36 (Procedure J)	13700 psi (25ºC), 10800 psi (130ºC)
Growth factors[b]	Customized, in-house	Minimum possible

[a]Needed for both flat stock and flow field plates.
[b]Needed for flow field plates only.

Other, less critical properties that were also measured were thermal stability, helium density, water immersion density, usable pH range, water absorption, tensile strength, and tensile modulus.

7.3.2.1 Experimental Design

Each graphite material/resin combination followed a two-level factorial design shown in the following table.

Table 12: Experimental Design for Graphite Mat/Resin Combinations

Treatment*	Resin Content	Molding Pressure
1	L	L
2	H	L
3	L	H
4	H	H
5	M	M
6	M	M
7	M	M

* The actual run order will vary with the particular graphite mat/resin combination.

Permeability and electrical resistivity were the primary quantitative responses monitored during processing since these properties, are critical to final plate performance and can be measured quickly and easily. Feature definition was monitored as a qualitative response. Other dependent properties were determined after the specifications for permeability, electrical resistivity, and feature definition were met.

Ideally, treatment run order is randomized across all process steps in order to mitigate systematic errors (e.g. the effect of solvent loss or resin aging over time). However, to improve efficiency and minimize variability in mat impregnation, all the impregnations for fixed resin content were done simultaneously. Mat positioning within the tank and the order of subsequent process steps were randomized.

7.3.3 Nitrogen and Helium Permeability (Leak) Testing

Permeability of the flat plates was tested initially in nitrogen, then helium. The availability of nitrogen leak testing made it the method of choice for initial screening and process optimization studies. Measurements on the flat composite stock showed no evidence of leaks. Results of the testing are summarized and shown in Appendix D. Similar testing was performed using helium gas with identical results.

7.3.4 Hydrogen Permeability Leak Testing

At the request of the Freedom Car Fuel Cell Technology Team, hydrogen permeability testing was performed on samples of the blank resin graphite composites. The testing was performed by Akron Rubber Development Laboratory (ARDL) an A2LA accredited contract testing laboratory specializing in gasket testing. Test method used was ASTM D1434-82 (2003) Procedure V. Test conditions were as shown in the following table.

Table 13: Hydrogen Permeability Testing Conditions

Test Condition	Value
Apparatus	Custom Scientific Model CS-135
Gas	Hydrogen
Test Temperature, °C	65.0

Test Condition	Value
Test Gas Pressure, psi	0.5-115.0
Test Sample Permeation Area, cm²	66.4
Capillary Diameter, cm	0.11696

Each sample was tested in duplicate with the exception of GRAFCELL FFP-300 @ 3.0 mm which was tested only once and the 2G resins sample @ 0.67 mm which was tested three times. Samples were purged with hydrogen for 20 min then held under the test pressure for a minimum of 1.5 hours. No positive flow readings were recorded for all samples unless they fractured under high pressure. The complete set of results is summarized in Appendix D.

7.3.5 Thermal and Mechanical Property Evaluations

7.3.5.1 Mechanical Testing Results on Resin Graphite Composite Samples.

Mechanical testing samples were prepared using the G1S1T1E1 graphite mat impregnated with the experimental 2G and 2H benzoxazine resin systems in 1-, 3-, and 5-ply sheets. Results from comparable samples consisting of the incumbent GRAFCELL FFP-300 standard resin composite system were used as controls. Testing was performed by the Lubrizol Corporation, Measurement Science Group, Brecksville, Ohio; using the protocols and equipment in the following table.

Table 14: Composite Mechanical Testing Information

Test	Method	Equipment	Rate, in/min	Span, in
Flexural	ASTM D790	Instron Model 1125	0.05	2.0
Tensile	ASTM D638	Instron Model 4430 Extensometer	0.20	2.0

Samples were analyzed in an environmental chamber at temperatures of -40, 23, 100, and 120 °C in 50% relative humidity. Statistical analysis of the results was performed using Minitab Version 14.2 assuming a 95% confidence interval (α=0.05). Four specimens were analyzed for each combination of resin, temperature, number of ply, and method. Data was examined for outliers which were removed from the data set prior to final analysis. Flexural and tensile strength values for the benzoxazine samples were compared to data collected on the incumbent GRAFCELL FFP-300 resin system using t-test statistics. Also, a paired t-test was conducted comparing results for the two benzoxazine resin systems. Detailed results of the testing and the statistical analysis of the data are shown in Appendix E.

The paired t-test results indicate that the flexural and tensile strengths of the 2G and 2H benzoxazine resin systems were not significantly different from each other. However, comparisons of results between each resin system and the GRAFCELL FFP-300 composite system indicate that both resins are similar to, or significantly higher, in flexural strength and modulus then the GRAFCELL FFP-300 composite at all temperatures tested. The improvements in mechanical testing properties are most pronounced at elevated temperatures (100 and 120 °C) where both benzoxazine resin systems are significantly stronger then the epoxy and have significantly higher modulus.

The tensile strength results are consistent with the flexural results showing that the benzoxazine resins are significantly higher in tensile strength then the GRAFCELL FFP 300 composite resin system. However, the results for the tensile modulus are less conclusive than the flexural modulus results. Values for this property show a high degree of variation with no clear indication of which resin is superior. See the figures below for box plots of the strength data which visually highlight the differences. Scatter plots of the flexural and tensile strength data (See Figures following the Boxplots) as a function of temperature show that the degradation in strength is less sever with increasing temperature for both of the benzoxazine resin systems than the control.

Figure 4: Box Plot of Flexural Strength vs. Resin Type and Number of Plies

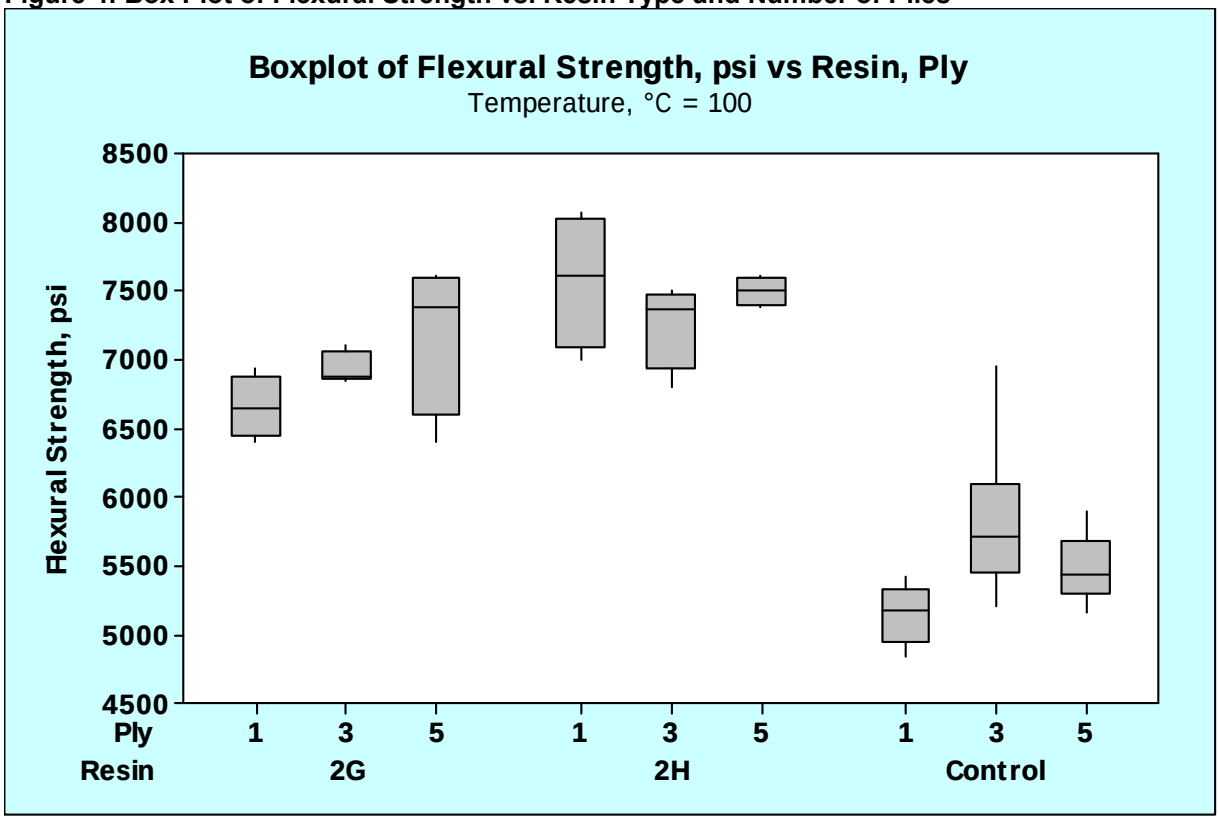

Figure 5: Box Plot of Tensile Strength vs. Resin Type and Number of Plies

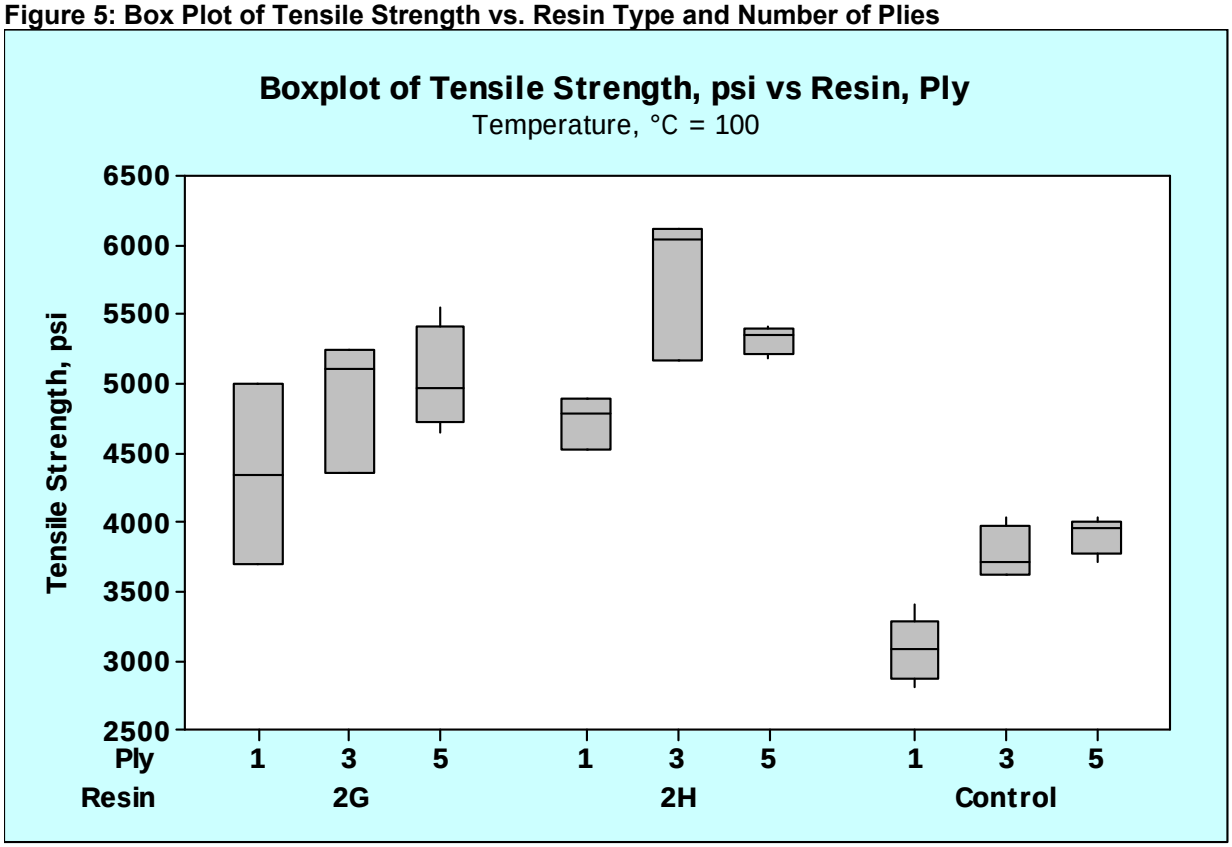

Scatter plots of the flexural modulus data as a function of temperature show that the flexural modulus has a maximum at room temperature and is higher for both benzoxazine resin systems then the control throughout the temperature range studied. Scatter plots of the tensile modulus data as a function of temperature show that the modulus also has a maximum at room temperature; however the difference between the benzoxazine resin systems and the control throughout the temperature range studied is not statistically significant.

Figure 6: Scatterplot of Flexural Strength vs. Temperature by Resin and Number of Plies

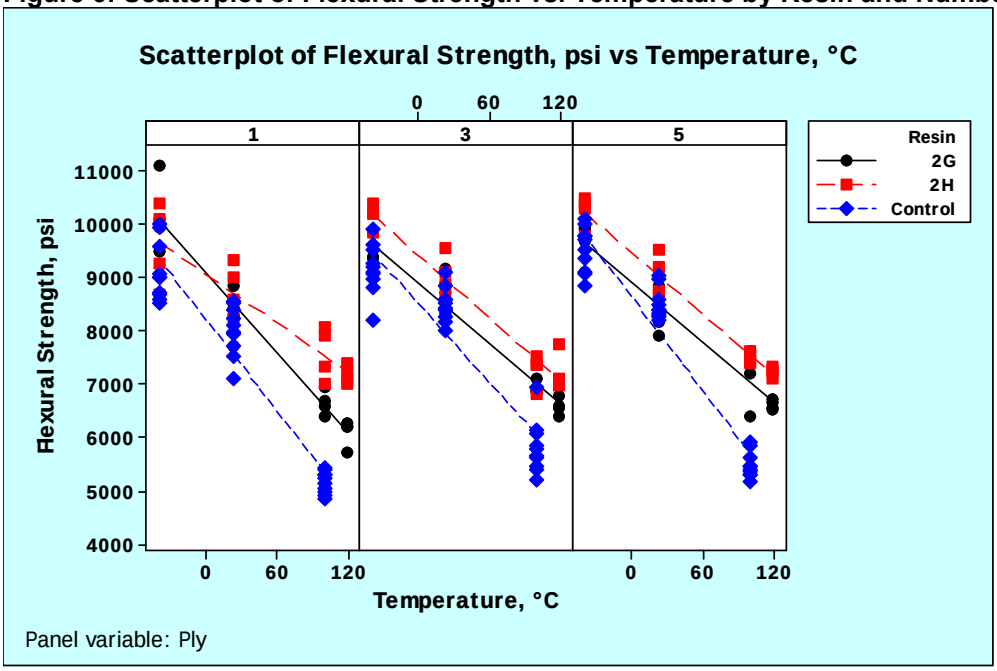

Figure 7: Scatterplot of Tensile Strength vs. Temperature by Resin and Number of Plies

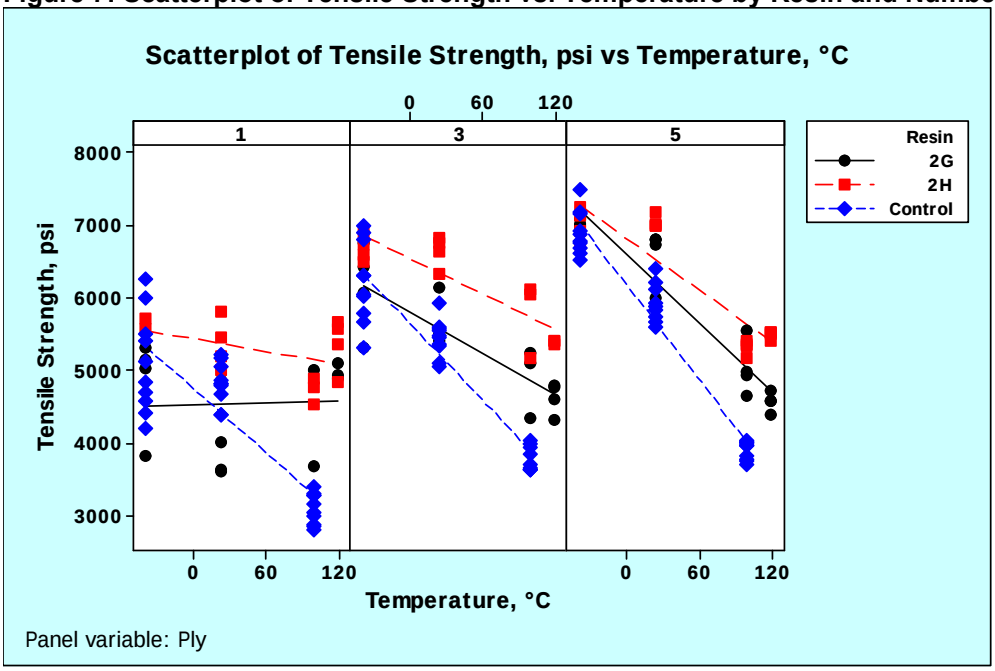

7.3.5.2 Work of Fracture Analysis

Work-of fracture analysis of the flexural strength data was similar to the flexural and tensile strength data. The summarized data and results of the statistical analysis are shown in Appendix F. The 2G resin composite had statistically higher values for work-of-fracture than the 2H resin composite based on a paired t-test comparison of data from similar treatments. Comparison of the work-of-fracture results between the

benzoxazine resin composite and the GRAFCELL FFP-300 composite system was not made since data for the FFP-300 composite was not available.

7.3.5.3 Compressive Strength Results

Compressive strength testing of the 2G resin composite was completed after fabrication of the final composites sheets since preparation of the test specimens required a large number of composite sheets. A minimum of 30 sheets were laminated to achieve the required specimen thickness for proper compressive strength testing. The delay in obtaining this data until late in the program made testing of the 2H or other previously eliminated composites moot, and therefore was not done. The results of the testing are summarized in Appendix G.

Example plots of the compressive stress strain-curves obtained on the test specimens are shown in the following figures.

Figure 8: Compressive Strength Stress-Strain Curves for the 2G Resin Flexible Graphite Composite System Comparing Thru-plane (TP) and In-Plane (IP) Results

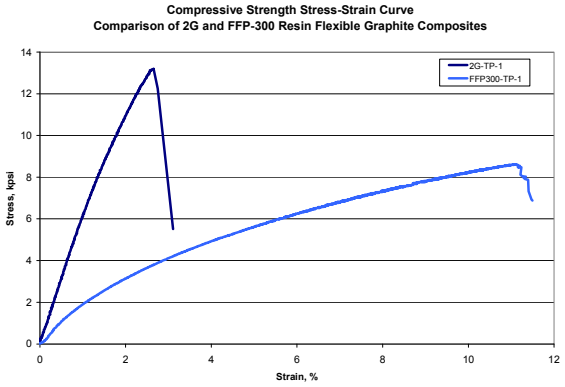

Figure 9: Compressive Strength Stress-Strain Curves Comparing the 2G Resin and FFP-300 Flexible Graphite Composite Systems Thru-plane (TP) Results

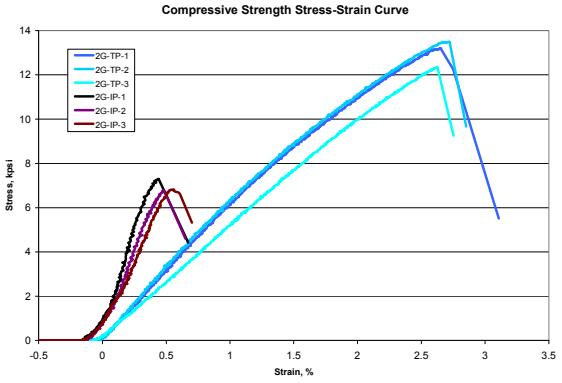

Based on the data and an examination of the failed samples, the following observations were made.

- All the samples exhibited brittle fracture characteristic of polymer resin systems.
- All thru-plane samples failed along the interface between composite layer sheets. Failure mode was by pulverizing at the specimen edge rather then by delaminating.
- All in-plane samples failed by cracking both thru and perpendicular to the composite layer sheets.
- All the resin composite systems had thru-plane compressive strength about twice the in-plane compressive strength.
- The benzoxazine 2G resin composite is approximately twice as strong as the FFP-300 resin system.

The increased compressive strength exhibited by the benzoxazine resin system should improve performance of bipolar plates manufactured using this system. Higher compressive strength will eliminate or minimize damage to the bipolar plates and the

fine structure of their flow field features which may occur during handling, manufacturing and/or stack assembly.

7.3.6 Long-Term Cycle Testing of Composite Samples

Samples of the resin expanded graphite flat stock were temperature cycled in an environmental chamber using a modified USCAR - III Test Protocol[9] for normal cycling and thermal shock cycle. The exposure conditions were as shown in the following table.

Table 15: USCAR - III Environmental Test Protocol

	Shock Test		Normal Cycle		
Cycles	100		40		
Step	1	2	1	2	3
Temperature, °C	125	-40	-40	87.5	125
Dwell, hrs	0.5		0.5		
Ramp Rate, °C/min	-328	328	4.25	1.25	-2.75
Hold Temp, °C	-40	125	87.5	125	-40
Relative Humidity, %	50	NA	80-90	NA	NA
Dwell, hrs	0.5	0.5	4	1.5	0.5

The samples were visually examined following the completion of the testing. All showed no visible evidence of adverse effects from the testing regime and were submitted for mechanical flexural and tensile strength testing. Results on the mechanical testing of the cycled composite samples are summarized in Appendix H in which they are compared to the results obtained on samples which were not environmentally cycled.

The mechanical property results of the environmentally cycled and shocked samples show that composites prepared with the 2G resin were statistically identical to, or better then, the unexposed samples for all properties evaluated for both 1- and 3-ply. However, the resin composites prepared with the 2H resin system did show degradation in both flexural and tensile properties for the 3-ply composite samples.

In this analysis the flexural and tensile strength were considered to be degraded when compared to unexposed specimens if their values were decreased after exposure. Conversely, a drop in the flexural and tensile modulus is viewed as beneficial since it indicates that the composite is more flexible and therefore more compliant with improved work of fracture. A more compliant material will be better able to compensate for minor variations when assembled under compression in a fuel cell stack then a stiffer material.

7.3.7 Plate Coolant Durability

Ballard developed a glycol permeation test based on ASTM D739-99a to evaluate the permeation of ethylene glycol across the resin expanded graphite composite. The extent of permeation of this coolant through the expanded graphite is important for plates with thinner webs. The testing protocol involved placing the test material in a fixture where the resin expanded graphite composite test sample was the only

separation between the ethylene glycol test fluid and the de-ionized water collection medium. Discrete sampling of the collection medium for the presence of the ethylene glycol was used to determine permeation rate. Gas chromatography with a field ionization detector was used to monitor the presence of ethylene glycol in the de-ionized water. The detection column was chosen specifically for this analysis and method optimization allowed quantitative ethylene glycol detection at 50 ppm, with a lower detection limit of 10 ppm.

In total, the analysis was conducted six times on the 2G resin composite and four times on the 2H resin composite. Initial attempts were complicated by a variety of operational issues which caused cracking of the composite plates and invalidated the results for those samples. The final results are summarized in Appendix I. Composite plates with the 2G resin showed significantly better performance then those made with the 2H resin.

7.4 Task 4: Machining and Embossing of Small-Scale Composites

In this task, test samples of molded composite plates were prepared and processing parameters for molding plates optimized. Using a proprietary oxidant flow field die, plates were molded from the composite materials which were fabricated as part of the designed experiment in Task 3.

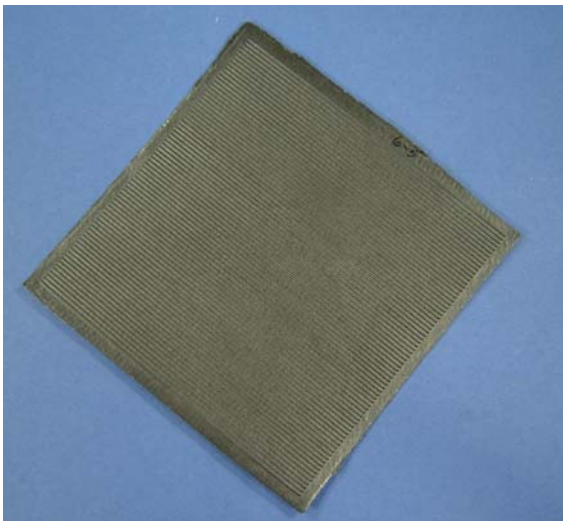

Figure 10: Molded Resin Expanded Graphite Composite Corrugated Flow Field Plate

Nitrogen gas permeability, in-plane and through-plane electrical resistance, and dimensional processing changes (growth factors) were measured on each plate. Samples of the composites were also tested for final properties.

A photograph of a non-proprietary molded plate typical of those used in the study is shown on the left. The plate in the figure has an active area similar to the actual test plates that is approximately 90 mm x 90 mm and is approximately 1 mm thick.

7.4.1 Permeability Results on Molded Test Plates

Permeability measurements for screening purposes on the molded test plates were made using a GrafTech Best Practice procedure and a test apparatus developed specifically for this purpose consistent with the specimen size and features. During the permeability testing, composites made using the G1S3P2T1E1 graphite mat were observed to be significantly higher in permeability than all others. Consequently composites made from this starting graphite mat were removed from additional consideration. The average value for the permeability measurements on each sample

set, for a fixed combination of material and process variables, is summarized in Appendix J. In this data table the process variables are coded.

A minimum of five specimens were analyzed for each combination of resin, graphite, and the three process variables resulting in the analysis of 180 composite samples. Data were examined for outliers; twelve of which were identified and removed from the final analysis. Statistical analysis was performed using Minitab Version 14.2 assuming a 95% confidence interval (α= 0.05; ß= 0.10). Analysis of variance (ANOVA) was performed using the General Linear Model (GLM) technique; since the removal of outliers resulted in a non-orthogonal data set. The analysis was limited to three factors: graphite, resin, and Process Variable 1 (PV 1). Process Variables 2 and 3 were also considered for analysis as factors in the ANOVA. Unfortunately, the range of samples based on these factors which could be fabricated was limited by process variable 1 (PV 1). The results of the ANOVA are summarized in Appendix J and shown graphically in the following figure.

Figure 11: Main Effects Plot for ANOVA Results on Leak rate vs. Graphite, Resin and Process Variable 1

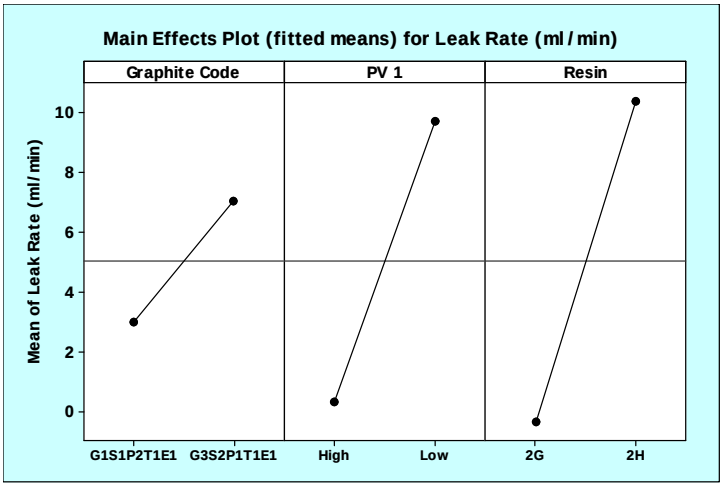

The ANOVA indicates that all three factors are statistically significant in determining the composite leak rate. Based on this result, minimum leak rates were obtained for samples of the G1S1P2T1E1 graphite; 2G resin; and with PV1 at the high level.

In order to perform additional analysis on the data the results were sorted into eight subsets each consisting of a different combination of graphite, resin, and PV1. Separate regression analyses were performed on all of the eight data subsets with the leak rate as the dependent variable and PV2, PV3, PV4, density, and thickness, as the independent variables. The results of the regression analyses are summarized and shown in Appendix J. An example plot is shown in the following figure.

Figure 12: Typical Regression Plot for Leak Rate vs. Process Variable 4

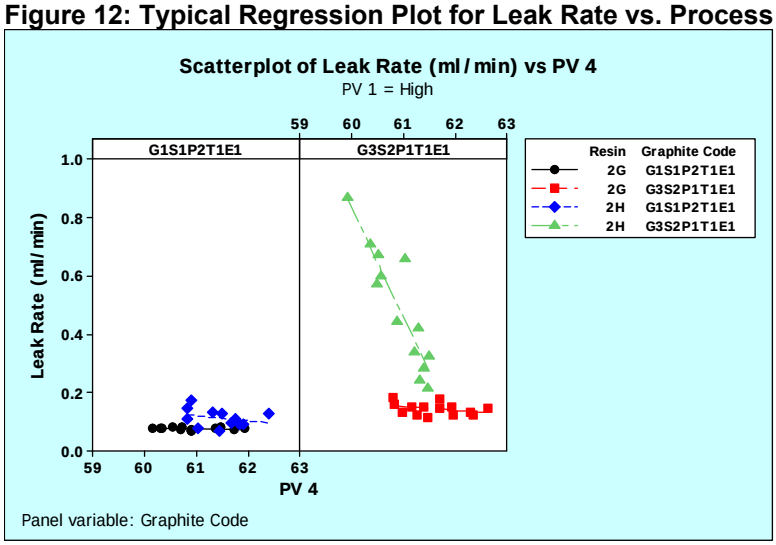

Only three of the data sub-sets had statistically significance regression results. This indicates that within the range of parameters studied, leak rates are at or near the minimum for the combination of process conditions that produced the best results. Additional improvement may be possible for these processing combinations; however, they may not improve the leak rate sufficiently to surpass the leak rate of the combination already providing the lowest value.

7.4.2 Graphite Resin Composite Dimensional Change (Growth Factor) Results

Composite dimensional changes (growth factors) resulting from the embossing and resin curing processes are affected by the resin formulation, and the number and type of flow field design features present in the composite. Minimizing these dimensional changes is beneficial for production of plates that meet customer specifications. Consequently, a processing optimization designed experiment was conducted on test plates containing flow field features similar to those anticipated to be in the final plate design. In this study, the composite dimensional changes (growth factors) were the dependent variables. Independent variables for the study were as shown in the following table. Sample dimensional changes were measured using an ROI Metrology System.

Table 16: Dimensional Changes to DoE Resin Graphite Composites

Independent Variable	Values
Graphite starting mats	G1S1P2T1E1 and G3S2P1T1E1
Resins systems	Benzoxazine 2G, 2H, GRAFCELL FFP
Processing Variable 1 (PV1)	Levels L1, L2, and L3
Processing Variable 2 (PV 2)	Levels L1, L2, and L3
Processing Variable 3 (PV 3)	Levels L1, L2, and L3
Thickness	Single Ply 0.47 - 0.88 mm

7.4.2.1 Data Analysis Procedure

A minimum of five specimens were analyzed for each treatment consisting of one combination of resin, graphite, PV1, PV2, and PV3. The total number of specimens

analyze was 180. Each specimen was measured for length, width, border thickness, landing thickness, and weight before impregnation, before curing, and after curing of the pressed composite. One of the treatments could not be measured for length and width since the composite had expanded to the point of being outside the range of ROI measurement. This treatment was dropped from further consideration and analysis. The final data set was examined for outliers of which there were none. Statistical analysis was performed using Minitab Version 14.2 procedures for Boxplots, t-tests, General Linear Model ANOVA, and regression analysis with α= 0.05; and ß= 0.10. The results of the analysis are summarized in the following sections.

7.4.2.2 Data Analysis T-test and Paired T-test Results

Results for the 2G and 2H composite resins were compared to comparable results for the GRAFCELL FFP-300 composite using a standard t-test. Additionally, a paired t-test analysis was performed between the 2G and 2H resin systems. The results are reported and summarized in Appendix K following the raw data.

The results of the t-test comparison indicate that both of the benzoxazine resins exhibit significantly less growth in length and width then the comparable GRAFCELL resin system for every treatment. The results of the paired t-test analysis indicate that the growth factors in the length direction are statistically the same for the two benzoxazine resin. However, the growth factor difference in the width direction is statistically significant. In both directions, the 2G resin grew less then the 2H resin. Pair t-test comparisons with the GRAFCELL FFP-300 resin were not made because the GRAFCELL data needed for each treatment level was not available.

General Linear Model (GLM) Analysis of Variance (ANOVA)

General Linear Model (GLM) ANOVA is a special case of ANOVA which is used for fitting of unbalanced designs, allows the use of covariates, and can be used to make multiple comparisons. The growth factor data was initially analyzed using the GLM ANOVA on all treatments. The results are shown in Appendix K following the raw date.

Both of the benzoxazine resin composites are significantly different in growth characteristics from the GRAFCELL resin composite. Since resin type was such a strong factor in this initial ANOVA the data set was subdivided for further analysis into the benzoxazine resin composites and the GRAFCELL resin composite subgroups. Elimination of the GRAFCELL resin composite data from the analysis improves the comparison between the two benzoxazine resins. The results of all these ANOVA calculations are summarized in the following table.

Table 17: Summary of ANOVA Analyses on Growth Factor Results

Growth Factor	Graphite	PV 1	Resin	PV 2	PV 3
Length	G3S2P1T1E1	NSS	2H	L3	L1
Width	NSS	L3	2G	L3	L1
Landing	NSS	NSS	2G	L1	NSS
Border	NSS	NSS	NSS	NSS	NSS
NSS = Not Statistically Significant					

The treatment giving the smallest growth factor is indicated in the table for each of the dependent variables. The results of the analysis did not produce a single treatment that was favored for all the dependent variables. Nonetheless, the general trend indicates that the following combination of process variables will produce a composite with the lowest growth factors.

Table 18: ANOVA Results for Growth Factor Measurements of Molded Composites

Treatment	Value
Graphite	G3P1S2T1E1
Resin System	2G
Process Variable PV1	Level L3
Process Variable PV2	Level L3
Process Variable PV3	Level L1

The results indicate that both of the benzoxazine resins exhibit significantly less growth in length and width than the comparable GRAFCELL resin system for every treatment. The results for the growth factors in the length direction are statistically the same for the two benzoxazine resins. However, the growth factor difference in the width direction is statistically significant for the two benzoxazine resins. In both directions, the 2G resin exhibited less expansion than the 2H resin. The growth factors measured on the test plates made with the test dies, were supplied to Ballard Power Systems for tooling and MEA design and to Innovative Tool and Die, the die fabricator, for final plate manufacturing.

7.4.3 Resistance Measurements of Molded Flow Field Plates.

Measurements of the in-plane and through-plane resistance of the molded composite plates for the 2G and 2H resin system were made using a modification of the ASTM C611 method for graphite[10]. A minimum of five specimens were analyzed in each orientation for each treatment consisting of one combination of resin, graphite, PV1, PV2, and PV3. The total number of specimens analyzed was 180 for each orientation. Data was examined for outliers of which there were none. Statistical analysis was performed using Minitab Version 14.2. General Linear Model ANOVA and regression analysis were conducted with $\alpha = 0.05$; and $ß = 0.10$. Results for the t-test comparisons with the incumbent GRAFCELL FFP-300 material were not made since the data for this material was not available.

The GLM ANOVA was conducted using graphite, resin and process variables PV1, PV2 and PV3 as independent variables and the resistance values as dependent variables. The condition that resulted in the lowest resistance values for each of the dependent variables in both of the measurement orientations is indicated in the following table.

Table 19: ANOVA Results for Resistance Measurements of Molded Composites

Dependent Variable	In Plane	Through Plane
Graphite	G3P1S1T1E1	Not Significant
Resin	2H	2H
Process Variable 1	L2	L2
Process Variable 2	L1	Not Significant
Process Variable 3	Not Significant	L2, L3

The 2H resin shows a statistically significant advantage over the 2G resin; however, the contribution is weak compared to the other processing variables.

7.4.4 Physical Property Measurement Summary

The following table summarizes all the physical property measurements made on the molded and un-molded resin flexible graphite composite samples. Where available, measurements are compared to similar results for the incumbent GRAFCELL FFP-300 composite.

Table 20: Comparison of Physical Property for Resin Flexible Graphite Composites

Property	Method	Units	GRAFCELL FFP 300	2G Resin	2H Resin
Immersion Density	ASTM C1039	g/cm^3	N.M.	1.67	1.72
Bulk Density	ASTM C559	g/cm^3	1.68	1.68	1.72
Thermal Conductivity (x, y)	ASTM D5470 Mod	W/m-K	275	286	294
Thermal Conductivity (z)	ASTM C714	W/m-K	4.7	4.0	4.03
Thermal Diffusivity	ASTM C714	cm^2/s	0.039	0.033	0.033
Electrical Resistivity (x, y)	ASTM C611	µΩm	7.8	8.2	10.7
Electrical Resistivity (x, y)	GTI BP	µΩm	N.M.	10.0	9.0
Electrical Resistivity (z)	GTI BP	µΩm	N.M.	760.4	807
Contact Resistance	GTI BP	$\mu\Omega cm^2$	N.M.	5.1	6.04
Electrical Conductivity (x, y)	GTI BP	S/cm	1470.0	1002	1111
Electrical Conductivity (z)	GTI BP	S/cm	N.M.	13.6	13.23
Thermal Expansion Coefficient (x,y)	ASTM E1545	µm/m-K	1.3	1.0	0.98
Thermal Expansion Coefficient (z)	ASTM E1545	µm/m-K	97.2	81.8	74.1
Flexural Strength, -40 °C	ASTM D790	MPa	63.9	67.3	69.0
Flexural Strength, 23 °C	ASTM D790	MPa	57.5	58.7	61.8
Flexural Strength, 100 °C	ASTM D790	MPa	37.8	47.8	51.3
Flexural Strength, 120 °C	ASTM D790	MPa	N.M.	44.3	49.7
Tensile Strength, -40 °C	ASTM D638	MPa	41.9	41.3	44.6
Tensile Strength, 23 °C	ASTM D638	MPa	38.6	37.4	43.8
Tensile Strength, 100 °C	ASTM D638	MPa	29.2	32.8	36.4
Tensile Strength, 120 °C	ASTM D638	MPa	N.M.	32.6	37.4
Work of Fracture, -40 °C	ASTM D790	mJ	N.M.	20.6	20.6
Work of Fracture, 23 °C	ASTM D790	mJ	N.M.	19.5	17.6
Work of Fracture, 100 °C	ASTM D790	mJ	N.M.	16.9	14.8
Work of Fracture, 120 °C	ASTM D790	mJ	N.M.	15.6	15.2
Compressive Strength (x, y)	ASTM C695	MPa	29.8	48.0	N.M.

Property	Method	Units	GRAFCELL FFP 300	2G Resin	2H Resin
Compressive Strength (z)	**ASTM C695**	**MPa**	**58.6**	**89.8**	**N.M.**
Growth Factors, Length	**GTI BP**	**%**	**0.6**	**0.4**	**0.43**
Growth Factors, Width	**GTI BP**	**%**	**0.8**	**0.6**	**0.64**
Growth Factors, Thickness, Land	**GTI BP**	**%**	**N.M.**	**1.1**	**1.06**
Growth Factors, Thickness, Board	**GTI BP**	**%**	**N.M.**	**2.9**	**1.80**

N.M. – Not Measured

The new benzoxazine resin system composites have bulk densities, thermal conductivities, and thermal diffusivities which are similar to each other and comparable to similar measurements for GRAFCELL FFP-300 composites. Electrical resistance and thermal expansion measurements for the benzoxazine composites are also similar to each other, but lower than the comparable values for GRAFCELL FFP-300 composites. As discussed in the preceding sections strength, dimensional stability, and thermal stability of the new resin system are significantly improved over the incumbent composite.

7.5 Task 5: Single Cell Testing

7.5.1 Machined Plates for Single Cell Testing

The flow field plate design selected for use in single cell testing of the new graphite/resin composites and control plates was a simple serpentine design. This design was selected to make the plates compatible with the remaining cell hardware. A photograph of one of the machined plates is shown in the figure to the right. The machined composite bipolar plate served as the cathode in the single cell fuel cell and was paired with a standard machined synthetic graphite cell component as the anode. The active area of the machined plate was 50 cm^2. Coupons of the neat cured 2G and 2H resin samples (1" x 1") were also used for leachate analysis.

Figure 13: Machined Resin Expanded Graphite Composite Single Cell Flow Field Plate

7.5.2 Single Cell Testing Components

Extended durability membranes were supplied by 3M. These membranes had no special properties for high temperature operation and were used as supplied. They consisted of a 0.002" thick membrane with platinum catalyst based anode and cathode electrodes. ETEK 1500 gas diffusion layers were used in all single cell testing.

7.5.3 Single Cell Testing Protocol

Materials were washed and subjected to ultrasonic treatment in diluted 50:50 water/isopropanol solutions to clean them before and after each use. Hydrogen crossover was measured under hydrogen (anode) / nitrogen (cathode) conditions at a potential of 0.4V vs. the anode. The last 30 second current average of a 5 minute potential hold was used as the measured current. The crossover current under these conditions took approximately 1 minute to reach a steady-state.

Autolab Eco Chemie PGSTAT 302 potentiostats were used for all electrochemical testing. Fuel cell tests were carried out on Fuel Cell Technologies test stands for the coupon testing. A Precision Flow test stand was used for all 50 cm^2 testing. The Precision Flow test stand was incapable of high temperature humidifier operation, thus reducing the testing conditions to 24% relative humidity at 120 °C. Cells were conditioned at 80 °C and 100% relative humidity for 24 to 48 hours before being run under the high temperature conditions. Each cell was checked for less than 5% variability over a chosen sample period at 600 mA/cm^2 and 80 °C.

Co-flow operation was used for all fuel cell tests. Cells were shut down once daily for cell resistance and performance characterization while on the Precision Flow test stand and at high temperature. A half cell setup was used for high potential testing. A potential of 1.2V was applied during high potential testing. An expanded view of the cell setup for coupon and single cell testing is shown in the following figures.

Figure 14: Single cell expanded view showing cell components and dimensions used for 1000 hour testing protocol.

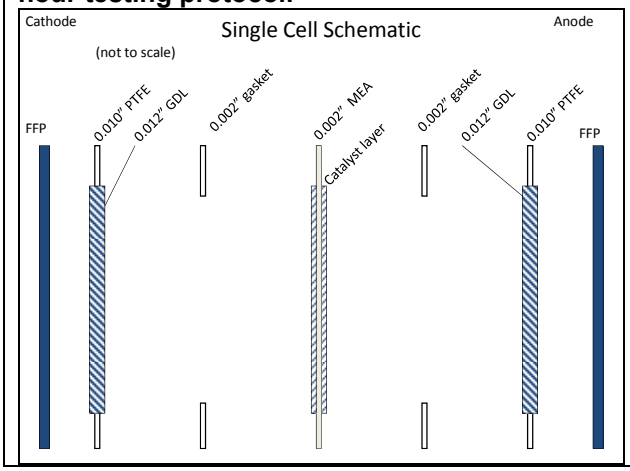

Figure 15: Half cell, half-MEA fixture diagram used for resin coupon testing.

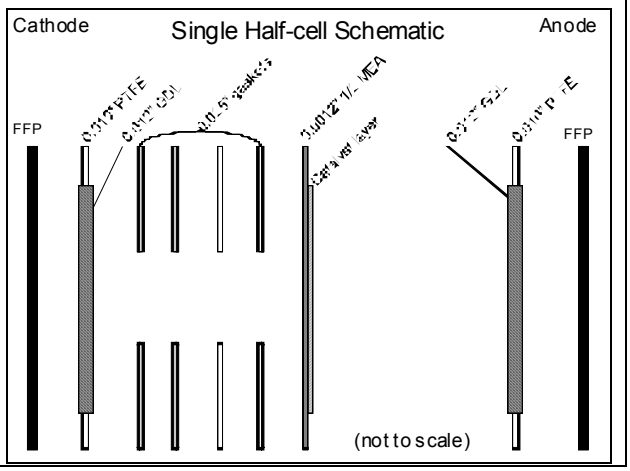

Resin composite testing was initially carried out on the coupons in fuel cell hardware. The resin coupon was sandwiched between the bipolar plate, with PTFE gaskets used to either isolate or center the coupon in the cell. Half MEA coupon experiments were conducted at 90 °C to slightly enhance possible thermal decomposition pathways versus operation at 80 °C, but were kept below 100 °C due to the complete lack of high temperature tolerance of the half MEAs. All components in direct contact with the plate and coupon materials were subjected to cleaning before and after individual tests.

7.5.4 Single Cell Test Results

The fuel cell polarization curves for the first cell tested (Cell 01), assembled with the 2G cathode plate are shown in the adjacent figure. Cells were set to operate in continuous voltage mode at 600mV vs. the anode reference hydrogen electrode (RHE) to better mimic operational requirements. The typical current draw at 600mV is below 100 mA/cm^2. As anticipated, cell performance at 120 °C is considerably worse than at 80 °C. There is approximately an order of magnitude reduction in current density versus ideal operation at 80 °C. This behavior is a consequence of the reduction in membrane

Figure 16: Fuel cell polarization curves for 2G Cell 01 cathode plate.

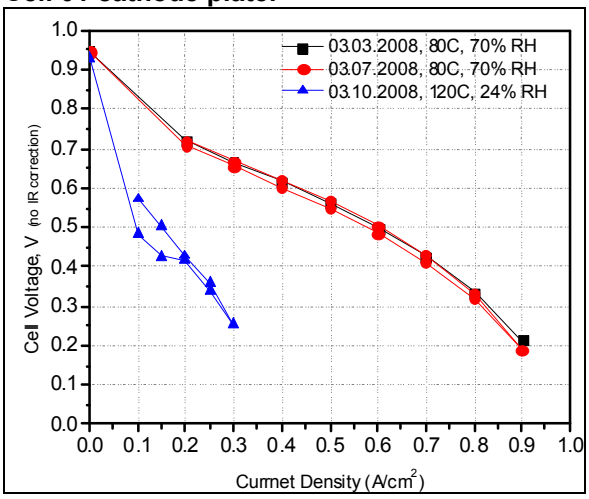

conductivity due to operation at lower relative humidity.

As a result of the harsh operating conditions, MEAs failed after approximately 100 hours of runtime at 120 °C. Consequently, a considerable portion of testing time was dedicated to breaking in and qualifying the cells before a short operational time at 120 °C. As is evident in the following figures, the cell resistance is shown to increase with time for each fresh cell.

Figure 17: Hydrogen crossover and cell high frequency resistance for all cells assembled with the 2G plates at 120 °C.

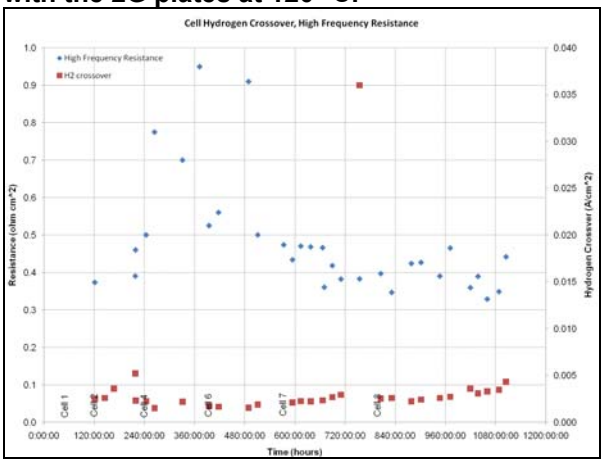

Figure 18: Potential and current density performance of cells assembled from the 2G plate over time.

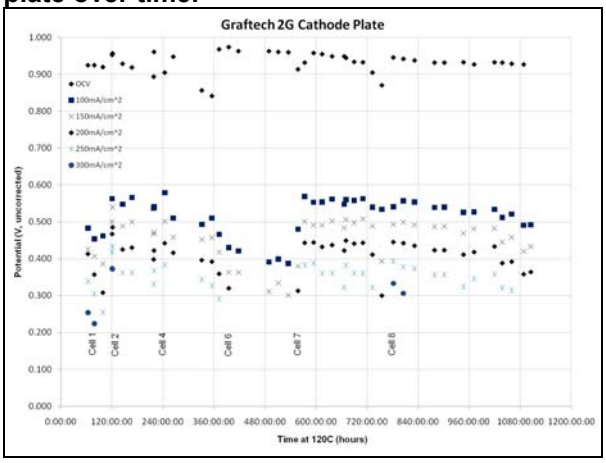

Hydrogen crossover increased over the lifespan of an individual MEA. As each individual cell aged a drop in the cell potential at a particular current density was observed, as well as a reduction in the maximum current density attainable by a particular cell. The maximum current drawn by an individual cell dropped with time as a function of the 1100 hour test of the 2G cathode plate at 120 °C. The open circuit potential of each cell dropped nearly linearly for most cells as a function of time.

Shutting cells down while maintaining inert gas flow can improve cell performance at 80 °C; however, the same is not the case at 120 °C. At 80 °C and operation with hydrogen / nitrogen (anode / cathode) gas flows, the membrane has time to return to equilibrium with the humidity of the incoming gas streams. At 120 °C, the cell shutdown is more damaging to the long term life of the membrane. Operation at 120 °C and low current densities produces water at the cathode that enhances the local membrane conductivity.

Due to the low current densities and high active cell area, the formation of localized hot spots that progress along the channel length of the cell with time is also a possibility. Sequential damage to the membrane would explain the gradual performance decay of each membrane and resultant performance loss. The co-flow operation mode of the cell exacerbates this problem. Upon disassembly, all of the MEAs used exhibited pinhole formation which is consistent with the drop in open circuit potential with time, and the increase in measured hydrogen crossover current with time.

The final test of the 2G plate was a potential hold at open circuit voltage (OCV) as an accelerated test to failure condition. Under normal fuel cell operating parameters, the potential at the cathode during startup and post-shutdown (if air infiltration of the anode is permitted while the cell is shutdown) is the open circuit potential of the operating cell, or higher[11]. The membrane performance and potential drop over the potential hold is shown in the following figure.

Figure 19: OCV potential hold for the 2G cathode plate

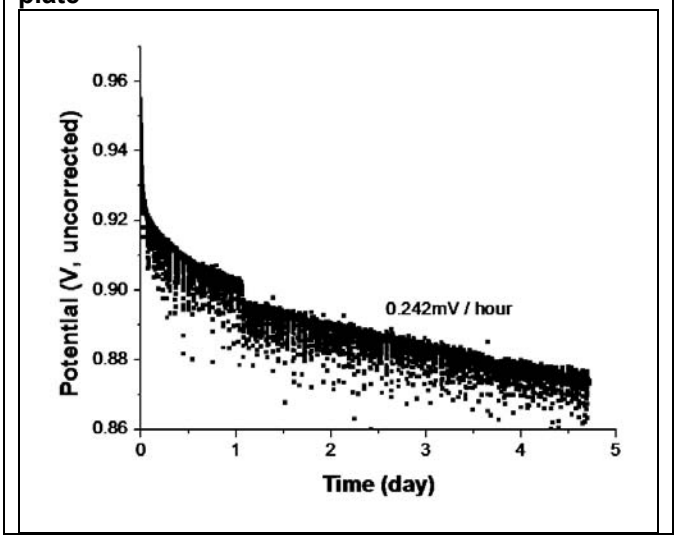

The cell exhibits a rapid loss in open circuit potential over the first few hours of operation before settling into a linear rate of decay over the next 3 days. A decay rate of 242mV/hour at open circuit was observed over days 2-4. It is unknown why a step transition occurs just past the 1 day mark, as the cell was running without interruption for the duration of the test.

Similar single cell testing was initiated for the 2H resin composite and over 200 hours of operation were completed with no evidence of plate degradation. Unfortunately, additional testing of the 2H plates was suspended due to consumption of the supply of MEA's. Additional MEAs could not be obtained in time and the decision was made to discontinue any additional single cell testing on the 2H resin system.

7.5.5 Single Cell Testing Effluent Analysis

The release of small amounts of organic material or inorganic ions into the fuel cell could have deleterious effects on performance. Ex-situ tests of bipolar plate materials in the form of 1" square cured neat resin coupons were used to develop a profile of possible organic and inorganic leachates. These test results were used in the post-test analysis of the plates and test effluents.

Analysis for organic leachates from the sample coupons used to develop the method was done by CWRU using resin system specific methods. An outline of the procedure is as follows.

- Three coupons of each resin expanded graphite composite were placed in a fuel cell single cell with flowing gases (air and/or hydrogen) and steam at 120 °C. The coupon rested in a cut-out in a Teflon gasket to seal and allow pressurization.
- In a second test, a similar configuration was used with a half-MEA added and a potential applied to the coupon.
- Background studies on effluent from the machined graphite blocks and gasket provided a contaminant baseline.

- Analysis of effluent solutions was carried out using liquid chromatography with mass spectral (LC-MS) detection.

A Hypersil C18 column (5µm, 120 A, 250mm x 4.6mm diameter) was used for all HPLC experiments. A Thermo Scientific Accela Pump and Autosampler were used in conjuction with a Thermo Scientific LCQ Fleet Mass Spectrometer for all HPLC-MS analysis. All samples had an injection volume of 5 µL, 125 µL/min flow rate. The flow program was 0-30minutes: 5-100% acetonitrile (ACN), balance water, 30-45 minutes, 100% ACN. The mass spectrometer was operated in negative polarity mode, over a range of 50-1000m/z. The NIST Chemistry Webbook was used to identify mass spectral data[12].

When liquid samples were collected, the first two samples of the collection phase were discarded. Collection of liquid samples from coupon testing was accomplished by diverting the high pressure exhaust of the fuel cell into a glass vial immersed in an ice water bath. Thus the collected coupon effluent consisted of liquid and condensed vapor portions of the fuel cell effluent. A collection time of 30 minutes resulted in 10-15mL of condensed liquid.

7.5.5.1 Coupon Testing

The supplied coupons were exposed to environments best representing fuel cell conditions encountered at 120 °C. The conditions judged most likely to lead to measurable degradation were:

1. Prolonged exposure to a reducing atmosphere.
2. Prolonged exposure to an oxidizing atmosphere.
3. High potential (1.2V) in the presence of pure oxygen.

Conditions were chosen to be exceedingly harsh on the composite plate materials. The test parameters were temperature, environment (oxidizing or reducing), and potential. Coupons were exposed to oxidizing (pure oxygen) and reducing (pure hydrogen) environments, to mimic conditions encountered at the cathode and anode, respectively. Hydrogen and oxygen were supplied at 100% relative humidity at both 80 °C and 120 °C. The cell fixture was operated at 0 atm backpressure at 80 °C, and 2.0 atm backpressure at 120 °C (the steam pressure at 120 °C). Though a low humidification level was expected in the final stack setup, gases were fed at 100% relative humidity to maximize liquid contact time with the coupons, as collected liquid was the means of assessing degradation products. Samples were collected approximately every 24 hours, except for the first hydrogen exposure test with the 2G coupon, which was extended. A summary of collected samples and conditions is presented in the following table.

Table 21: Summary of sampling intervals for coupon tests, and exposure conditions.

Test	2G			2H		
H_2	24hrs	48hrs	9d	24hrs	48hrs	72hrs
O_2	24	48	72	24	48	72
O_2 + 1.2V	24	48	72	-	-	-

For high potential testing, half of the cell was the coupon, and the other side was a standard fuel cell electrode in humidified oxygen. The cell diagram for half MEA experiments was shown previously. A carbon cloth was located between the graphite plate and the coupon. The coupon was in direct contact with the non-catalyst coated side of the half MEA (the “cathode”). The gasket fit around the coupon was not air-tight, to allow some flow of O_2 around the coupon. Gas flow rates for the half MEA experiment were 50 sccm O_2 (cathode), 50 sccm H_2 (anode), with the cell polarized to 1.2V versus the anode (RHE). Typical current under these conditions fluctuated between 25 and 35 mA/cm^2.

No physical change in the surface of the coupons was observed during any testing. However, the carbon cloth in contact with the coupon exhibited a change from hydrophobic to hydrophilic behavior with time at high potential. This change was observed by placing a water droplet on the carbon cloth after the experiment was completed. This behavior is consistent with carbon loss and direct oxidation of the carbon cloth. Half MEA electrodes were missing sections of the Pt/C catalyst which was observed once the cells were disassembled. These areas did not correspond to any visible changes in the surface of the coupon in contact with the half MEA. The primary mechanism for carbon loss from the electrode and carbon cloth was thought to be via the oxidation of carbon to carbon dioxide[13].

Figure 20: HPLC-MS spectrum of 2H coupon sample, post background subtraction

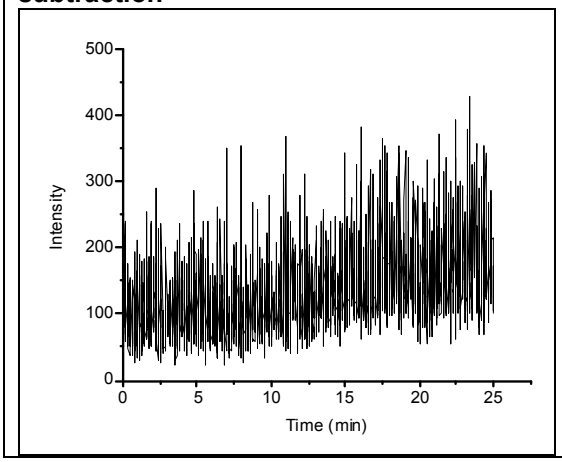

Shown to the left is a sample spectrum similar to that obtained for most coupon samples. The measured intensity is approximately 2 orders of magnitude below that seen in later HPLC-MS experiments. HPLC-MS was not an effective means of analyzing the liquid samples collected during the coupon tests. The signal intensity in this spectrum is very low, and noisy. Fuel cell effluent testing was based on Zhou’s thesis and some work using an HPLC with a UV Visible spectrometer as the detector by Wang[14,15].

The lack of existing literature on the topic of fuel cell effluent analysis led to the development of in house methods for the analysis of collected effluent. With no literature reference for expected fragment sizes, and with the intention of distinguishing between membrane and balance of plant components of the effluent, significant time was spent on exploratory HPLC-MS, with Wang's procedure as the only reference for a separation study that was able to identify degradation products from a membrane. Stability between samples was not always present. Samples were stored in the dark at room temperature for several weeks between collection and actual HPLC analysis.

7.5.5.2 Resin Degradation

Due to the lack of observable degradation products in the collected effluent from the coupon tests, and the unknown class of the resin during coupon effluent analysis, a number of chemical exposure and chemical attack methods were applied to a sample of the cured resin. Intentional degradation of a resin sample at high apparent concentrations was carried out to determine the properties of the resin, to understand how the resin would interact with the HPLC column, or in what form the degraded resin would be present in a liquid solution (if any). A summary of the solvents used and results of solvent exposure are present in the following table.

Table 22: Resin Exposure Conditions at 21 °C and Solvent-Resin Interaction Results

Solvent	Result	Solvent	Result
1M HF	wets	DMSO	swells
1M Na + 1M HF	wets	NMP	swells
0.5M H_2SO_4	wets	Chloroform	swells
1M KOH	wets	Methanol	does not wet

For the solvent-resin interactions described in the table, approximately 10 mg of a finely divided, shaved resin sample was stirred overnight with 10 mL of the chosen solvent. The DMSO solvent sample was also heated to 120 °C, but no apparent increase in the dissolution of the solid resin was observed. Strong organic solvents were seen to swell the resin sample, whereas the highly acidic and basic aqueous solvents simply wet the surface of the polymer. Addition of water to methanol was observed to wet the resin.

None of the solvents used dissolved the resin sample to any appreciable extent. A Fenton's reagent at a concentration of 100 mM was prepared to rapidly degrade the resin sample. The ordinarily dark brown resin dissolved vigorously in the presence of the Fenton's reagent and turned the liquid solution a dark orange-brown. After 24 hours at room temperature, no solid portion of the resin remained, but a yellow powder had settled to the bottom of the solution vial. A further 24 hours did not result in an increase in the amount of solids present. The dark orange liquid portion of the solution was filtered and diluted to 10 mM.

A further aliquot of hydrogen peroxide (H_2O_2) was added to the solution, and after a further 24 hours, a bright yellow powder had accumulated at the bottom of the vial, indicating that the initial resin sample was soluble in the solution, but not degraded entirely by the 100 mM Fenton's reagent. Further filtration and dilution of the 10 mM solution to 1 mM also resulted in a bright yellow settled powder after the addition of H_2O_2. Separate 1mM Fenton's solution containing the degraded resin became and remained (dissolving the precipitate) clear after the addition of sulfuric acid to a final concentration of 0.5 M. Addition of potassium hydroxide (KOH) to 0.5 M did not dissolve the precipitate.

The conclusion from the chemical exposure tests is that strongly acidic conditions in the presence of hydrogen peroxide and metal cations are needed to degrade the resin binder.

7.5.5.3 2G Composite Single Cell Test Effluent Analysis

Summary tables of collected mass spectral data along with identifiable compounds for the 2G resin sample are shown in Appendix L. A background sample of pure HPLC grade water (Fisher) was used as the reference against the effluent samples. Prior to each experiment, the HPLC column was continuously flushed, while the mass spectrometer was run in scan averaging mode for several column volumes. Fragments were detected exiting the HPLC column, but these fragments did not resolve into a peak. Nor were the detected fragments of any specific mass value. Components of the HPLC effluent exiting the column consist of the injected sample, the introduced solvents, and possible long retention time fragments strongly bound to the column medium.

None of the fragments common to the samples containing the Graftech plate samples were found in the coupon HPLC-MS results. The coupon testing effluent was indistinguishable from the background spectra. This would indicate the collected fluid was insufficiently concentrated in degradation products, or the onset of plate binder degradation does not occur over the time scale of the coupon tests. The flow field plate used for durability testing was run for substantially longer than any of the individual coupon tests.

Long chain fluorocarbons or group fragments containing sulfonic acid were not detected under the experimental conditions, but were expected in the effluent based on past investigations of membrane decomposition products[16]. Most identifiable compounds contained nitrogen in the form of -amines, -amides, or –azines, as well as large fragments containing silica side groups. The only identifiable compound found in multiple spectra was daniquidone ($C_{15}H_{11}N_3O$), in the 2G Cell 04 and 08 mass spectral data, after 240 and 1104 hours time at 120 °C. Approximately one half of the compounds present in the cell effluent samples were identifiable compounds, with the remainder described only empirically in Appendix L.

7.5.5.4 Single Cell Testing Effluent Analysis Conclusions

The resin impregnate used in the composite plates is a benzoxazine, formed from the reaction of amine, phenol, and formaldehyde[17]. In light of this information, and the unknown status of the side chains attached to the phenolic or amine groups, the presence of the amine group and any nitrogen containing side chain groups would be responsible for the observed nitrogen containing compounds to some extent. Some of the nitrogen containing compounds detected in the fuel cell effluent would appear too complex to be attributable to decomposition of a single benzoxazine monomer unit. However, the amine functional group is subject to attack by protonation under acidic conditions, resulting in the detachment at the amine group. Hydrogen adsorbs on the surface of graphite[18]. The stability of both the amine and phenol groups is dependent on the exact structure of the side groups.

Other sources of nitrogen within the system may have been the result of the acetonitrile mobile phase associating with membrane polymer or resin binder effluent products.

Though effluent samples were stored in PTFE containers, samples were transferred to glass vials for HPLC-MS analysis. No silicone based adhesives were used in the construction of the fuel cells, thus the observed silicon containing compounds are the result of interaction with sample vial side walls, or destructive reaction with the HPLC column substrate. There are many fragments of various atomic weights present in the HPLC-MS results that are not accounted for by background subtraction nor are the fragments part of the identifiable resin degradation products. Empirical formulas for the heavier fragments are tabulated based on elements present in the identifiable components of the mass spectra.

At the cathode, hydrogen is present as a crossover gas, and though the rate of hydrogen crossover is low under normal operating conditions, the long expected life of the stack may result in substantial degradation of the bipolar plate. The work presented here has used membranes that were unsuited to high temperature operation, and had abnormally high hydrogen crossover rates. The rate of hydrogen crossover was consistently increasing with time. Thus the test conditions were a worst case scenario for the resin plates, combining high temperature, low relative humidity, and high potential by operation as the cathode, and high hydrogen crossover. No suggestion is made as to the rate of degradation of the resin binder, as hydrogen present at the cathode can be consumed partially or fully in the cathode catalyst layer.

In a fuel cell stack designed for operation at 120 °C and with high temperature membranes, the rate of hydrogen crossover with, for example, polybenzImidazole (PBI) membranes can be comparable to the values obtained in this work, approximately 7.8 mA/cm^2 at 800 hours[19]. It is possible that the rate of decomposition of the resin binder is low enough within the fuel cell over the lifetime of the plate to limit concerns of resin degradation. Quantifying the rate of decomposition *in situ* over a long duration experiment is necessary to determine whether the 2G resin is sufficiently stable over the stack design life.

7.5.6 Single Cell Testing Teardown Observations

Photographs of the 2G cathode plates taken between MEA replacements are shown in the following figure. Visual examination did not reveal any indication of degradation or contamination of the composite after the more than 1120 hrs of operation at 120 °C.

In contrast, the 2H plate exhibited deformation around both of the gas inlets after 300 hours of runtime at 120 °C. As the transfer line temperatures were below that of the cell (90 °C vs. 120 °C), the deformation was not the result of plate erosion by the incoming gases. The other possible results of deformation are overly high compression, or local heating of the inlet leading to thermoplastic deformation of the plate, which is exacerbated by the co-flow operation of the cell. The gas crossover of the cell was measured over the lifetime of the cell, and increased throughout testing of the 2H plate. Additionally, the surface of the 2H plate exhibited large pores. The most likely explanation is that the 2H resin material began decomposing or off gassing, forming the

visible pores, and increasing the porosity of the plate. The 2G plate did not exhibit physical changes with time.

Figure 21: 2G Resin Composite Cathode Plate Photographs Between MEA Replacements

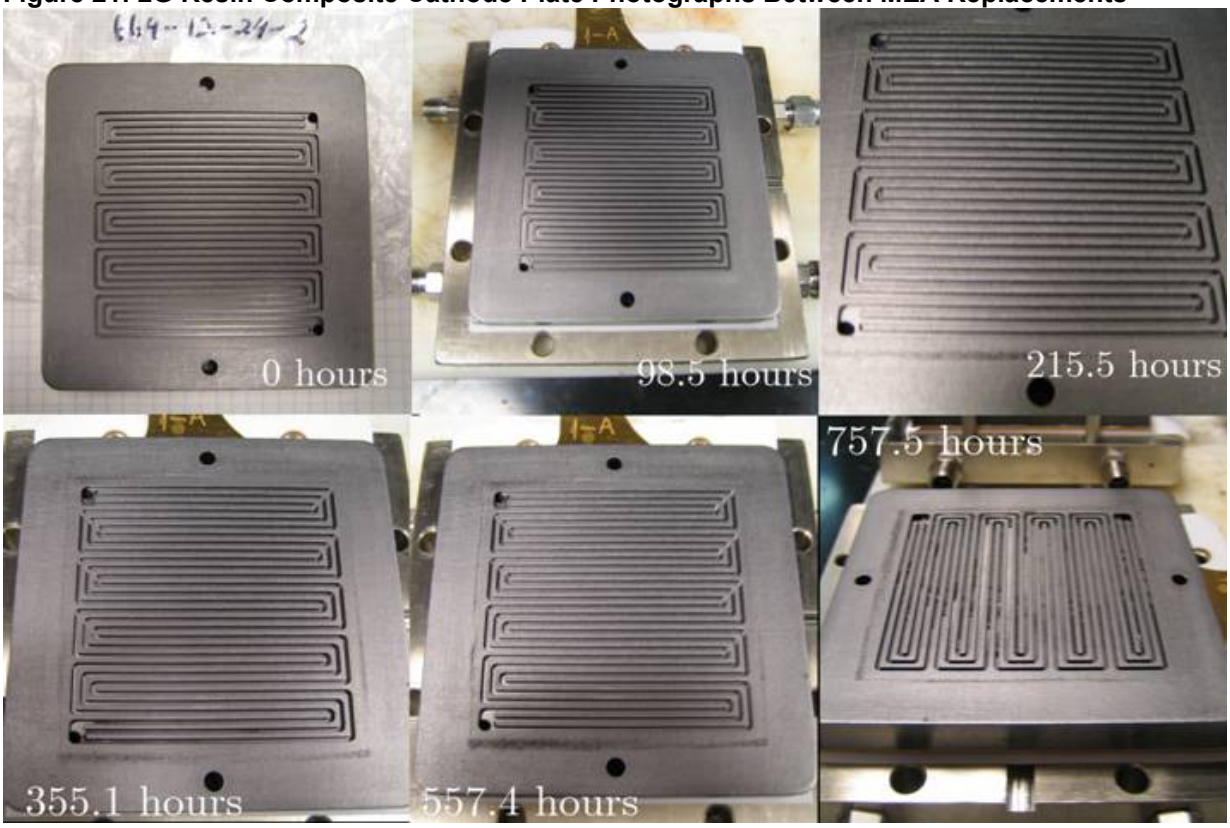

The end of life average hydrogen crossover for all cells using the supplied MEAs was 11.3mA/cm^2. The expected hydrogen crossover for Nafion 112 is 2.1 mA/cm^2 at 120 °C and 25% relative humidity[20]. The low initial conductivity and high hydrogen crossover of the membranes is not unexpected, due to the low relative humidity of the incoming gases. Water is required to transport protons in Nafion-type membranes, and with low relative humidity comes poor conductivity. The low operating current density of the 50 cm^2 cells was insufficient for complete wetting of the membrane. Additionally, the membrane was not specifically engineered to encourage water retention. The stable phase of water at 120 °C is as a gas, which precludes the full hydration of the membrane.

7.6 Task 6: Design and Manufacture Full-size Bipolar Plates

7.6.1 Selection of Final Starting Materials

Prior to initiation of the fabrication of the final full size plates, a meeting was held to review all available data on resin performance. At this review the final selection of graphite and resin for full sized plate fabrication was made. The following table summarizes the selection criteria that were considered in the decision process.

Table 23: Summary of Composite Testing Results

Property	Preferred Graphite	Preferred Resin
Thermal Properties	No preference	Benzoxazine
Mechanical Properties	No preference	Benzoxazine
Resistance In-Plane	G3P1S1T1E1	2H Benzoxazine
Resistance Through-Plane	No preference	2H Benzoxazine
Nitrogen Permeability	G1P2S1T1E1	2G Benzoxazine
Growth Factor Analysis	G3P1S1T1E1	2G Benzoxazine
Coolant Compatibility	No preference	2G Benzoxazine
Preliminary Leachate Analysis	No preference	2G Benzoxazine
Single Cell Testing	No preference	2G Benzoxazine
Environmental Cycling	No preference	No preference

The 2G benzoxazine resin system clearly demonstrated better performance than the 2H resin composite and was selected for final plate fabrication. The selection of graphite mat was less obvious since the results for most of the criteria were statistically inconclusive. Both the G1 and G3 graphites were preferred for at least one of the criteria. The final decision was made in favor of the G3P1S1T1E1 graphite based on the fact that this material is a purified grade and was readily available in inventory. Use of a purified starting graphite material minimized the presence of contaminates which could potentially leach out of the plates during fuel cell operation and poison the MEA catalysts.

7.6.2 Selection Molding Press for Use in Fabricating Full-Size Bipolar Plates

Calibration and certification of the GrafTech AFGF molding press, was performed prior to pressing of the final full sized plates. The press flatness characteristics were more than adequate for the plate tolerance specifications. Based on the results, Ballard approved use of the press for final plate fabrication. Use of the GrafTech AFGF equipment significantly improved the project scheduling and product quality by reducing the number of hand-offs between GrafTech and Ballard during the plate fabrication process.

7.6.3 Alternative Methods of Plate Formation

During the course of the program two alternative methods of plate formation; roller embossing and high-speed adiabatic forming were considered for use, but due to the time constraints of the program, not evaluated in final part fabrication.

Roller embossing technology had been evaluated in a joint development effort between Ballard and GrafTech previously. This technology shows promise for application to fuel cell bipolar plate formation which will significantly decrease embossing rates over static pressing, but the method is in need of significant additional development work which was outside the scope of this program[21].

High speed adiabatic forming as practiced by Cellimpact AG is another high speed manufacturing technique which could potentially result in additional manufacturing cost reductions over roller embossing and static pressing. In an effort to evaluate the viability of this methodology for future work, samples of the program's resin-impregnated flexible graphite mat were sent to Cellimpact for embossing studies with their process. These initial samples of uncured plates showed excellent feature definition with little to no evidence of blistering. Based on these results, an additional set of samples with optimized forming properties were selected and sent to Cellimpact for further evaluation. Results on these samples were also positive and additional work is planned under alternative funding.

The positive results obtained with both of these forming technology justified their inclusion into the cost estimates of future bipolar plate production conducted by Directed Technologies Inc. as part of Task 8.

7.6.4 Selection of Flow Field Plate Architecture

Ballard selected a flow field plate design based on a modification of a plate from a previous design for use in the final full-size plate production. The modified plate design had a plate assembly thickness below 1.6 mm and a plate area greater than 250 cm². The chosen design incorporated known design features to aid in part formation during processing. The plate dimensions met the program requirements and were a size suitable for use in the GrafTech AFGF press.

7.6.5 Full Size Embossing Die Set Fabrication

The final full scale flow field plate design was reviewed and approved by both Ballard and GrafTech. The final plate design is considered business confidential by Ballard and details of the design will not be presented here. The growth factors measured by GrafTech on the test tools were supplied to Ballard Power Systems for tooling and MEA design and to Innovative Tool and Die, the die fabricator, for final plate manufacturing.

7.6.6 Final Graphite Mat Manufacture

The G3P1S1T1E1 graphite mat for use in final plate fabrication was manufactured in the GrafTech AFGF in early July of 2008. Approximately 300 mats were produced. Specification testing of the production lot was conducted and the found to be within current limits.

7.6.7 Manufacture of Final Resin for Full Size Plate Impregnation

Manufacture of the 2G resin for test tool and full size plate production was completed by Huntsman and received by GrafTech in June of 2008.

7.6.8 Embossing of Full-Size Bipolar Plates

Approximately 60 of each of the fuel and oxidant plates were pressed using the selected graphite mat and resin. All of the plates appeared to be flawless based on a cursory visual inspection. Measured gas leak rates on individual plates were below, or near, the detection limits of the measurement equipment. Samples of the cured individual plates were sent to Ballard for dimensional verification. All were within the target thickness value of <0.8 mm and had length and width measurements within Ballard's specifications. Checks of growth factors on the cured plates were consistent with previous measurements. Additionally, the plates for both the anode and cathode end-plate assemblies were pressed, cured, and machined. Four sets of each assembly were fabricated.

7.6.9 Post Production Sealing of Bipolar Plates

As a precautionary measure, post curing impregnation with a sealing resin was performed on all the fuel and oxidant plates to insure gas impermeability. The average sealing resin pick-up was measured to be approximately 2%, a value which is consistent with plates that are low in porosity and have low leak rates.

7.7 Task 7: Short Stack Test of Full-Size Plates

7.7.1 Plate Gluing and Pressure Drop Testing

In a change from the original project plan, GrafTech was responsible for gluing the individual flow field plates to form the bipolar plate. The gluing technology needed to perform this process was obtained via a technology transfer agreement between GrafTech and Ballard. Ballard provided a sufficient quantity of their proprietary glue system for final plate gluing.

New glue dispensing equipment was purchased and installed in a GrafTech Parma R&D pilot plant module equipped with independent temperature and humidity controls needed to insure reproducible dispensing and curing of glue joints. Operational training and start-up of the new gluing equipment was completed and the unit was used to glue the anode and cathode plates pressed during Task 6. All the glued assemblies were successfully cured.

Fabrication of the leak check apparatus was completed by GrafTech in Parma. Leak checking of the glued and cured bipolar plate assemblies and end plate assemblies was performed using this device. With the exception of a few assemblies, leak rates on the final glued and cured assemblies were very low or not detectable. The leak testing results were used to rank the bipolar plate assemblies prior to shipment to Ballard for final stack assembly.

7.7.2 MEA Fabrication

Design and fabrication of the MEAs to be used in final stack testing was completed by Ballard. The hardware for the final stack assembly was obtained by Ballard.

7.7.3 Full Size Stack Assembly and Leak Checking

GrafTech delivered the first plate assemblies to Ballard and they passed preliminary dimensional inspection related to stack integration with MEA and stack hardware components. The plates were successfully assembled into a 10-cell stack that met leak check criteria enabling fuel cell testing to begin. A photograph of a 5 cell assembled stack is shown in the following figure.

Figure 22: Assembled 5-Cell Stack Prior to Testing at Ballard

7.7.4 High Temperature Stack Testing Initial 1000 Hours

Testing of the 10-cell stack began with operational characterization to allow monitoring of stack and cell performance over the test period. Characterization included overall stack performance at various load conditions and pressure drop analysis. As part of the initial diagnostics two issues were identified. A cell was not performing well and was replaced. Additionally, hot operation attempts to a 120ºC coolant outlet temperature revealed several cells were not able to meet minimum cell performance.

Investigation into the cause of the initial operational problems revealed that lower than anticipated cell performance was not related to the bipolar plate material but rather to a combination of MEA temperature limitations, and non-optimal operating conditions within the cells. To address potential MEA temperature limitations the decision was made to limit stack operation temperature to a maximum of 95°C until 500 hours of operation were achieved and sufficient baseline performance established.

7.7.5 High Temperature Stack Testing Final Results

In June of 2009, the 10-cell stack began operational characterization to allow monitoring of stack and cell performance over the test period. Characterization included overall stack performance at various load conditions and pressure drop analysis. The duty cycle was developed to simulate automotive drive cycle conditions including high temperature excursions.

The stack was operated on a dynamic test station with automated macro control of operational conditions. General stack operations were monitored continuously and weekly diagnostics were performed to characterize changes in stack and cell performance. The duty cycle used to test the stack simulated automotive drive cycle conditions including the high temperature excursions. Duty cycle coolant temperature range was 65ºC to 75ºC with the high temperature excursion capped at 95ºC. At the completion of the 500 hour baseline testing, higher temperature operation was initiated with a target stack coolant outlet temperature of 110ºC to 115ºC. The renewed efforts to run at the high temperature conditions were hindered by a seal failure requiring the stack to be taken off test. Fortunately, the seal was fixed without having to replace any MEAs and the stack was successfully reassembled and returned to test. Operation continued under these conditions until completion.

The following table provides a simplified chronological summary of key operational hours at different times.

Table 24: Functional Baseline Tests

Event start	Event	Conditioning hours	Diagnostics and FBT hours	Duty cycle Coolant Inlet 65ºC Max coolant cycle temp≤95ºC hours	Steady State Coolant Inlet ≥100ºC hours	Total Hours with load on Stack hours
June 5th	Stack conditioning	75				72
	Stack Diagnostics +FBT		88			163
	Duty cycle operation ≤95ºC		5	447		615
July 28th	Stack Diagnostics +FBT		20			635
Aug 4th	Duty cycle operation ≤95ºC		3	130		768
Aug 14th	Hot operation Coolant Inlet ≥100ºC				9	777
	Duty cycle operation ≤95ºC			11		788
	Stack conditioning	17				805
	Hot operation Coolant Inlet ≥100ºC				63	868
Aug 21st	Stack conditioning	66				934
Aug 24th	Hot operation Coolant Inlet ≥100ºC		2		47	981
Aug 26th	End of Test (totals)	158	118	588	119	983

Stack configuration consisted of stack hardware, two interface plates, 9 glued plate assemblies and 10 MEAs. An air bladder controlled stack compression load. Test station coolant was 100% ethylene glycol required for operation up to 120ºC. Stack polarization data is shown in the following figure at the beginning of duty cycle testing.

Figure 23: Full Size Stack Testing - Beginning of Duty Cycle Test

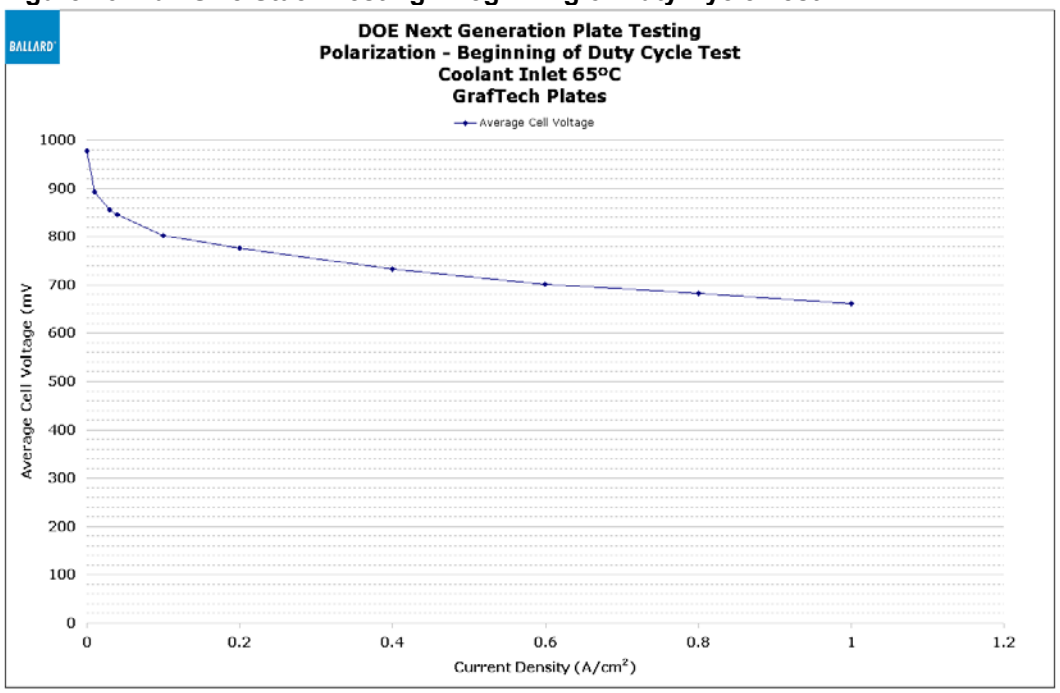

The degradation rate for the duty cycle operational conditions is charted in the following figure including the first portion of operation with coolant inlet temperature greater than 100ºC. The average cell degradation rate was 26μV/hour.

Figure 24: Full Size Stack Testing - Drive Cycle Test Performance Tracking

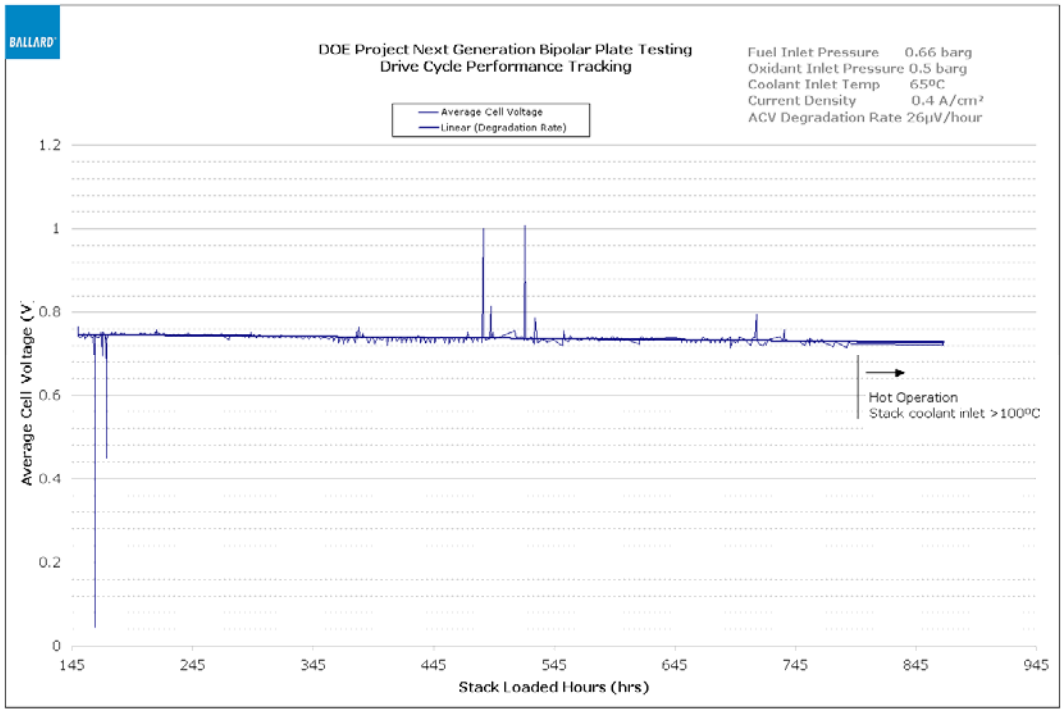

The hot operation with coolant inlet temperature greater than 100ºC resulted in a significant change in operational conditions. A required change was an increase to the stack bladder pressure to account for the increased internal gas pressures specified by the operation conditions. Stack bladder pressure was increased from 30 psig to 40 psig.

Operation with coolant inlet temperatures greater than 100ºC was done initially in intervals of 4 hours followed by two larger continuous runs of 55 hours and 45 hours. The cell performance was seen to drop quickly in the last 45 hours of operation. Under hot operation, average stack coolant outlet temperature was about 115ºC. Stack coolant pressure drop over the hot operation test time remained stable.

At completion, the stack had been operated successfully for over 980 total loaded hours which included conditioning, steady state, duty cycle and steady state hot operation hours with coolant inlet greater than 100ºC. Stack operation was terminated just short of 1000 hours due to a large internal fuel to air transfers.

7.7.6 Freeze Thaw Stack Testing

A separate 5-cell stack for freeze/thaw testing was assembled by Ballard using additional bipolar plates supplied by GrafTech. The 5-cell configuration consisted of 2 interface plates and 4 plate assemblies with 5 MEAs. The test focused on monitoring coolant pressure drop. The coolant channels and coolant fluid flow are isolated from the MEA. Therefore, the coolant pressure drop is a good metric to evaluate mechanical changes to the plate assemblies in a stack configuration, since it is largely independent of MEA mechanical changes. A large permanent increase in coolant pressure drop may be an indication of plate material change associated with the temperature exposure. Coolant pressure drop was measured using dry room temperature air connected to a mass flow meter with the stack at room temperature.

The stack was placed in a freezer set to –40ºC with thermocouples attached to monitor the actual stack temperature. The test period began once the stack temperature reached –40ºC. The stack was exposed to –40ºC for 48 hours not including the cooling or thawing phases. The stack was allowed to return to room temperature and the stack coolant pressure drop retested. The results showed no significant change in stack coolant pressure drop.

Additional high temperature testing was performed using the same 5-cell stack. The stack was exposed to temperatures of 95ºC, 110ºC and 120ºC incrementally for 1 hour at each temperature. The stack coolant pressure drop was measured after each 1 hour temperature exposure once the stack had returned to room temperature. The incremental temperature exposures were included to capture possible intermediate mechanical changes versus temperature before proceeding with a longer exposure at 120ºC. The results showed no significant change to stack coolant pressure drop at any of the temperatures tested.

The stack was then placed back into the environmental chamber set at 120ºC for a period of 100 hours to extend the exposure time to further evaluate high temperature plate robustness. After the exposure time and once the stack had returned to room temperature, the stack coolant pressure drop was measured. No significant change to stack coolant pressure drop was observed.

7.7.7 Post-Test Analysis of Parts and Performance

7.7.7.1 Water Analysis

Water effluent analysis was completed for water samples collected during the periods of duty cycle testing. The anode and cathode effluent water was collected at intervals corresponding to stack loaded hours of 70 hours, 500 hours and 750 hours. An external lab performed trace metals analysis and semi-volatiles analysis on the effluent samples. Water analysis of a 34 elements profile showed all values below 1 mg/L per element. The elements with the highest detected levels were silicon (0.93 mg/L) and sulfur (0.7 mg/L) in the 500 hour cathode effluent sample. Since neither element is present in the bipolar plate composite at a detectable level, the source of these potential contaminates must be due to other stack components. Additionally, the concentration measured for these metals are lower than any levels believed to be detrimental to fuel cell operation.

Semi-volatile analysis of the effluent showed levels of N-butyl-benzenesulfonamide (CAS 3622-84-2) of 11.6 µg/L at 500 hours and 7.54 µg/L at 750 hours in the cathode effluent water. Dibutyl phthalate (CAS 84-74-2) was detected at a level of µg/L 9.64 in the 70 hour effluent sample; but, was not detected in later stack operation. These detected levels of organics were significantly lower than any levels believed to be detrimental to fuel cell operation. Cyclosiloxanes were also found at all 3 test times. A likely source of this contaminant is the seal polymer used in stack assemble.

7.7.7.2 Stack Leak Rate

The stack leak rates of interest are coolant to fuel and coolant to air. The leak rates are determined by pressurizing the coolant fluid stream and measuring collected air passing into the fuel and air streams respectively. Each fluid stream is tested separately. This is a common measurement method for the leak-rate though the plate material in a stack configuration.

Dry air set at 0.5 bar-gage pressure was used to pressurize the coolant fluid stream. The stack was allowed to stabilize for 5 minutes before the leak rate was measured. Measurement was done by collecting any air passing into the fluid stream (air or fuel) using a graduated cylinder. The collection time is noted in the summary table.

Table 25: Full Size Stack Leak Rate Testing Summary

Leak Rate Beginning of Test (after cell 6 replacement)		**Leak Rate End of Test**	
Coolant to Fuel:	2.8 cc/min	Coolant to Fuel:	0.2 cc/min (in 5 min)
Coolant to Air:	0 bubbles (in 2 min)	Coolant to Air:	0.4 cc/min (in 5 min)

7.7.7.3 Plate Assembly Thickness Comparison

Prior to stack operation all plate assemblies were tested using a thickness under compression test to measure plate assembly thickness. Five data points along the length of the plate active area were measured. The average of these five data points is the average plate assembly thickness. The same test was repeated after completion of stack testing. Thickness measurements unfortunately were not made in the exact same locations and introduce a source of error.

The difference in average plate assembly thickness before and after stack operation were collected and compared. All differences were less than or equal to 4 μm and 7 of 9 plate assemblies were less than or equal to 2 μm. The differences are within measurement error. Additionally, there was no trend from inlet to outlet associated with operational temperature.

7.7.7.4 Plate Visual Observations after Completion of Stack Testing

The 10-cell stack was disassembled and the plates were visually inspected. Inspection of the active area and transition area showed no visual signs of change.

Some minor plate material deformation was observed in a localized area of the seal groove near the ports. This deformation appeared on some but not all plate assemblies and was usually on, but was not limited to, the fuel plate side. Material deformation was more pronounced on the transition plates in the same area. Preliminary indications suggested localized improper mechanical support between the plate assemblies where the seal force exerts pressure on the plate. The area is parallel to the plate assembly glue joint. The seal load is on or adjacent to the glue joint in this area.

Samples of these plate sections were taken and prepared for optical microscopy analysis by the GrafTech microscopy laboratory. The results of the analysis indicated that deformation in these regions was due to a reduction in plate thickness near the outside of the assembly. This change is postulated to have reduced the compressive and/or flexural strength of the plate edge and resulted in compressive failure of the plate edges. The failed regions were only observed in single localized sections of two of the bipolar plate assemblies. These failed regions represent less then a fraction of a percent of the total stack area.

7.7.8 Deliver Full Size Plate Stack to DoE

Ballard assembled and shipped an additional 10-cell stack for evaluation by a group at Argonne National Laboratory (ANL) which was selected by the DoE to perform independent verification of bipolar plate performance. As of the completion of this report the stack was on the Argonne test stand and testing was scheduled to begin using a low temperature drive cycle for long term stability testing.

7.8 Task 8: Economic Assessment of New Technologies

To ensure consistency with previous bipolar plate manufacturing cost estimates, the DoE requested that the manufacturing cost estimates for the GRAFCELL process be calculated using a methodology employed by Directed Technologies Inc. (DTI). The analysis was performed by DTI and the results are shown in the following sections.

The "Best Case Scenario" section represents the final conclusion of the analysis. This estimate for the cost of resin impregnated flexible graphite systems is based on projections to high volumes with assumptions about implementation of process improvements which have not yet been demonstrated, but have a high probability of success. The final result of this analysis for the high volume manufacturing scenario ($6.85 /kW) is above the DoE target of $3 to $5/kW. However, the result is close enough, and the error of the estimate high enough, to justify continued development by GrafTech of the manufacturing technology required to ultimately meet the DoE transportation cost target.

7.8.1 Best Case Scenario

The results summarized below represent the "best case scenario" where all of the low cost parameters identified by the Monte Carlo analysis are adopted (with the exception of labor rate). The following tables list these "best case" parameters. A cost of $6.85/kWnet is achievable under these conditions.

Table 26: Best Case Scenario Cost – 500k Systems/year

Best Case Low Cost Scenario High Speed Forming 500K Systems/year		
Material	**$/kW$_{net}$**	$2.85
Manufacturing	**$/kW$_{net}$**	$3.91
Tooling	**$/kW$_{net}$**	$0.12
Total Annual Cost	**$/kW$_{net}$**	$6.85

Table 27: Best Case Scenario Parameters

Solvent-less System (500k/year)			
Parameter	**Unit**	**Minimum Cost**	**Rationale**
Line Speed - Resin Impreg	**m/s**	0.0508	10ft/min is projected as the maximum attainable speed under any conditions.
Capital Cost - Resin Impreg	**$**	$6,100,000	Projected Lowest attainable Capital Cost for Resin Impreg System
Resin Cost	**$/kg**	$5.43	Projected lowest possible resin price
Graphite Cost	**$/kg**	$5.51	Graftech best case possible
Labor Rate	**$/hr**	$21.50	Current Graftech fully burdened labor rate

Note that this is a domestic best-case scenario and does not include the foreign labor rate used in the sensitivity analyses. Were this rate used there would be an additional $0.17 in savings

In the following sections the details of the DTI cost analysis are presented.

7.8.2 Cost Analysis of GrafTech Advanced Graphite Bipolar Plate Manufacturing by Directed Technologies Inc. (DTI)

7.8.2.1 Introduction

Directed Technologies Inc. (DTI) has examined three variants of a GrafTech specified bipolar plate manufacturing process to assess the expected plate cost at various annual manufacturing rates. The cost analysis is based on a Design for Manufacturing and Assembly (DFMA) methodology and draws heavily on the previous work done by DTI on PEM fuel cell system cost estimation for the US Department of Energy. Manufacturing process parameters and cost analysis assumptions are based primarily on GrafTech supplied values, but are augmented by DTI based on their engineering judgment and data base of similar procedures. To the extent possible, assumptions were consistent with those used by DTI's cost estimate project for the DoE[22] so that the GrafTech bipolar plate estimates can be directly compared to other DoE funded manufacturing approaches.

7.8.2.2 Bipolar Plate Manufacturing Processes

Figures 25 through 27 schematically detail the bipolar plate manufacturing steps modeled in the cost analysis. Three manufacturing processes are defined and can be chiefly described by how the flow field is imparted onto the graphite plate. Thus the three manufacturing process trains are denoted as:

1. Compression Molding,
2. Embossing,
3. Stamping.

Each process train represents an incremental advance in technology.

While each process train can be conducted over a range of annual production rates, for this analysis the processes are labeled as 10k stacks/year, 100k stacks/year, and 500k stacks per year to approximately match the advances in technology with the expected increase in manufacturing rate with time. Consequently, cost results were generated for Compression Molding at 10k stacks per year, Embossing at 100k stacks per year, and Stamping at 500k stacks per year.

Figure 25: Compression Molding Production Flow Diagram

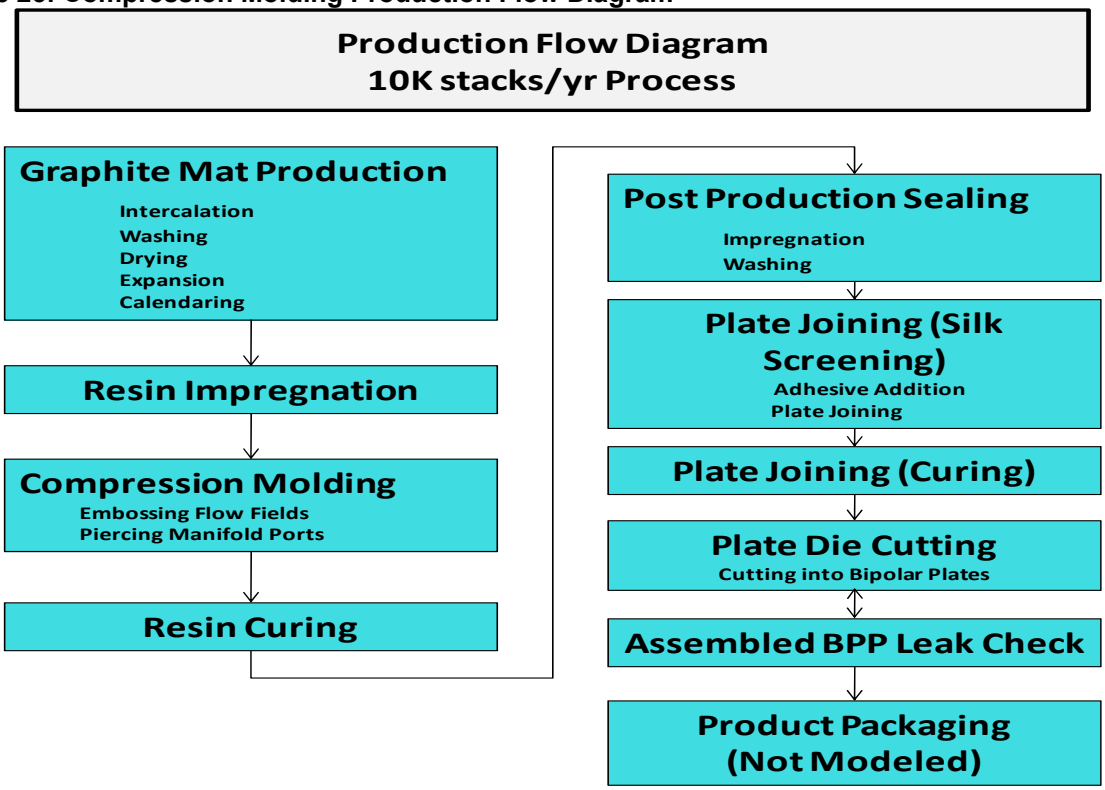

Figure 26: Embossing Production Flow Diagram

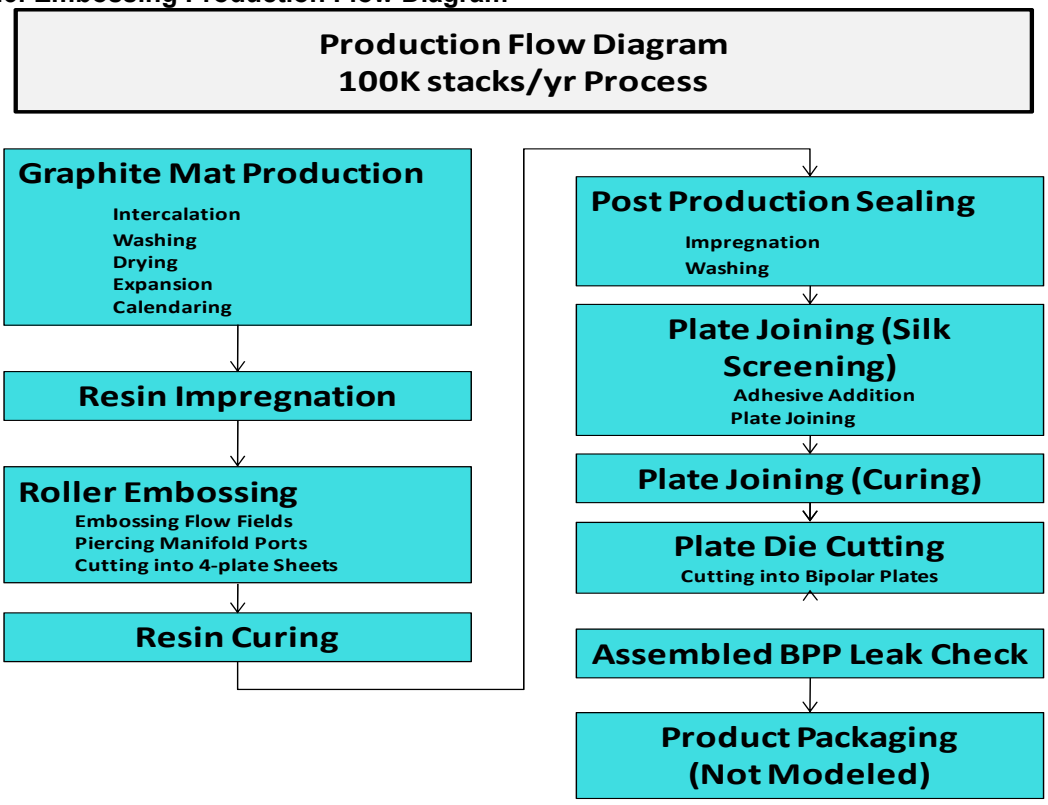

Figure 27: Stamping Production Flow

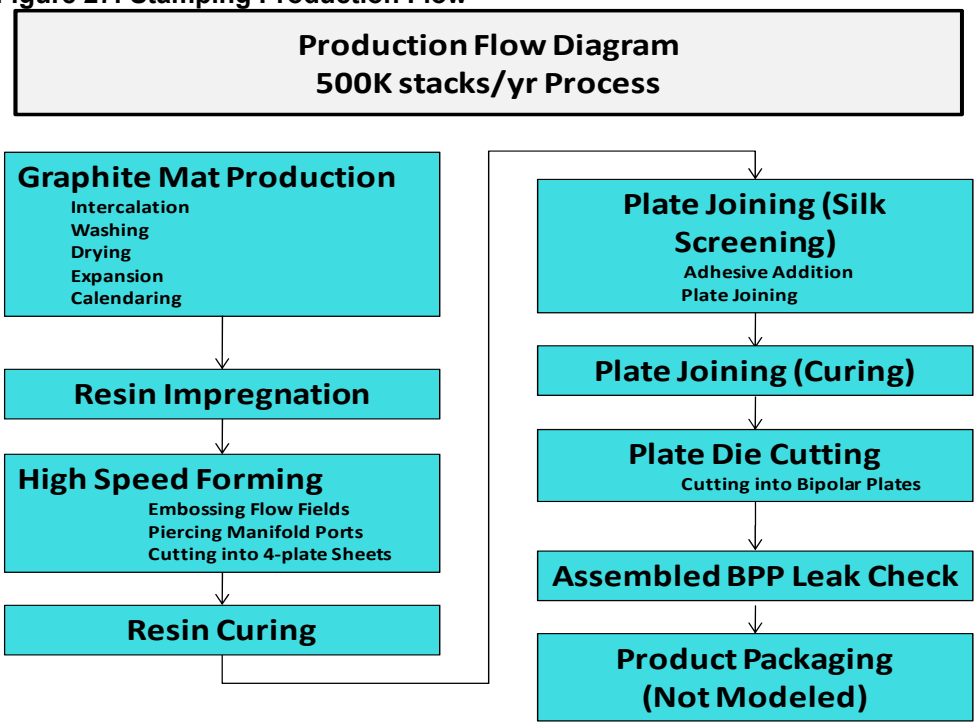

7.8.3 Study Assumptions

7.8.3.1 Stack and Standard Machinery Assumptions

In order to create an accurate comparison with similar fuel cell systems analyzed previously for the DoE by DTI, some of the GrafTech supplied assumptions for both stack performance and standard machinery parameters were altered. The updated assumptions used in the cost analysis are shown in the following tables.

Table 28: Basic Stack and Bipolar Plate Assumptions

Dimensions		
Width	cm	15.5
Length	cm	58.4
Thickness	cm	0.08
Power Density	mW/cm^2	833
Number of BPP	BPP/system	150
Power per Plate	kW_{net}/BPP	0.53
	kW_{gross}/BPP	0.60
Stack Power		
Gross	kW	90.2
Net	kW	80
Assumed Active to Total Area Ratio*		0.8

*Ratio of membrane area to total BPP area.

Table 29: Standard Machinery Parameters

Interest Rate	10%
Corporate Income Tax Rate	40%
Capital Recovery Factor* (% of capital cost)	20.5%
Equipment Installation Factor	1.4
Maintenance/Spare Parts (% of capital cost)	10%
Miscellaneous Expenses (% of capital cost)	12%
Labor Rate	$22.5/hr
Equipment Lifetime	10 years

*The capital recovery factor is effectively a loan payment percentage. It is defined as the percentage of equipment/system capital cost that must be paid every year to cumulatively payback the capital plus interest charges.

This analysis and the corresponding spreadsheets use several different phrases to describe the various stages of sheet formation. A sheet refers to a ~60 cm by ~60 cm sheet of graphite/resin composite that contains four contiguous plates. When two of these plate sheets are stacked, adhesively bonded together, and subsequently cut, they generate four bipolar plates (BPP). A BPP is the repeat unit within the fuel cell stack and functionally serves as an anode plate, cathode plate, and channels for coolant flow in the region between the plates.

7.8.3.2 Manufacturing Assumptions

The primary manufacturing parameters for each of the different stages of plate production are considered to be business confidential by GrafTech and are not reproduced here. Organizations or individuals wishing to review the details of these cost estimate parameters will need to submit a formal request with the GrafTech Legal Department. The values used in DTI's calculations are primarily based on data provided by GrafTech but have been augmented by DTI assumptions.

7.8.3.3 Resin Impregnation

While titled "resin impregnation", this step actually encompasses the entire conversion of raw flake graphite into approximately 60 cm wide by 0.8 mm thick sheets of resin impregnated graphite mat. The capital cost and other key processing parameters are based on GrafTech's Advanced Flexible Graphite Facility (AFGF) but are modified to reflect a lengthened vacuum chamber (2 times in length), operating at twice the line speed, and costing 1.5 times the base facility capital cost.

The resin is the proprietary high temperature 2G benzoxazine resin developed as part of this program as a replacement for the standard lower temperature FFP-300 resin typically used by GrafTech. Further, the 2G resin used with the Compression Molding plate forming method is solvent-based resin whereas the resin used in the Roller Embossing and High Speed Stamping forming methods is postulated as a future solvent-less version of the 2G resin. Capital cost of the resin impregnation line is reduced when the solvent-less resin is used as a result of the elimination of the solvent recovery system. Material costs are based on volume pricing. Note that at 500,000 systems per year, 29 parallel processing lines are required.

When followed by compression molding, the resin impregnation step is assumed to include cutting the mat into 4-plate sheets (ie. approximately 60 cm x 60 cm). However, when followed by roller embossing or high speed stamping, the resin impregnation step is assumed to supply a continuous graphite sheet (i.e. 60 cm wide by ~1500 m long coil on a large diameter spool).

7.8.3.4 Compression Molding

The compression molding process is envisioned for use at relatively low production rates and entails individually loading a 4-plate graphite sheet into a compression molding press to impart flow field features and manifold ports into the plates. Robotic loading of the compression molding press was examined and found to have nearly identical cost as manual loading. Consequently to maintain model simplicity, robotic operation was assumed for the cost analysis. Finished parts exit the molding press to an automated conveyer system which stacks them for transport to the next processing step.

7.8.3.5 Roller Embossing

Roller embossing is envisioned for moderate production rates and entails using a rotary drum to impart flow field features onto the plates. The advantages of roller embossing are a much higher rate of production (approximately 1.9 times the capacity per line that compression molding) and the ability to process the graphite in continuous coils rather than discrete sheets, thereby minimizing handling time and cost.

The speed of the roller embosser is set to match that of the resin impregnation line so the units may be connected in series. While this eliminates buffering and parts handling in-between the lines, it also causes the roller embosser to run below capacity. While the upper roller embosser speed is not known, it is expected to be well in excess of the 0.0457 m/s rate of resin impregnation.

In addition to embossing a flow field pattern onto the graphite mat, the roller also pierces the mat to form manifold openings, and cuts the continuous mat into 4-plate sheets. (Note that when roller embossing is used, the graphite mat must come from the resin impregnator in a continuous sheet rather than in 4-plate sheets. Previously, the mat-to-sheet cutting cost had been included within the resin impregnation step but is now assumed to be performed in the roller embosser. While this slight miss-allocation of capital cost introduces error into the cost analysis, it is expected to be minor and for analysis simplicity is ignored.

7.8.3.6 High Speed Forming

High speed forming is envisioned for high production rates and entails using a high speed stamping press to press flow field features onto the graphite mat while simultaneously cutting them into 4-plate sheets. Like the roller embosser, the graphite mat is fed as a continuous coil. However, stamping is inherently an indexed process rather than a continuous one. Consequently the graphite mat is rolled into a coil as it comes off the resin impregnation line; the coil is transferred to the stamping line, and

then unrolled in an indexed fashion for the stamping operation. (Alternately, the resin impregnation line could be linked to the high speed stamping line and some mechanical mechanism used to adjust for the indexing. Cost is expected to be about the same.) Additional capital is added for these two roll/un-roll units. Part processing is considerably faster than continuous embossing. Finished parts are automatically stacked and prepared for transport to the next processing step.

7.8.3.7 Resin Curing

This process entails curing the formed 4-plate sheets at temperature for 2 hour total duration. Since the sheets must be rigidly clamped top-and-bottom to prevent warping during the curing process, a rigid rack system using a batch oven is envisioned. Two robots load a total of four 4-plate sheets to a flat oven rack. A third robot stacks the oven rack onto a wheeled assembly. Each rack layer nests into the layer below it to provide the appropriate anti-warping confinement and gas flow passages as well as edge support so the plates are not crushed. Upon stacking of 250 rack layers, the assembly is complete and a worker manually rolls the rack assembly into the curing oven. After curing, the rack assembly is manually removed from the oven and allowed to convectively cool prior to unloading. The unloading process is performed by the same three robots but in reverse direction.

7.8.3.8 Post Production Sealing

Post production sealing represents a series of steps to seal the surface of the plates to make them water and gas impermeable. It is a batch process and is only used in combination with compression molding and roller embossing.

7.8.3.9 Plate Joining (Step #1: Screen Printing)

Plate joining is modeled in two steps: application of adhesive via a screen printing process and plate curing to bond the two plates together. The first step is modeled as follows: a loading robot is used to lift a 4-plate sheet from a magazine and properly orient it onto an indexed carrier table. The carrier table is next advanced into the screen printer wherein an optical camera system is used to verify proper alignment, a screen having the proper adhesive pattern and orientation is lowered over the 4-plate sheet, a wiper bar pushing adhesive is swept over the top of the screen, the screen is lifted, and the 4-plate sheet is advanced out of the machine. Cycle time for the screen printing is conservatively modeled as 0.42 minutes/cycle, although investment in advanced machinery holds the potential to reduce this cycle time considerably. Upon exit, a second loading robot deposits an inverted 4-plate sheet onto the bottom (adhesive covered) 4-plate sheet to form a loosely joined bipolar plate. This newly formed bipolar plate is removed by a third robot and carefully stacked for transfer to the next processing stage.

7.8.3.10 Plate Joining (Step #2: Plate Curing)

As stated above, plate joining is modeled in two steps: adhesive addition via screen printing and plate curing. The second step (plate curing) is modeled in a similar fashion to the resin curing process. Two robots load a total of four 4-bipolar plate sheets to a flat oven rack. A third robot stacks the oven racks onto a wheeled assembly. Each rack

layer nests into the layer below it to provide the appropriate anti-warping surface and gas flow passages as well as edge support so the plates are not crushed. Upon stacking of 250 rack layers, the assembly is complete and a worker manually rolls the rack assembly into the curing oven. After curing, the rack assembly is manually removed from the oven and allowed to convectively cool prior to unloading. The unloading process is performed by the same three robots but in reverse direction.

7.8.3.11 Plate Die Cutting

After plate joining, the bipolar plates are virtually complete and need only be cut into individual bipolar plates from their bonded 4-plate sheet form. Die cutting is done via a conventional die cutting press however the cyclic speed of the press is reduced to allow 4 seconds of actual shearing time to avoid fracturing the brittle bipolar plate material. A loading robot is used to position the 4-bipolar-plate sheet prior to indexing into the die cutter. A second robot is used to stack the individual bipolar plates.

7.8.3.12 Assembled Bipolar Plate Leak Check

Joined bipolar plates are potentially susceptible to gas/water leakage through the adhesive bonded joints. At very low volumes, every bipolar plate can be tested. However, at even moderate production rates, testing of all assemblies is onerous. Consequently, future manufacturing systems must be created that have high quality control standards that obviate individual bipolar plate testing. Quality control equipment is assumed at each stage of the manufacturing process. For this analysis, additional finished plate sampling is postulated to ensure quality control. Generic testing that takes ten minutes for five plates and is conducted by two human testers is assumed. Additionally, the fraction of plates tested is assumed to decline with manufacturing rates. Other assumptions include 5% parts tested for 10k systems/year, 1% for 100k systems/year, and 0.5% for 500k systems/year.

Parts inspectors must regularly collect parts from the multiple parallel processing lines and test them while carefully keeping track of lot numbers so that “failed” parts can be traced back to their batch mates. The careful analysis required to determine actual quality control personnel headcount and procedures is beyond the scope of this cost analysis. However, this representative approach reflects expected quality control costs and is consistent with the assumed parts yield assumptions.

7.8.4 Cost Results for Three Main Production Configurations

The following table sums the costs of each relevant step for each of the process trains, namely the “Compression Molding” at 10k systems/year, “Embossing” at 100k systems/year, and “Stamping” at 500k systems/year. Each manufacturing step is broken down into materials, manufacturing, and tooling (i.e. amortization of custom/expendable dies, etc.). All values are reported in $\$/kW_{net}$ and include both material yields and part yields. Note that while the cost of all 10 manufacturing steps are computed at each of the three annual production rates, not all 10 steps are used in each of the three process trains.

Normally a mark-up charge is applied to manufacturing and assembly costs to account for the real world expenses due to research & development (R&D), general & administrative (G&A), scrap, and profit. Consistent with DoE directives for reporting of fuel cell system costs, markup has not been applied to any of the cost estimates. Typical mark-up rates for automotive supplies are 15% to 25% at high rates of manufacture (100k-500k/year) and a higher percentage at lower rates of manufacture.

Table 30: Bipolar Plate Cost Summary

		Comp. Molding (10k/year)	Roller Embossing (100k/year)	High Speed Forming (500k/year)
Material	**$/kW$_{net}$**	$9.78	$5.55	$4.78
Manufacturing	**$/kW$_{net}$**	$14.11	$7.77	$5.97
Tooling	**$/kW$_{net}$**	$0.17	$0.13	$0.12
Total Annual Cost	**$/kW$_{net}$**	$24.06	$13.46	$10.87

The following figures are graphic representations of the relative cost for the three manufacturing processes.

Figure 28: Cost Breakdown of the Compression BPP Process at 10k Systems/Year

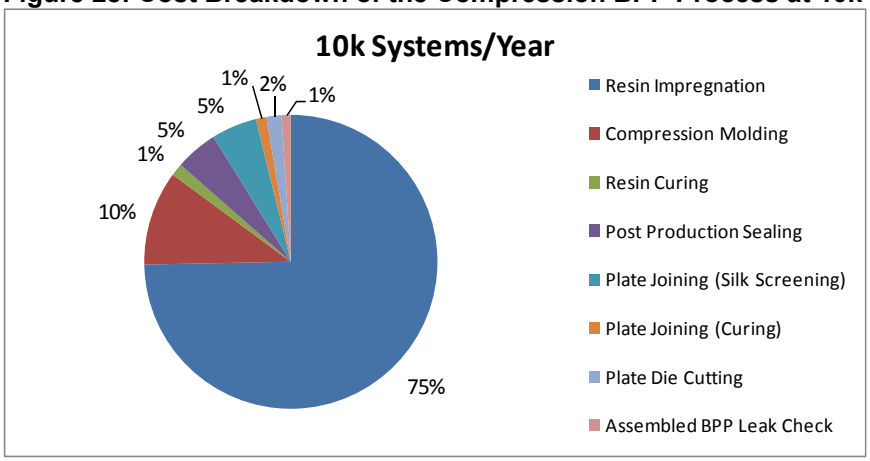

Figure 29: Cost Breakdown of the Embossing BPP Process at 100k Systems/Year

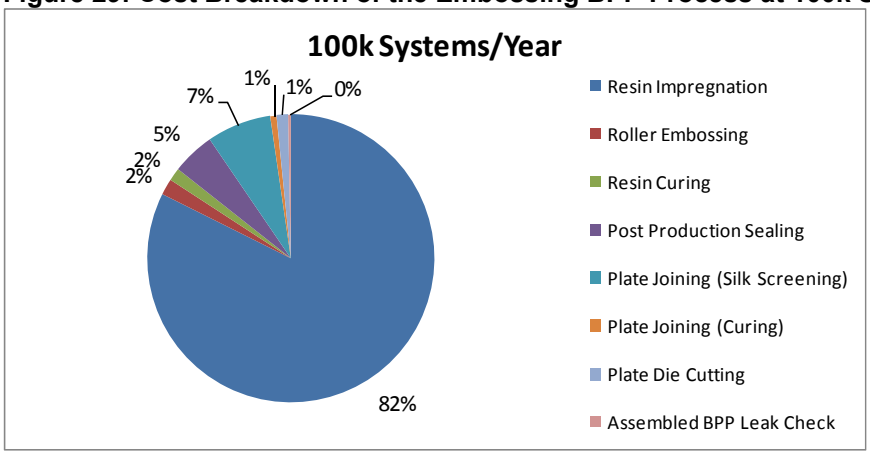

Figure 30: Cost Breakdown for the Stamping BPP Process at 500K Systems/Year

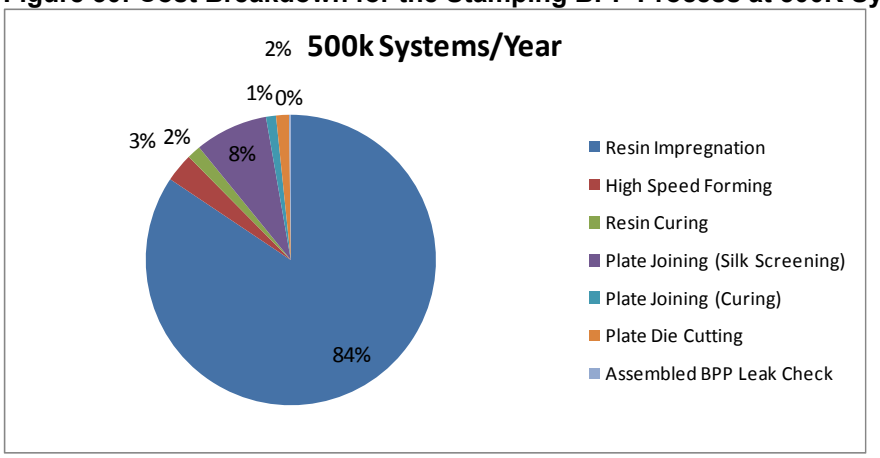

7.8.5 Sensitivity Analysis

In addition to the baseline assumptions, both a Monte Carlo sensitivity analysis and a single variable sensitivity were conducted. The parameters used were primarily based on GrafTech's projected improvements in system design and materials costs. For simplicities sake, only three different values for each parameter were used, giving a triangular probability distribution function, with the "likeliest cost" option representing the baseline assumptions. A future solvent-less resin impregnation system that could potentially lower costs was hypothesized for the Roller Embossing and High Speed Forming production methods, and thus the Monte Carlo parameters differ among the three production methods. The following tables show the varied parameters for the 10k units/year solvent resin system and the 100k and 500k bipolar plate/year solvent-less resin systems.

Table 31: Monte Carlo Parameters for 10k systems/year

Solvent-Based Resin System (10k/year)							
Parameter	**Unit**	**Minimum Cost**	**Rationale**	**Likeliest Cost**	**Rationale**	**Maximum Cost**	**Rationale**
Capital Cost - Resin Impreg	$	$7,100,000	Projected Lowest attainable Capital Cost for Resin Impreg System	$12,798,750	Based on AFGF cost of 8,532,500. Cost is increased 1.5x for a speed increase of 2x.	$14,078,625	10% increase over Medium Cost.
Resin Cost	$/kg	$5.43	Projected lowest possible resin price	$38.59	Graftech projected high volume price	$46.31	Current cost of resin bought by AFGF facility
Graphite Cost	$/kg	$5.51	Graftech best case possible	$6.84	Graftech projected high volume price	$11.57	Current cost of graphite bought by AFGF facility
Labor Rate	$/hr	$9.45	Graftech foreign labor rate	$21.50	Current Graftech fully burdened labor rate	$45.00	Current auto industry labor standard

Table 32: Monte Carlo Parameters for 100k and 500k systems/year

Solvent-less Resin System (100k/year, 500k/year)							
Parameter	**Unit**	**Minimum Cost**	**Rationale**	**Likeliest Cost**	**Rationale**	**Maximum Cost**	**Rationale**
Capital Cost - Resin Impreg	$	$6,100,000	Projected Lowest attainable Capital Cost for Resin Impreg System	$11,298,750	Reduction of solvent removal system cuts $1M from cost. Cost is increased 1.5x for a speed increase of 2x.	$12,428,625	10% increase over Medium Cost.
Resin Cost	$/kg	$5.43	Projected lowest possible resin price	$24.26	Projected price for a solvent-less resin system	$29.11	20% increase from solvent-less resin system
Graphite Cost	$/kg	$5.51	Graftech best case possible	$6.84	Graftech projected high volume price	$11.57	Current cost of graphite bought by AFGF facility
Labor Rate	$/hr	$9.45	Graftech foreign labor rate	$21.50	Current Graftech fully burdened labor rate	$45.00	Current auto industry labor standard

Because line speed and capital cost are not independent variables, the Monte Carlo analysis was run at a constant 0.04572 m/s (9 ft/min.) line speed while varying capital cost. The effect of line speed on cost is examined in the single variable sensitivity analysis.

7.8.5.1 Monte Carlo Results

The results of the Monte Carlo analysis are show in the following figures. In these plots the blue area indicates the middle 90% of Monte Carlo runs. This region gives a high degree of confidence that the actual result will be in the indicated range.

Figure 31: Monte Carlo Results - 10k Systems/Year

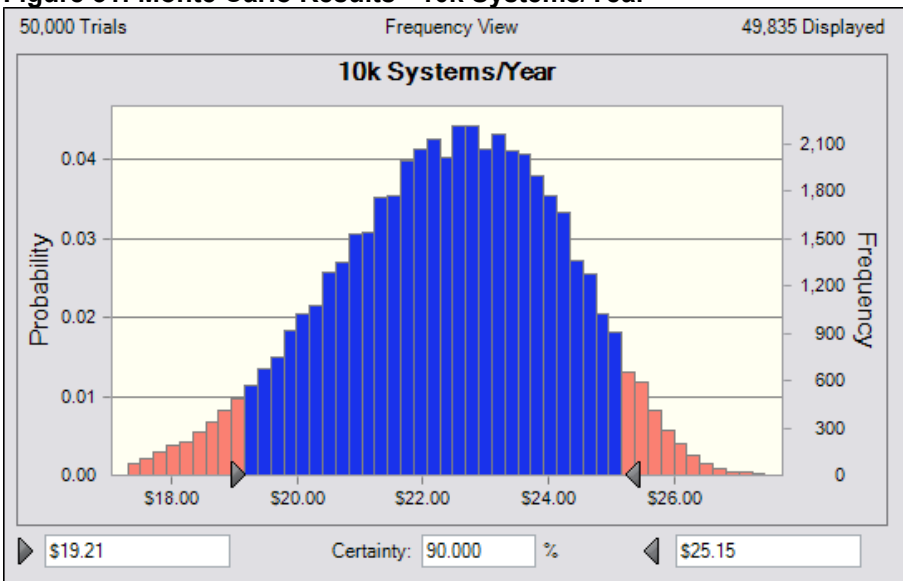

Figure 32: Monte Carlo Results - 100K Systems/Year

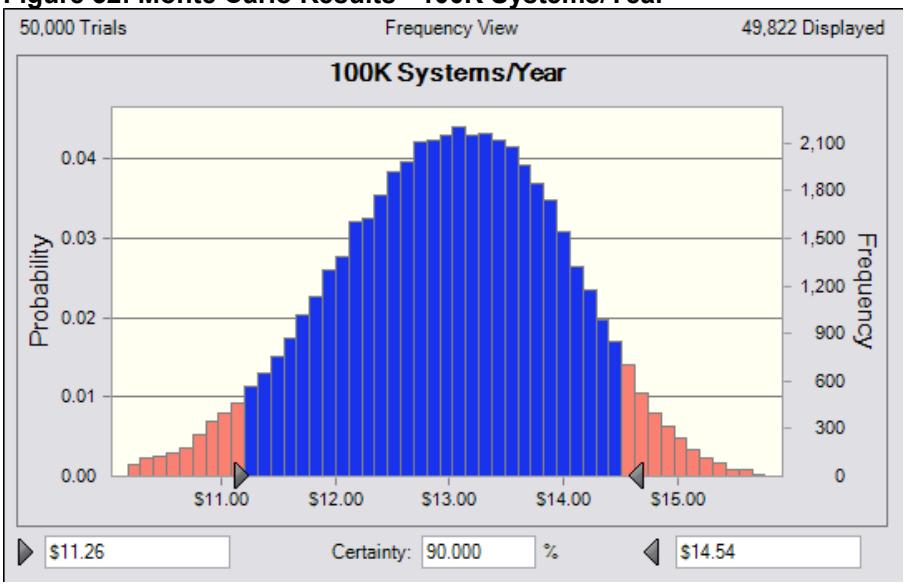

Figure 33: Monte Carlo Results - 500K Systems/Year

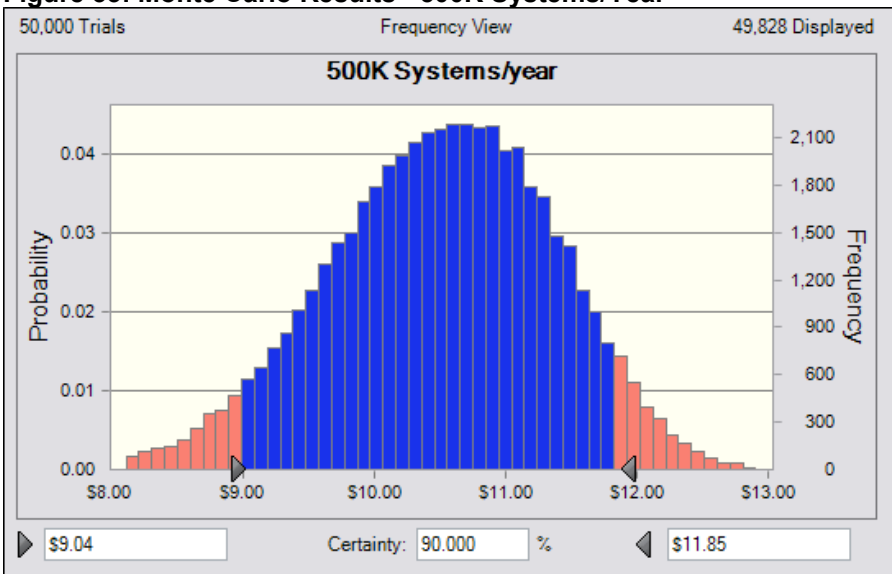

The baseline cost, mean and median of the above probability distributions are shown in the following table.

Table 33: Baseline, Mean, and Median costs for Monte Carlo Analysis

Systems/Year	Baseline Cost	Median Cost	Mean Cost
10k	$24.06	$22.49	$22.37
100k	$13.46	$13.02	$12.97
500k	$10.87	$10.55	$10.51

7.8.5.2 Single Variable Sensitivity

The parameters for the single variably sensitivity are similar to the parameters in the Monte Carlo, but include variation in the capital cost of the resin impregnation system. These parameters are shown in the following table. The analysis was conducted on the 500k systems/year case. The subsequent plot shows the results of this analysis. Line speed is seen to be a critical parameter and clearly shows that speeds of ~9 ft/min. are highly desirable.

Table 34: Single Variable Sensitivity Parameters for 500k systems/year

Solvent-less Resin System (500k/year)							
Parameter	Unit	Minimum Cost	Rationale	Likeliest Cost	Rationale	Maximum Cost	Rationale
Line Speed - Resin Impreg	m/s	0.0508	10ft/min is projected as the maximum attainable speed under any conditions.	0.04572	Doubling of current max line speed (2x4.5ft/min=9ft/min). Line length and cap cost are also increased.	0.0165	Current effective speed in AFGF facility. (3.26ft/min)
Capital Cost - Resin Impreg	$	$6,100,000	Projected Lowest attainable Capital Cost for Resin Impreg System	$11,298,750	Reduction of solvent removal system cuts $1M from cost. Cost is increased 1.5x for a speed increase of 2x.	$12,428,625	10% increase over Medium Cost.
Resin Cost	$/kg	$5.43	Projected lowest possible resin price	$24.26	Projected price for a solvent-less resin system	$29.11	20% increase from solvent-less resin system
Graphite Cost	$/kg	$5.51	Graftech best case possible	$6.84	Graftech projected high volume price	$11.57	Current cost of graphite bought by AFGF facility
Labor Rate	$/hr	$9.45	Graftech foreign labor rate	$21.50	Current Graftech fully burdened labor rate	$45.00	Current auto industry labor standard

Figure 34: Single Variable Sensitivity Analysis

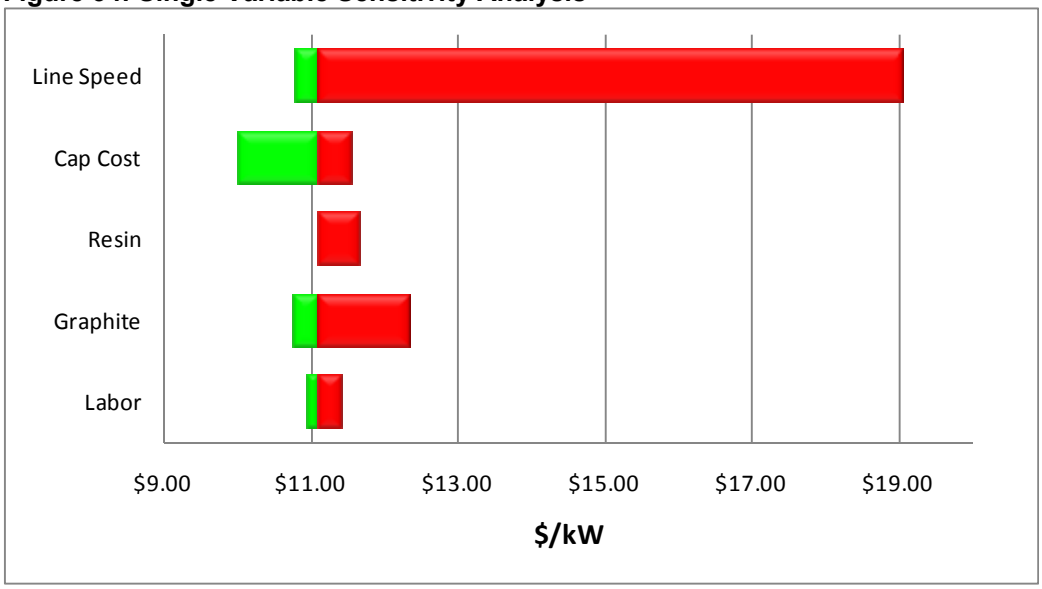

7.8.5.3 Impact of the Solvent-Less Resin System

For completeness, the bipolar plate cost for all systems and all production methods was calculated using both the solved-based and solvent-less resin systems. The following figures graphically show these cost values. Note that for both resin systems, the "knee" in the curve occurs somewhere between 10k systems/year and 100k systems/year for all production methods. Ultimately, switching to a solvent-less system reduces cost and the magnitude of this reduction is dependent on production rate for all manufacturing methods. There is a savings of \$2.93/kW_{net} for 10k systems/year, \$2.39/kW_{net} for 100k systems/year, and \$2.11/kW_{net} for 500k systems/year.

Figure 35: Cost Results for All 3 Production Methods Using a Solvent-Based Resin

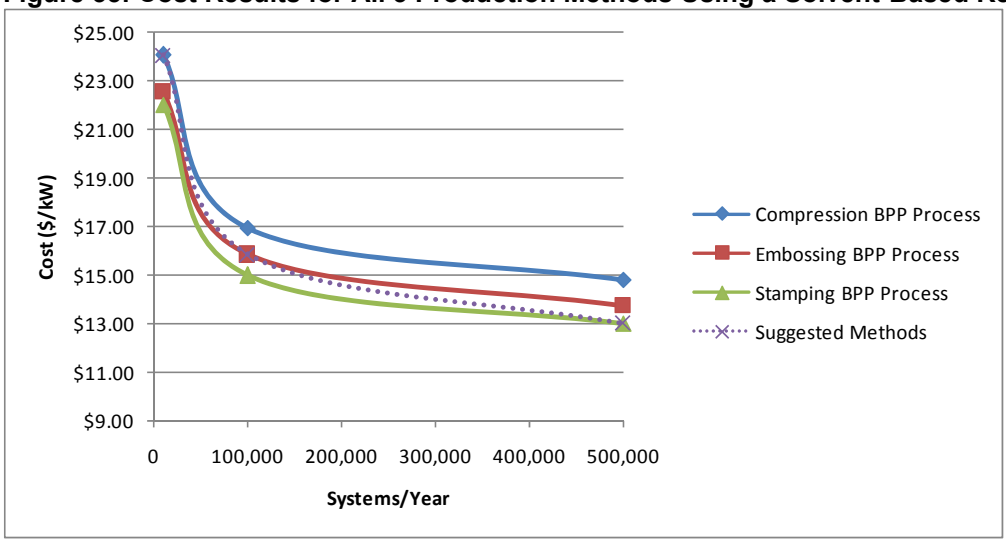

Figure 36: Cost Results for All 3 Production Methods Using Solvent-less Resin

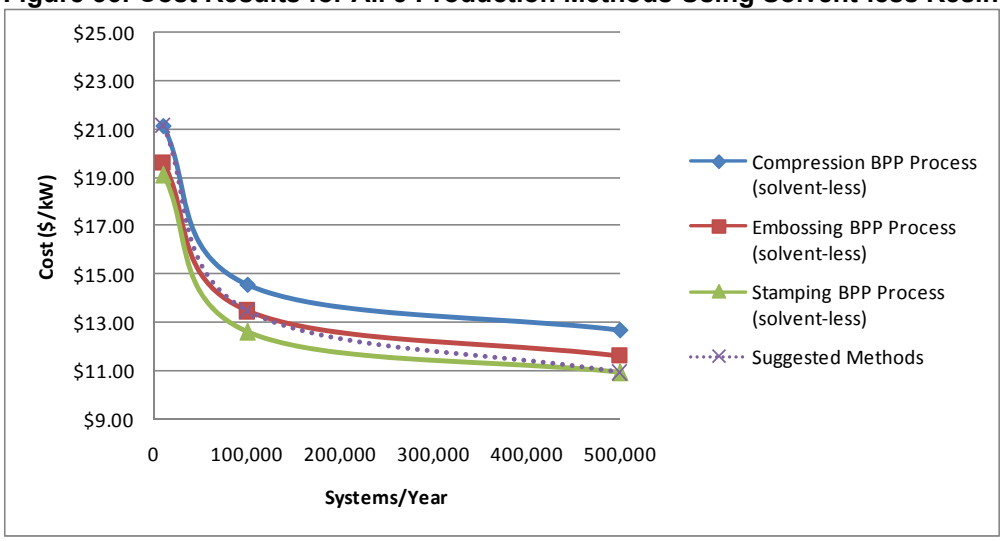

7.8.6 Best Case Scenario

The results listed in the following table represent a "best case scenario" where all of the low cost parameters from the Monte Carlo analysis are adopted (with the exception of labor rate). The second table lists these "best case" parameters. A cost of $6.85/kWnet is achievable under these conditions. This number represents the best case cost scenario given the current performance projections.

Table 35: Best Case Scenario Cost – 500k Systems/year

Best Case Low Cost Scenario High Speed Forming 500K Systems/year		
Material	**$/kW$_{net}$**	$2.85
Manufacturing	**$/kW$_{net}$**	$3.91
Tooling	**$/kW$_{net}$**	$0.12
Total Annual Cost	**$/kW$_{net}$**	$6.85

Table 36: Best Case Scenario Parameters

Solvent-less System (500k/year)			
Parameter	**Unit**	**Minimum Cost**	**Rationale**
Line Speed - Resin Impreg	**m/s**	0.0508	10ft/min is projected as the maximum attainable speed under any conditions.
Capital Cost - Resin Impreg	**$**	$6,100,000	Projected Lowest attainable Capital Cost for Resin Impreg System
Resin Cost	**$/kg**	$5.43	Projected lowest possible resin price
Graphite Cost	**$/kg**	$5.51	Graftech best case possible
Labor Rate	**$/hr**	$21.50	Current Graftech fully burdened labor rate

Note that this is a domestic best-case scenario and does not include the foreign labor rate used in the sensitivity analyses. Were this rate used there would be an additional $0.17 in savings

8. APPENDIX A – ELEMENTAL ANALYSIS OF CANDIDATE GRAPHITES

Table 37: Natural Graphite Characterization ICP AES and Sulfur Results

	Graphite Code											
Element	Limit	G1S1P2	G1S1P1	G1S2P1	G1S3P1	G2S1P2	G2S2P2	G3S2P1	G4S1P1	G4S2P1	G6S1P2	G6S2P2
Aluminum (Al)	1.1	1600	ND	ND	ND	14	800	ND	180	150	4300	7200
Barium (Ba)	0.01	3	ND	ND	ND	0.092	7.5	ND	1.6	1.3	27	7.7
Calcium (Ca)	0.2	3900	ND	ND	ND	5.2	420	ND	130	190	31	27
Chromium (Cr)	0.03	1.6	ND	ND	ND	0.033	0.49	ND	5.8	3.5	5.3	5.9
Copper (Cu)	0.06	10	ND	ND	ND	0.075	3	ND	6.6	2.9	16	9.7
Iron (Fe)	0.3	2500	ND	ND	ND	36	1100	ND	1600	380	3600	3700
Magnesium (Mg)	0.03	1200	ND	ND	ND	5.6	420	ND	160	150	130	80
Manganese (Mn)	0.02	22	ND	ND	ND	0.62	3.9	ND	5.2	3	150	59
Molybdenum (Mo)	0.03	44	ND	ND	ND	ND	1.9	ND	8	1.1	1.5	ND
Nickel (Ni)	0.07	2.7	ND	ND	ND	0.1	1.1	ND	2	1.5	9.3	7.9
Potassium (K)	1.6	350	ND	ND	ND	2.1	140	ND	34	54	74	81
Silicon (Si)	1.9	5300	ND	ND	ND	40	2200	ND	1500	830	5800	9200
Sodium (Na)	1	280	ND	ND	ND	ND	120	ND	420	200	26	28
Strontium (Sr)	0.01	9.7	ND	ND	ND	0.022	2.5	ND	0.7	0.74	1.3	1.5
Titanium (Ti)	0.1	40	ND	ND	ND	0.42	18	ND	130	49	44	37
Vanadium (V)	0.08	0.75	ND	ND	ND	0.083	1.7	ND	4.4	1.5	23	25
Zinc (Zn)	0.02	3.4	ND	ND	ND	0.081	ND	ND	2.1	1.8	7.5	ND
Zirconium (Zr)	0.03	10	ND	ND	ND	0.084	20	ND	19	14	11	18
Trace Ash		38702	40	180	76	25099	11021	175	7667	4148	33595	75982
Ash, %		3.87	ND	0.02	0.01	2.51	1.1	0.02	0.77	0.41	3.36	7.6
Leco Sulfur	50	620	ND	ND	ND	110	180	ND	130	100	80	ND

ND - Not Detected
All Values are in ppm unless noted

9. APPENDIX B – INTERCALATED GRAPHITE CHARACTERIZATION RESULTS

Table 38: Natural Graphite Raw Material Evaluation Treat Property Data

Graphite	Treat	Expansion Volume @ 600 °C	Expansion Volume @ 800 °C	pH	Surface Acid	Onset Temp	Leco Ash	Leco Moisture	Leco Volatiles
Code	Code	cc/g	cc/g		%	°C	%	%	%
G1S1P1T1	T1	51	179	2.46	2.70	174.2	<0.03	1.51	17.42
G1S1P2T1	T1	22	139	2.58	2.26	222.3	1.74	0.64	13.66
G1S2P1T1	T1	69	293	2.07	2.84	187.6	<0.03	1.53	18.26
G1S3P1T1	T1	38	131	2.14	2.80	178.3	<0.03	1.88	15.32
G2S1P2T1	T1	19	97	2.60	2.84	175.9	1.20	1.22	10.62
G2S2P1T1	T1	32	159	2.27	2.87	175.7	0.41	1.07	13.16
G3S2P1T1	T1	31	192	2.54	1.84	174.6	<0.03	0.32	13.64
G4S1P1T1	T1	26	133	2.57	3.38	174.3	0.41	1.02	12.50
G4S2P1T1	T1	30	162	2.47	3.43	174.6	0.11	1.24	13.65
G6S1P2T1	T1	58	95	2.81	2.38	251.5	1.85	0.54	10.44
G6S2P2T1	T1	69	130	3.00	2.30	171.6	2.71	0.77	12.21
G1S1P1T2	T2	107	272	2.10	1.89	163.3	<0.03	1.66	22.99
G1S1P2T2	T2	113	284	2.77	1.32	158.4	1.10	0.68	30.99
G1S2P1T2	T2	163	388	1.97	2.21	163.0	<0.03	1.68	24.69
G1S3P1T2	T2	88	225	2.43	1.28	159.6	<0.03	2.00	25.94
G2S1P2T2	T2	62	190	2.61	0.98	161.6	0.95	0.95	16.80
G2S2P1T2	T2	91	283	2.57	1.32	162.3	0.68	3.09	18.34
G3S2P1T2	T2	92	299	2.79	1.18	161.6	0.05	0.34	20.36
G4S1P1T2	T2	81	219	3.04	1.23	161.8	0.37	1.08	17.62
G4S2P1T2	T2	101	302	2.92	1.35	160.2	0.15	1.20	20.10
G6S1P2T2	T2	121	179	3.10	1.13	162.0	1.64	1.93	16.68
G6S2P2T2	T2	156	261	3.10	1.15	160.9	2.42	0.99	16.71
G5S1P2T3	T3	66	177	5.08	0.05	162.0	0.78	0.14	8.31

10. APPENDIX C – SELECTED RESIN SYSTEMS THERMAL ANALYSIS RESULTS

Table 39: DSC Date Uncured Resin Systems

Resin Formulation	Catalyst	Peak Onset Temperature, °C	Exotherm Peak Temperature, °C	Exothermic Heat, J/g
Benzoxazine				
1	No	239.1	260.7	187.4
2	No	239.4	262.5	186.9
3	No	242.8	263.8	219.2
4	No	202.2	205.5	150.9
5	No	245.4	266	249.6
Epoxy				
1	Yes	137.2	175.9	249.9
2	Yes	NA	NA	NA
3	Yes	140.5	169.5	187.5
4	No	154.3	193.5	220.5
5	No	141.9	178.4	168.5
6	No	130.7	194.3	118.3

Table 40: Glass Transition Temperatures for Neat Resin Systems

System	Catalyst	DMA Tan Delta Tg, °C	DMA Storage Modulus Tg, °C	TMA Tg, °C	TMA CTE, µm/m °C
Benzoxazine Resins					
1	No	215	185	183	64
2	No	171	137	128	82
2A	No	232	198	216	85
2B	No	225	183	195	159
2G	No	282	252	247	61
2H	No	282	255	261	52
3	No	298	183	175	67
4	No	148	120	114	75
5	No	183	148	104	65
Epoxy Resins					
1	Yes	205.0	178.0	172.0	82.0
2	Yes	208.0	191.0	184.0	81.0
3	Yes	242.0	210.0	197.0	72.0
4	No	156.0	125.0	NA	NA
5	Yes	143.0	96.0	NA	NA
6	No	95.0	88.0	NA	NA
	Selected Resin Systems				

APPENDIX C (cont)

Table 41: Gel Time, Softening Point and TGA Results for Neat Resin Systems

System	Catalyst	Gel Time @ 200 °C, s	TGA Decomp Temp, °C	TGA Wt Loss, %	Softening Point, °C
Benzoxazine Resin					
1	No	>600	339	2.2	70.5
2	No	>600	319	1.9	84.8
2A	No	>600	351	3.1	Liquid
2B	No	>600	343	2.6	Liquid
2G	No	364.9	343	3.8	88.1
2H	No	440.9	347	3.8	74.6
3	No	>600	317	2.5	80.5
4	No	420	NA	NA	98
5	No	>600	NA	NA	87
Epoxy Resin					
1	Yes	30.3	336.0	3.8	Liquid
2	Yes	170/150 °C	309.0	3.5	Liquid
3	Yes	100/150 °C	341.0	3.5	Liquid
4	No	155/150 °C	NA	NA	Liquid
5	Yes	31.3	286.0	3.2	Liquid
6	No	>600	NA	NA	Liquid
	Selected Resin Systems				

11. APPENDIX D - PERMEABILITY (LEAK) TESTING RESULTS

Table 42: Nitrogen Leak Rate Measurements on Resin Expanded Graphite Flat Stock

Resin Type	Molding Pressure	Average Molded Thickness, (mm)	Cured Immersed Density, (g/cc)	Leakage In Plane, (ml/min)	Leakage Through Plane, (ml/min)
2G	L	0.638	1.508	<0.0025	<0.0025
2G	L	0.654	1.519	<0.0025	<0.0025
Average			1.538		
2G	H	0.634	1.450	<0.0025	<0.0025
2G	H	0.651	1.477	<0.0025	<0.0025
Average			1.464		
2H	L	0.597	1.612	<0.0025	<0.0025
2H	L	0.604	1.631	<0.0025	<0.0025
Average			1.626		
2H	H	0.598	1.621	<0.0025	<0.0025
2H	H	0.603	1.610	<0.0025	<0.0025
Average			1.621		

Torque 5" lb, 0.8 Bar N_2

Table 43: Hydrogen Permeability on Resin Expanded Graphite Flat Stock

Sample ID	Thickness, mm	Permeation Rate	Hold Time	Fracture? (Pressure, psi)
DoE 2G	0.673	< LDL	2.5	Yes, (15)
DoE 2G	0.686	< LDL	2.5	Yes, (5)
DoE 2G	0.682	< LDL	2.0	Yes, (5)
DoE 2G	3.770	< LDL	3.0	No
DoE 2G	3.785	< LDL	3.5	No
FFP-300	0.726	< LDL	2.0	Yes, (80)
FFP-300	0.7522	< LDL	2.0	Yes (40)
FFP-300	1.0442	< LDL	4.0	No
FFP-300	1.0282	< LDL	3.0	No
FFP-300	1.985	< LDL	1.5	No
FFP-300	1.9614	< LDL	2.0	No
FFP-300	3.0464	< LDL	4.0	No

LDL = $5.72 \times 10^{-7} cm^3/min/cm^2$

12. APPENDIX E - MECHANICAL TESTING RESULTS ON RESIN GRAPHITE COMPOSITE SAMPLES

Table 44: Flexural Strength Testing Results for Resin Flexible Graphite Composites

Resin	Ply	Temp, °C	N	Flexural Modulus, Mpsi			Flexural Strength, psi		
				Avg.	Std. dev.	T-test	Avg.	Std. dev.	T-test
2G	1	-40	4	2.44	0.12	-1.00	10200	695	3.11
2G	3	-40	4	2.4	0.2	7.65	9430	303	1.72
2G	5	-40	4	2.5	0.151	6.03	9660	392	0.64
2G	1	23	4	2.88	0.197	-1.12	8320	462	1.36
2G	3	23	4	3.06	0.056	38.57	8790	347	1.51
2G	5	23	4	2.85	0.136	6.76	8420	457	-0.37
2G	1	100	4	2.18	0.115	18.52	6660	226	13.32
2G	3	100	4	2.36	0.173	12.49	6930	121	18.51
2G	5	100	4	2.24	0.116	13.02	7190	500	6.84
2G	1	120	4	2.35	0.142	17.39	6100	264	7.16
2G	3	120	4	2.34	0.148	14.32	6570	149	10.20
2G	5	120	4	2.29	0.094	17.13	6610	84	26.90
2H	1	-40	4	2.43	0.185	-0.76	9610	778	1.26
2H	3	-40	4	2.32	0.148	9.26	10100	223	8.34
2H	5	-40	4	2.51	0.213	4.37	10300	334	4.58
2H	1	23	4	3.07	0.199	0.80	8790	475	3.31
2H	3	23	4	3.36	0.112	24.64	9060	385	2.71
2H	5	23	4	3.17	0.02	78.00	9030	401	2.62
2H	1	100	4	2.28	0.113	20.62	7580	496	9.78
2H	3	100	4	2.51	0.089	27.64	7260	314	9.24
2H	5	100	4	2.3	0.12	13.58	7500	108	37.41
2H	1	120	4	2.35	0.083	29.76	7180	181	22.38
2H	3	120	4	2.41	0.096	23.54	7220	354	7.97
2H	5	120	4	2.38	0.132	13.56	7240	87	40.46
Control	1	-40	5	2.50	0.597		9120	743	
Control	3	-40	5	1.64	0.213		9170	694	
Control	5	-40	5	2.05	0.226		9535	327	
Control	1	23	5	2.99	0.544		8005	460	
Control	3	23	5	1.98	0.219		8490	374	
Control	5	23	5	2.39	0.163		8505	324	
Control	1	100	5	1.12	0.144		5155	245	
Control	3	100	5	1.28	0.232		5810	545	
Control	5	100	5	1.49	0.121		5480	245	
Paired T-test (P-value)				0.02			0.00		
Critical Value			4	0.05		2.353	0.05		2.353

T-test Results Legend		
No Difference	Worse	Better

APPENDIX E (cont)

Table 45: Tensile Strength Testing Results for Resin Flexible Graphite Composites

Resin	Ply	Temp., °C	N	Tensile Modulus. Mpsi			Tensile Strength, psi		
				Avg.	Std. dev.	T-test	Avg.	Std. dev.	T-test
2G	1	-40	4	4.28	0.95	1.66	4830	684	-0.80
2G	3	-40	4	4.10	0.34	1.35	6140	610	-0.25
2G	5	-40	4	3.54	0.98	-0.89	7000	59	3.39
2G	1	23	4	3.90	0.58	2.60	4040	589	-2.65
2G	3	23	4	4.90	0.32	2.69	5630	337	1.22
2G	5	23	4	4.53	0.59	0.12	6590	398	3.34
2G	1	100	4	3.35	0.16	20.63	4340	930	2.69
2G	3	100	4	4.24	1.48	-1.47	4900	479	5.09
2G	5	100	4	3.55	1.41	-0.23	5030	377	15.33
2G	1	120	4	3.35	0.55	5.95	4970	107	35.14
2G	3	120	4	2.53	0.28	-20.29	4630	265	7.17
2G	5	120	4	3.11	0.48	-2.49	4570	139	34.95
2H	1	-40	4	5.10	0.65	4.97	5700	250	4.76
2H	3	-40	4	3.67	0.24	-1.69	6690	168	5.65
2H	5	-40	4	3.23	0.16	-9.14	7010	223	0.99
2H	1	23	4	5.71	0.64	8.03	5360	347	3.11
2H	3	23	4	5.21	0.38	3.85	6640	218	12.51
2H	5	23	4	4.96	0.23	4.12	7050	95	23.68
2H	1	100	4	3.20	0.47	6.31	4730	188	17.45
2H	3	100	4	4.05	0.74	-3.47	5780	533	7.88
2H	5	100	4	3.34	0.33	-2.22	5320	99	64.22
2H	1	120	4	3.24	0.60	5.10	5360	366	12.40
2H	3	120	4	3.23	0.23	-17.95	5420	240	14.50
2H	5	120	4	3.35	0.39	-1.83	5490	61	109.80
Control	1	-40	5	3.50	1.64		5105	1024	
Control	3	-40	5	3.87	1.78		6215	777	
Control	5	-40	5	3.98	1.60		6900	416	
Control	1	23	5	3.15	0.39		4820	399	
Control	3	23	5	4.47	1.67		5445	354	
Control	5	23	5	4.50	1.10		5925	360	
Control	1	100	5	1.72	0.28		3090	197	
Control	3	100	5	5.33	3.13		3680	446	
Control	5	100	5	3.71	1.58		2141	179	
Paired T-test (P-value)				0.21			0.00		
Critical value			4	0.05		2.353	0.05		2.353

T-test Results Legend		
No Difference	Worse	Better

APPENDIX E (cont)

Table 46: T-test Results for Benzoxazine Resin vs GRAFCELL FFP-300 Composite Flexural Testing

Ply	Temp., °C	Flexural Modulus		Flexural Strength		Flexural Stain	
		2G	2H	2G	2H	2G	2H
1	-40	-1.00	-0.76	3.11	1.26	-5.67	-12.50
3	-40	7.65	9.26	1.72	8.34	-23.00	-44.00
5	-40	6.03	4.37	0.64	4.58	-6.50	-11.00
1	23	-1.12	0.80	1.36	3.31	-1.50	-2.00
3	23	38.57	24.64	1.51	2.71	-437.52	-951.84
5	23	6.76	78.00	-0.37	2.62	-7.50	-6.33
1	100	18.52	20.62	13.32	9.78	-45.50	-19.80
3	100	12.49	27.64	18.51	9.24	-27.33	-47.00
5	100	13.02	13.58	6.84	37.41	-12.00	-39.00
1	120	17.39	29.76	7.16	22.38	-26.25	-33.00
3	120	14.32	23.54	10.20	7.97	-43.00	-46.00
5	120	17.13	13.56	26.90	40.46	-70.00	-24.00
Critical Value		2.35	2.35	2.35	2.35	2.35	2.35
Paired T-test (2G-2H)							
P-value		0.02		0.00		0.00	
Critical Value		0.05		0.05		0.05	
Code		Higher	Same	Lower			
Table values are t-test results for a 95% confidence interval with 3 degrees of freedom							

Table 47: T-test Results for Benzoxazine Resin vs. GRAFCELL FFP Composite Tensile Testing

Ply	Temp., °C	Tensile Modulus		Tensile Strength		Tensile Strain	
		2G	2H	2G	2H	2G	2H
1	-40	1.66	4.97	-0.80	4.76	-5.00	-2.73
3	-40	1.35	-1.69	-0.25	5.65	-4.14	-5.50
5	-40	-0.89	-9.14	3.39	0.99	-20.00	-8.75
1	23	2.60	8.03	-2.65	3.11	-6.67	-13.33
3	23	2.69	3.85	1.22	12.51	-274.16	-252.22
5	23	0.12	4.12	3.34	23.68	-3.03	-12.73
1	100	20.63	6.31	2.69	17.45	-11.49	-55.00
3	100	-1.47	-3.47	5.09	7.88	-14.26	-15.48
5	100	-0.23	-2.22	15.33	64.22	-12.75	-18.28
1	120	5.95	5.10	35.14	12.40	-19.74	-12.10
3	120	-20.29	-17.95	7.17	14.50	-16.34	-20.29
5	120	-2.49	-1.83	34.95	109.80	-13.41	-12.79
Critical value		2.353	2.353	2.353	2.353	2.353	2.353
Paired T-test (2G-2H)							
P-value		0.21		0.00		0.92	
Critical Value		0.05		0.05		0.05	
Code		Higher	Same	Lower			
Table values are t-test results for a 95% confidence interval with 3 degrees of freedom							

13. APPENDIX F - WORK-OF FRACTURE ANALYSIS OF THE FLEXURAL STRENGTH DATA

Table 48: Work of Fracture Analysis for 2G and 2H Resin Composites

Resin	Ply	Temp, °C	Span, in	Mean, (in-lb)	Std dev	N	T-test (2G-2H)
2G	1	-40	1	0.045	0.003	4	6.67
2G	3	-40	1.5	0.161	0.006	4	0.67
2G	5	-40	2	0.341	0.040	4	-0.55
2G	1	23	1	0.038	0.004	4	1.50
2G	3	23	1.5	0.163	0.015	4	3.60
2G	5	23	2	0.318	0.028	4	1.57
2G	1	100	1	0.034	0.002	4	2.00
2G	3	100	1.5	0.132	0.010	4	3.80
2G	5	100	2	0.283	0.048	4	1.50
2G	1	120	1	0.027	0.004	4	-2.00
2G	3	120	1.5	0.123	0.007	4	2.00
2G	5	120	2	0.265	0.004	4	4.50
2H	1	-40	1	0.035	0.005	4	
2H	3	-40	1.5	0.159	0.007	4	
2H	5	-40	2	0.352	0.020	4	
2H	1	23	1	0.035	0.004	4	
2H	3	23	1.5	0.136	0.013	4	
2H	5	23	2	0.296	0.036	4	
2H	1	100	1	0.032	0.005	4	
2H	3	100	1.5	0.113	0.008	4	
2H	5	100	2	0.247	0.014	4	
2H	1	120	1	0.031	0.003	4	
2H	3	120	1.5	0.116	0.012	4	
2H	5	120	2	0.256	0.021	4	
Paired t-test (2G-2H)				**2.60**			
Critical value (95% C.I.)				**2.20**			**3.18**

	Difference is statistically significant
	Difference is not statistically significant

14. APPENDIX G - COMPRESSIVE STRENGTH TESTING RESULTS

Table 49: Compressive Strength Testing of Resin Flexible Graphite Composites

Sample ID	Peak Load (N)	Modulus (MPa)	Extension at Yield (mm)	Peak Strength (MPa)
Thru-Plane				
FFP-300-1	7,694	1,404	2.81	59.3
FFP-300-2	7,548	1,399	2.68	58.2
FFP-300-3	7,607	1,423	2.69	58.2
Average	**7,616**	**1,409**	**2.73**	**58.6**
2G-1	11,825	4,348	0.67	91.0
2G-2	12,107	4,621	0.69	93.1
2G-3	11,087	3,598	0.67	85.2
Average	**11,673**	**4,189**	**0.68**	**89.8**
In-Plane				
FFP-300-1	3,772	8,184	0.13	29.1
FFP-300-2	3,843	9,761	0.12	29.6
FFP-300-3	3,967	8,653	0.14	30.6
Average	**3,861**	**8,866**	**0.13**	**29.8**
2G-1	6,538	14,143	0.11	50.3
2G-2	6,072	11,216	0.12	46.7
2G-3	6,103	9,567	0.14	47.0
Average	**6,238**	**11,642**	**0.12**	**48.0**

15. APPENDIX H - MECHANICAL TESTING RESULTS ON TEMPERATURE CYCLED COMPOSITE SAMPLES

Table 50: Flexural Testing Results Comparison for Environmentally Cycled Resin Flexible Graphite Composites

Resin	Ply	Flexural Modulus Before, Mpsi		Flexural Strength Before, psi		Flexural Modulus Cycle, Mpsi				Flexural Strength Cycle, psi			
		Avg	Std	Avg	Std	Avg	Std	Delta	T-test	Avg	Std	Delta	T-test
2G	1	2.88	0.200	8323	462	2.49	0.105	-14%	8.45	8870	229	7%	-5.20
2G	3	3.06	0.059	8785	350	2.40	0.158	-22%	19.21	8610	290	-2%	1.89
2H	1	3.07	0.196	8793	475	2.47	0.170	-20%	11.37	9138	160	4%	-3.37
2H	3	3.36	0.112	9063	385	2.36	0.072	-30%	37.01	8770	184	-3%	3.36
Paired T-test (Before-After)									5.21				0.53
Critical t-value									2.45				2.45
Averages are based on results from 4 specimens, Statistical analysis based on α= 0.05													

Table 51; Tensile Testing Results Comparison for Environmentally Cycled Resin Flexible Graphite Composites

Resin	Ply	Flexural Modulus Before, Mpsi		Flexural Strength Before, psi		Flexural Modulus Shock, Mpsi				Flexural Strength Shock, psi			
		Avg	Std	Avg	Std	Avg	Std	Delta	T-test	Avg	Std	Delta	T-test
2G	1	2.88	0.200	8323	462	2.22	0.139	-23%	13.4	8775	324	5%	-3.93
2G	3	3.06	0.059	8785	350	2.35	0.081	-23%	34.8	8705	253	-1%	0.91
2H	1	3.07	0.196	8793	475	2.26	0.174	-26%	15.0	8868	80	1%	-0.76
2H	3	3.36	0.112	9063	385	2.35	0.180	-30%	23.4	8390	401	-7%	5.92
Paired t-test (Before-After)									10.3				0.24
Critical t-value									2.45				2.45
Averages are based on results from 4 specimens, Statistical analysis based on α= 0.05													

Table 52: Flexural Testing Results Comparison for Environmentally Shocked Resin Flexible Graphite Composites

Resin	Ply	Tensile Modulus Before, Mpsi		Tensile Strength Before, psi		Tensile Modulus Cycle, Mpsi				Tensile Strength Cycle, psi			
		Avg	Std	Avg	Std	Avg	Std	Delta	T-test	Avg	Std	Delta	T-test
2G	1	3.91	0.573	4035	587	3.81	0.844	-2%	0.46	4443	602	10%	-2.38
2G	3	4.90	0.319	5638	337	4.55	0.564	-7%	2.67	5483	412	-3%	1.4
2H	1	5.71	0.639	5365	347	3.88	0.241	-32%	13.11	5263	455	-2%	0.9
2H	3	5.21	0.387	6635	218	4.95	0.640	-5%	1.69	5535	585	-17%	8.6
Paired t-test (Before-After)									1.58				0.76
Critical t-value									2.45				2.45
Averages are based on results from 4 specimens, Statistical analysis based on α= 0.05													

APPENDIX H (cont.)

Table 53: Tensile Testing Results Comparison for Environmentally Shocked Resin Flexible Graphite Composites

Resin	Ply	Tensile Modulus Before, Mpsi		Tensile Strength Before, psi		Tensile Modulus Shock, Mpsi				Tensile Strength Shock, psi			
		Avg	Std	Avg	Std	Avg	Std	Delta	T-test	Avg	Std	Delta	T-test
2G	1	3.91	0.573	4035	587	3.31	0.442	-15%	4.0	4958	660	23%	-5.12
2G	3	4.90	0.319	5638	337	4.67	0.379	-5%	2.4	5490	200	-3%	1.84
2H	1	5.71	0.639	5365	347	3.46	0.127	-39%	16.9	5328	535	-1%	0.29
2H	3	5.21	0.387	6635	218	4.40	0.424	-16%	6.9	5098	556	-23%	12.62
Paired t-test (Before-After)									2.2				0.39
Critical t-value									2.45				2.45

	Improvement
	No Significant Change
	Degradation

Averages are based on results from 4 specimens, Statistical analysis based on α= 0.05

16. APPENDIX I - BIPOLAR PLATE COOLANT DURABILITY TESTING RESULTS

Table 54: Final Results for Coolant Durability Testing

Run Num	Resin Type	Sampling Time, hours							
		0	1	2	4	8	24	48	120
6	2H	NS	ND	ND	ND	5294	5291	5261	5542
7	2G	NS	148	155	159	184	183	194	210
10	2G	ND	ND	ND	ND	ND	ND	ND	ND
ND =	Not Detected								
NS =	Not Sampled								

17. APPENDIX J - PERMEABILITY TESTING RESULTS ON MOLDED TEST PLATES

Table 55; Summary of Permeability Measurements on Molded Flexible Graphite Resin Composite

Graphite Code	PV 1	Resin	PV 2	Average Thickness (mm)	Average Density (g/cc)	PV 3	Avg. PV4	Average Leak Rate (ml/min)
G1S1P2T1E1	High	**2G**	Low	0.599	1.008	Low	48.08	0.08
G1S1P2T1E1	High	**2G**	Low	0.711	0.859	Medium	48.62	0.21
G1S1P2T1E1	High	**2G**	Low	0.846	0.811	High	48.30	0.31
G1S1P2T1E1	High	**2H**	Low	0.589	1.035	Low	56.69	0.16
G1S1P2T1E1	High	**2H**	Low	0.721	0.854	Medium	56.01	0.10
G1S1P2T1E1	High	**2H**	Low	0.869	0.817	High	56.93	0.18
G1S1P2T1E1	Low	**2G**	Medium	0.495	1.031	Low	47.54	2.07
G1S1P2T1E1	Low	**2G**	Medium	0.556	0.915	Medium	47.86	1.74
G1S1P2T1E1	Low	**2G**	Medium	0.688	0.818	High	48.47	0.97
G1S1P2T1E1	Low	**2G**	High	0.470	1.182	Low	54.13	5.06
G1S1P2T1E1	Low	**2G**	High	0.533	1.066	Medium	54.58	2.27
G1S1P2T1E1	Low	**2G**	High	0.673	0.923	High	55.07	1.54
G1S1P2T1E1	Low	**2H**	Medium	0.475	1.034	Low	61.08	12.50
G1S1P2T1E1	Low	**2H**	Medium	0.544	0.920	Medium	61.62	10.53
G1S1P2T1E1	Low	**2H**	Medium	0.701	0.815	High	62.07	6.59
G1S1P2T1E1	Low	**2H**	High	0.574	0.945	Low	60.64	14.36
G1S1P2T1E1	Low	**2H**	High	0.668	0.816	Medium	60.58	18.28
G1S1P2T1E1	Low	**2H**	High	0.828	0.751	High	61.26	9.47
G3S2P1T1E1	High	**2G**	Low	0.579	1.055	Low	51.08	0.18
G3S2P1T1E1	High	**2G**	Low	0.668	0.923	Medium	50.89	0.15
G3S2P1T1E1	High	**2G**	Low	0.805	0.851	High	50.92	0.13
G3S2P1T1E1	High	**2H**	Low	0.582	1.043	Low	55.55	0.86
G3S2P1T1E1	High	**2H**	Low	0.673	0.900	Medium	56.84	0.95
G3S2P1T1E1	High	**2H**	Low	0.808	0.840	High	57.53	0.33
G3S2P1T1E1	Low	**2G**	Medium	0.482	0.997	Low	49.13	3.23
G3S2P1T1E1	Low	**2G**	Medium	0.543	0.895	Medium	49.98	1.22
G3S2P1T1E1	Low	**2G**	Medium	0.688	0.775	High	50.71	1.36
G3S2P1T1E1	Low	**2G**	High	0.495	1.145	Low	54.25	2.51
G3S2P1T1E1	Low	**2G**	High	0.533	1.050	Medium	54.52	2.90
G3S2P1T1E1	Low	**2G**	High	0.660	0.914	High	55.57	5.09
G3S2P1T1E1	Low	**2H**	Medium	0.495	0.960	Low	60.42	23.06
G3S2P1T1E1	Low	**2H**	Medium	0.559	0.857	Medium	61.13	92.66
G3S2P1T1E1	Low	**2H**	Medium	0.706	0.779	High	61.57	26.42
G3S2P1T1E1	Low	**2H**	High	0.584	0.927	Low	60.97	23.11
G3S2P1T1E1	Low	**2H**	High	0.673	0.811	Medium	61.62	70.02
G3S2P1T1E1	Low	**2H**	High	0.831	0.743	High	62.04	12.64

APPENDIX J (cont.)

Table 56: ANOVA Results for Leak Rate (ml/min) vs. Graphite, PV 1, and Resin

Factor	Type	Levels	Values			
Graphite	fixed	2	G1S1P2T1E1, G3S2P1T1E1			
PV 1	fixed	2	High, Low			
Resin	fixed	2	2G, 2H			
Source	**DF**	**Seq SS**	**Adj SS**	**Adj MS**	**F**	**P**
Graphite	1	575.6	689.2	689.2	11.66	0.001
PV 1	1	3292.7	3154.3	3154.3	53.37	0.000
Resin	1	4790.6	4790.6	4790.6	81.06	0.000
Error	164	9692.0	9692.0	59.1		
Total	167	18350.8				

Table 57: Regression Analysis of Permeability Testing Results

Mat Composition			Correlation Coefficients			
Graphite	Resin	PV 1	PV 3	PV 4	Blank Density	Thickness
G1S1P2T1E1	2G	Low	NC	NC	NC	NC
G1S1P2T1E1	2G	High	NC	NC	NC	NC
G1S1P2T1E1	2H	Low	-2.323	NC	-117.8	NC
G1S1P2T1E1	2H	High	NC	NC	NC	NC
G3S2P1T1E1	2G	Low	NC	NC	NC	NC
G3S2P1T1E1	2G	High	NC	NC	NC	NC
G3S2P1T1E1	2H	Low	NC	NC	NC	-495.3
G3S2P1T1E1	2H	High	NC	-0.370	NC	NC
Optimum						
NC = No Statistical Correlation						

18. APPENDIX K - GRAPHITE RESIN COMPOSITE DIMENSIONAL CHANGE (GROWTH FACTOR) RESULTS

Table 58: Two Sample T-tests Comparing Benzoxazine and GRAFCELL Resin Composites

Graphite	Resin	PV 1	PV 2	PV 3	Growth Factor Length, Avg. (%)	T-test vs GRAFCELL	Growth Factor Width Avg (%)	T-test vs GRAFCELL
G3S2P1T1E1	2G	L1	L1	L1	0.3903	-9.9	0.5989	-21.2
G3S2P1T1E1	2G	L1	L1	L2	0.4253	-18.9	0.6170	-14.7
G3S2P1T1E1	2G	L1	L1	L3	0.4266	-11.1	0.6525	-8.7
G3S2P1T1E1	2G	L1	L2	L1	0.4025	-8.6	0.5771	-27.0
G3S2P1T1E1	2G	L1	L2	L2	0.4407	-6.7	0.5674	-11.6
G3S2P1T1E1	2H	L1	L1	L1	0.4088	-10.8	0.6675	-10.6
G3S2P1T1E1	2H	L1	L1	L2	0.3943	-11.4	0.6304	-5.3
G3S2P1T1E1	2H	L1	L1	L3	0.4148	-6.3	0.6653	-8.7
G3S2P1T1E1	2H	L1	L2	L1	0.2896	-66.2	0.6514	-23.3
G3S2P1T1E1	2H	L1	L2	L2	0.2900	-11.6	0.6433	-4.1
G3S2P1T1E1	2H	L1	L2	L3	0.3230	-19.5	0.6318	-14.2
G3S2P1T1E1	GRAFCELL	L1	L2	L2	0.5983		0.8164	
G3S2P1T1E1	2G	L3	L2	L1	0.3930	-21.1	0.6138	-28.6
G3S2P1T1E1	2G	L3	L2	L2	0.4200	-24.0	0.6111	-23.1
G3S2P1T1E1	2G	L3	L2	L3	0.4143	-10.7	0.6584	-14.1
G3S2P1T1E1	2H	L3	L1	L1	0.4018	-19.9	0.6079	-16.9
G3S2P1T1E1	2H	L3	L1	L2	0.3994	-31.2	0.6286	-22.4
G3S2P1T1E1	2H	L3	L1	L3	0.3990	-21.8	0.6747	-7.7
G3S2P1T1E1	GRAFCELL	L3	L3	L2	0.5812		0.9531	
G1S1P2T1E1	2G	L1	L1	L1	0.4182	-10.2	0.6050	-21.4
G1S1P2T1E1	2G	L1	L1	L2	0.4416	-20.4	0.6217	-11.7
G1S1P2T1E1	2G	L1	L1	L3	0.4500	-11.2	0.5731	-13.3
G1S1P2T1E1	2G	L1	L3	L1	0.4018	-13.8	0.5564	-16.4
G1S1P2T1E1	2G	L1	L3	L2	0.4141	-16.6	0.5971	-18.7
G1S1P2T1E1	2G	L1	L3	L3	0.4038	-39.5	0.5912	-19.0
G1S1P2T1E1	2H	L1	L1	L1	0.4103	-17.3	0.6474	-17.0
G1S1P2T1E1	2H	L1	L1	L2	0.4038	-24.7	0.7264	-7.1
G1S1P2T1E1	2H	L1	L1	L3	0.4172	-34.7	0.7382	-4.9
G1S1P2T1E1	2H	L1	L2	L1	0.4135	-20.5	0.5906	-14.7
G1S1P2T1E1	2H	L1	L2	L2	0.4416	-26.5	0.5657	-19.0
G1S1P2T1E1	2H	L1	L2	L3	0.4455	-16.8	0.6143	-22.7
G1S1P2T1E1	GRAFCELL	40	L2	L3	0.6548		0.8962	
G1S1P2T1E1	2G	L3	L1	L1	0.4294	-13.4	0.5868	-15.1
G1S1P2T1E1	2G	L3	L1	L2	0.4350	-9.2	0.6106	-42.5
G1S1P2T1E1	2G	L3	L1	L3	0.4397	-7.7	0.6000	-11.6
G1S1P2T1E1	2H	L3	L1	L1	0.4198	-49.5	0.6301	-11.3
G1S1P2T1E1	2H	L3	L1	L2	0.4261	-11.4	0.5992	-11.9
G1S1P2T1E1	2H	L3	L1	L3	0.4526	-8.7	0.6161	-14.9
G1S1P2T1E1	GRAFCELL	L3	L2	L2	0.5555		0.7911	
					Critical Value	**2.78**		**2.78**
Less Expansion		More Expansion				Not Significant		

APPENDIX K (cont.)

Table 59: Paired T-test Comparing Benzoxazine Resin Systems Against Each Other.

Graphite	PV 1	PV 2	PV 3	Resin 2G		Resin 2H	
				Growth Factor Length, Avg. (%)	Growth Factor Width Avg (%)	Growth Factor Length, Avg. (%)	Growth Factor Width Avg (%)
G3S2P1T1E1	L1	L2	L1	0.390	0.599	0.409	0.651
G3S2P1T1E1	L1	L2	L2	0.425	0.617	0.394	0.667
G3S2P1T1E1	L1	L2	L3	0.427	0.653	0.415	0.630
G3S2P1T1E1	L1	L3	L1	0.403	0.577	0.290	0.643
G3S2P1T1E1	L1	L3	L3	0.441	0.567	0.290	0.632
G3S2P1T1E1	L2	L1	L1	0.393	0.614	0.402	0.608
G3S2P1T1E1	L2	L1	L2	0.420	0.611	0.399	0.629
G3S2P1T1E1	L2	L1	L3	0.414	0.658	0.399	0.675
G1S1P2T1E1	L1	L2	L1	0.418	0.605	0.410	0.647
G1S1P2T1E1	L1	L2	L2	0.442	0.622	0.404	0.591
G1S1P2T1E1	L1	L2	L3	0.450	0.573	0.417	0.726
G1S1P2T1E1	L1	L3	L1	0.402	0.556	0.413	0.566
G1S1P2T1E1	L1	L3	L2	0.414	0.597	0.442	0.614
G1S1P2T1E1	L1	L3	L3	0.404	0.591	0.446	0.738
G1S1P2T1E1	L2	L1	L1	0.429	0.587	0.420	0.630
G1S1P2T1E1	L2	L1	L2	0.435	0.611	0.426	0.599
G1S1P2T1E1	L2	L1	L3	0.440	0.600	0.453	0.616
Paired T (p-value)						0.13	0.01
Critical Value						0.05	0.05
Significantly Different Growth							
Not Statistically Different							

APPENDIX K (cont.)

Table 60: Analysis of Variance Results for Growth Factor Width, %

Source	DF	Seq SS	Adj SS	Adj MS	F	P
Graphite	1	0.20040	0.01596	0.01596	6.38	0.012
Resin	2	2.64400	0.85887	0.42944	171.58	0.000
PV 1	2	0.10387	0.08198	0.04099	16.38	0.000
PV 2	2	0.11127	0.11146	0.05573	22.27	0.000
PV 3	2	0.01324	0.01324	0.00662	2.64	0.073
Error	208	0.52059	0.52059	0.00250		
Total	217	3.59337				

Table 61: Analysis of Variance Results for Growth Factor Length, %

Source	DF	Seq SS	Adj SS	Adj MS	F	P
Graphite	1	0.00013	0.04663	0.04663	34.16	0.000
Resin	2	1.63701	0.48634	0.24317	178.11	0.000
PV 1	2	0.08580	0.05230	0.02615	19.15	0.000
PV 2	2	0.04205	0.04224	0.02112	15.47	0.000
PV 3	2	0.01305	0.01305	0.00653	4.78	0.009
Error	208	0.28398	0.28398	0.00137		
Total	217	2.06202				

19. APPENDIX L – SINGLE CELL TESTING EFFLUENT ANALYSIS RESULTS

The results of high performance liquid chromatography – with mass spectral detection (HPLC-MS) of the effluent from the single cell testing of the 2G composite are presented in the following figures and tables. In the following figures and tables, the results on the basis of retention time are shown first with retention times labeled; followed by the mass spectra of the contents of the effluent at a specific retention time. The compounds that were identified are summarized in a table for the specified analysis conditions.

Figure 37: Background Spectrum of HPLC Grade Water.

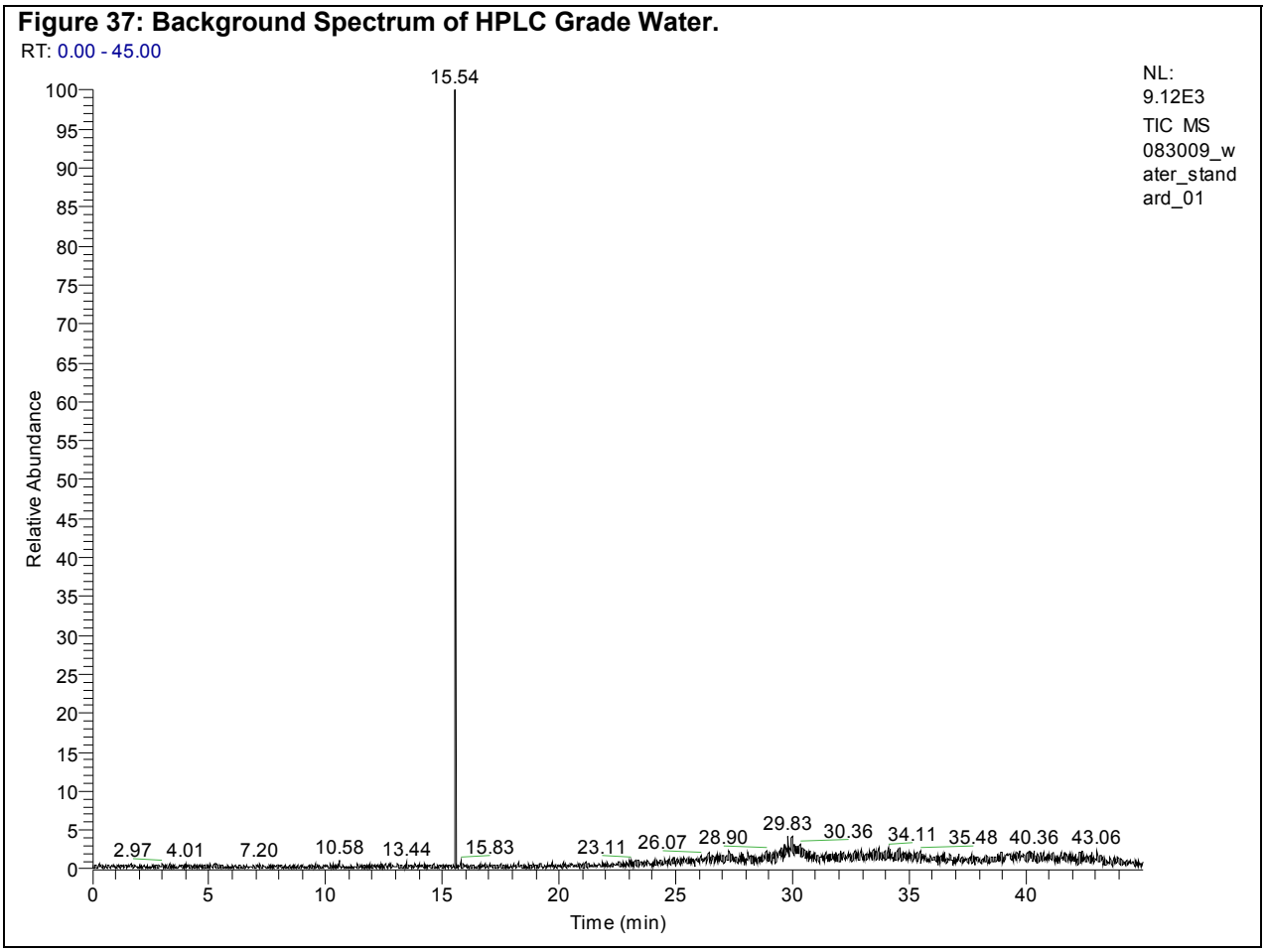

HPLC – MS Results for 2G Resin Impregnated Plate After 99 Hours of Single Cell Testing (Cell 01)

Shown in the figure below is the entire HPLC-MS scan for the 2G resin plate Cell 01 effluent after 99 hours of single cell runtime. A grouping of peaks is present with retention times between 7.99 and 9.52 minutes with a major peak at a retention time of 8.54 minutes.

Figure 38: Background Corrected HPLC-Mass Spectral Scan of the Effluent From 2G Plate Cell 01 after 99 Hours of Singe Cell Testing Runtime.

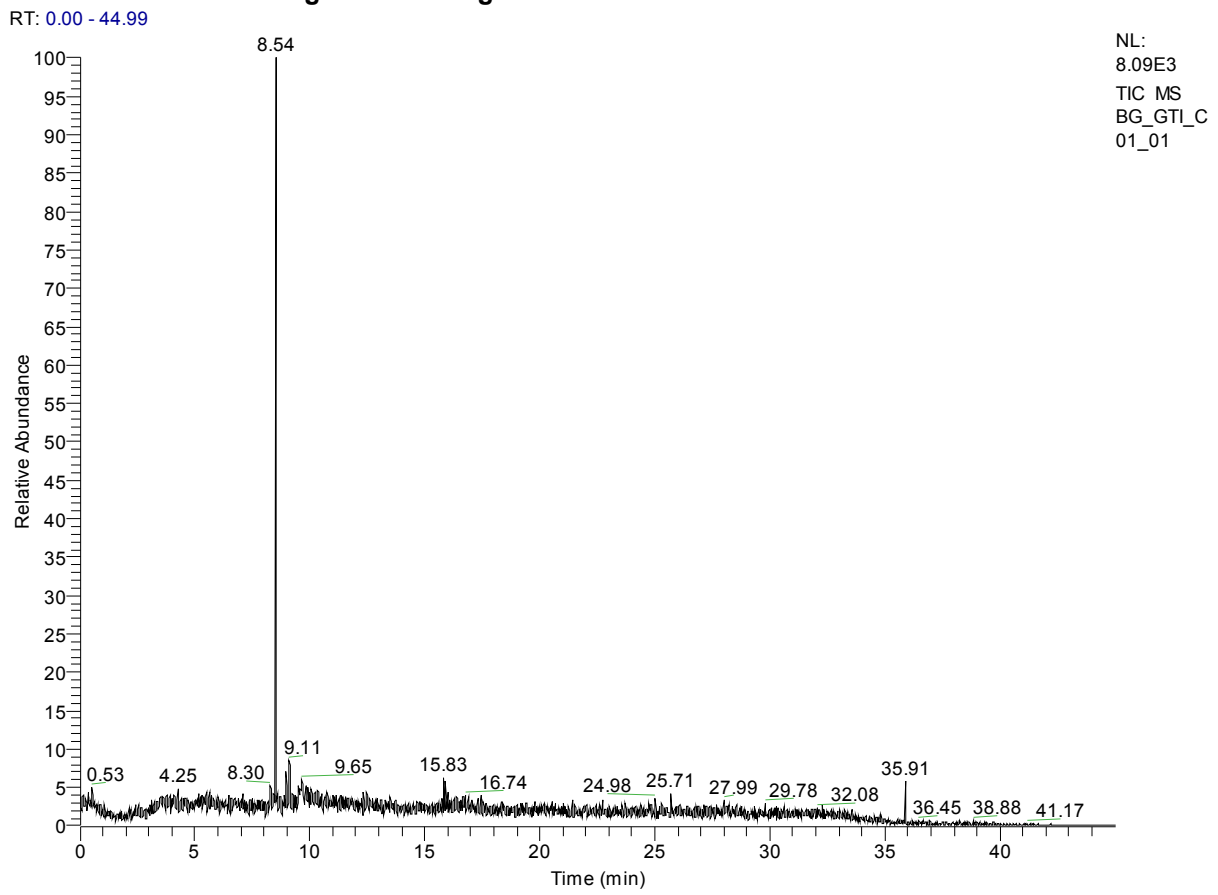

The following figures are individual mass spectra obtained of the effluent at the indicated retention time.

Figure 39: Background Corrected HPLC-Mass Spectral Scan of the Effluent From 2G Plate Cell 01 after 99 Hours of Singe Cell Testing Runtime at a Retention Time of 8.54 Minutes.

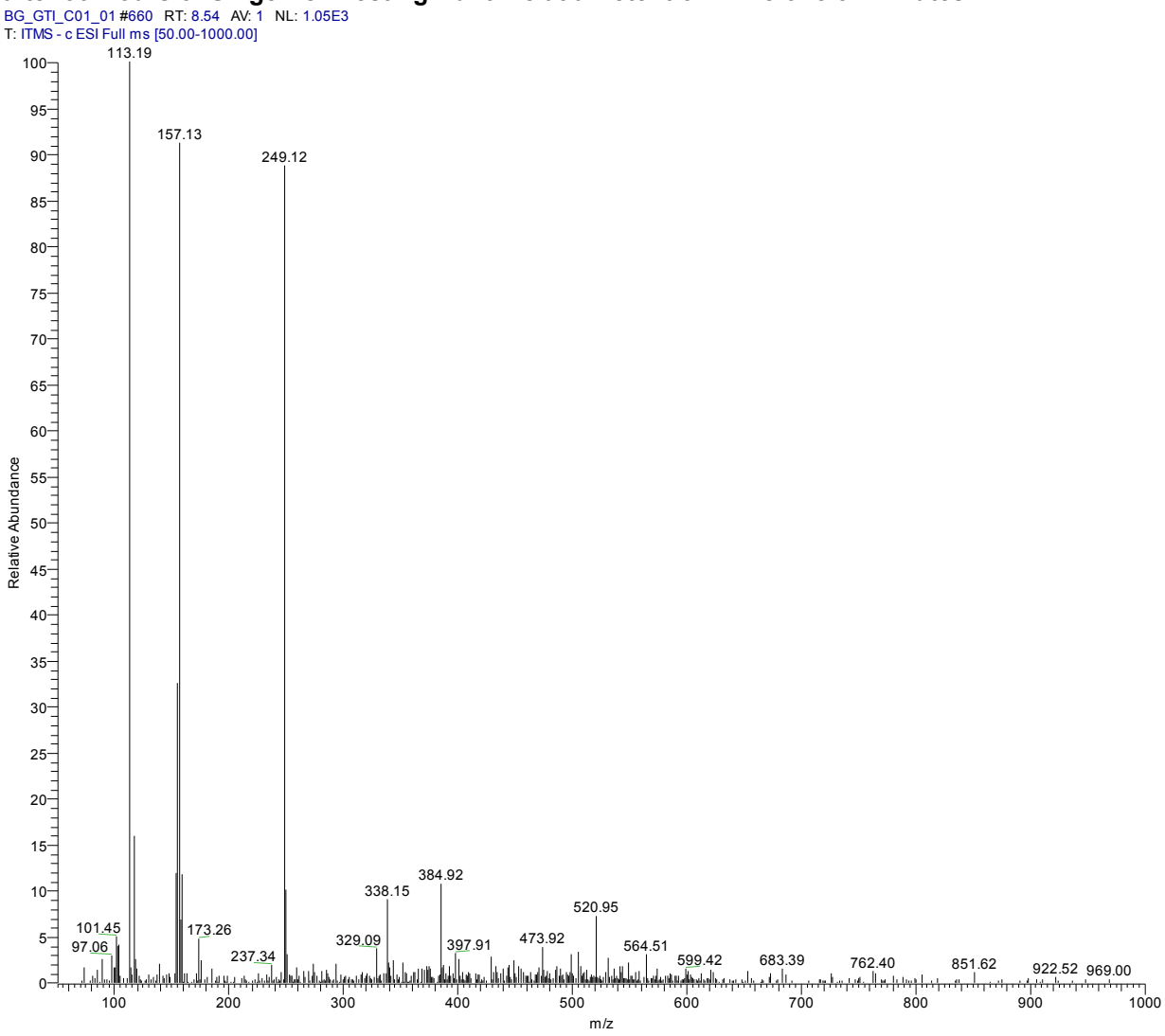

Figure 40: Background Corrected Mass Spectrum of the Effluent From 2G Plate Cell 01 Collected after 99 Hours of Single Cell Runtime at a Retention Time Between 7.99 and 9.52 Minutes.

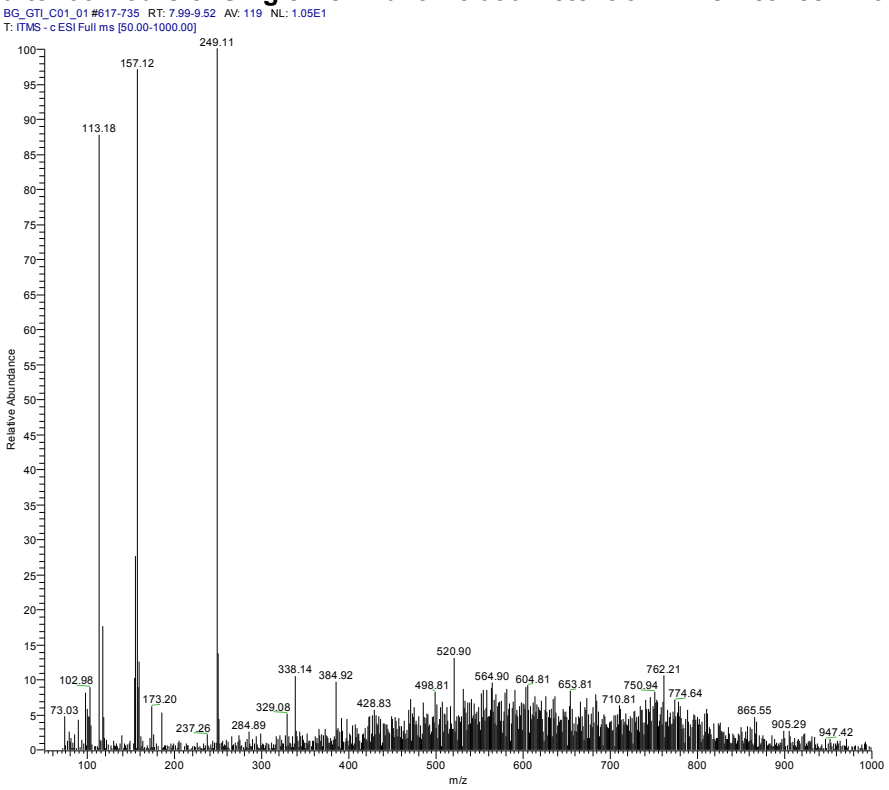

A summary of the highest peaks and corresponding compounds detected is present in the following table with empirical formulas for compounds corresponding to unknown mass fragments.

Table 62: Identified Compounds at a Retention Time of 8.54 Minutes for the 2G Resin Cell 01 after 99 Hours of Single Cell Operation.

mass	status	name or formula
97.06	ident.	1-Ethyl-1,2,4-triazole, 1-methyl-5-aminopyrazole
101.45	unknown	CO2N2FSi4
113.19	unknown	C4H9N4
157.13	ident.	C8H19NSi, 1-[2-(trimethylsilyl)ethyl]-azetidine
249.12	ident.	C13H19NO2Si, dimethyl(4-cyanophenoxy)isobutoxy-silane
338.15	ident.	3,5-dinitrobenzoate
384.92	ident.	C7H21Cl8 (-)
520.95	unknown	C23O10N2F3

Unknown compounds have an assigned empirical formula, and have a charge value of 1 unless otherwise specified.

HPLC – MS Results for 2G Resin Impregnated Plate after 240 hours of single cell testing (Cell 04)

Figure 41: Background Corrected HPLC-Mass Spectral Scan of the Effluent from 2G Resin Cell 04 After 240 Hours of Single Cell Operation.

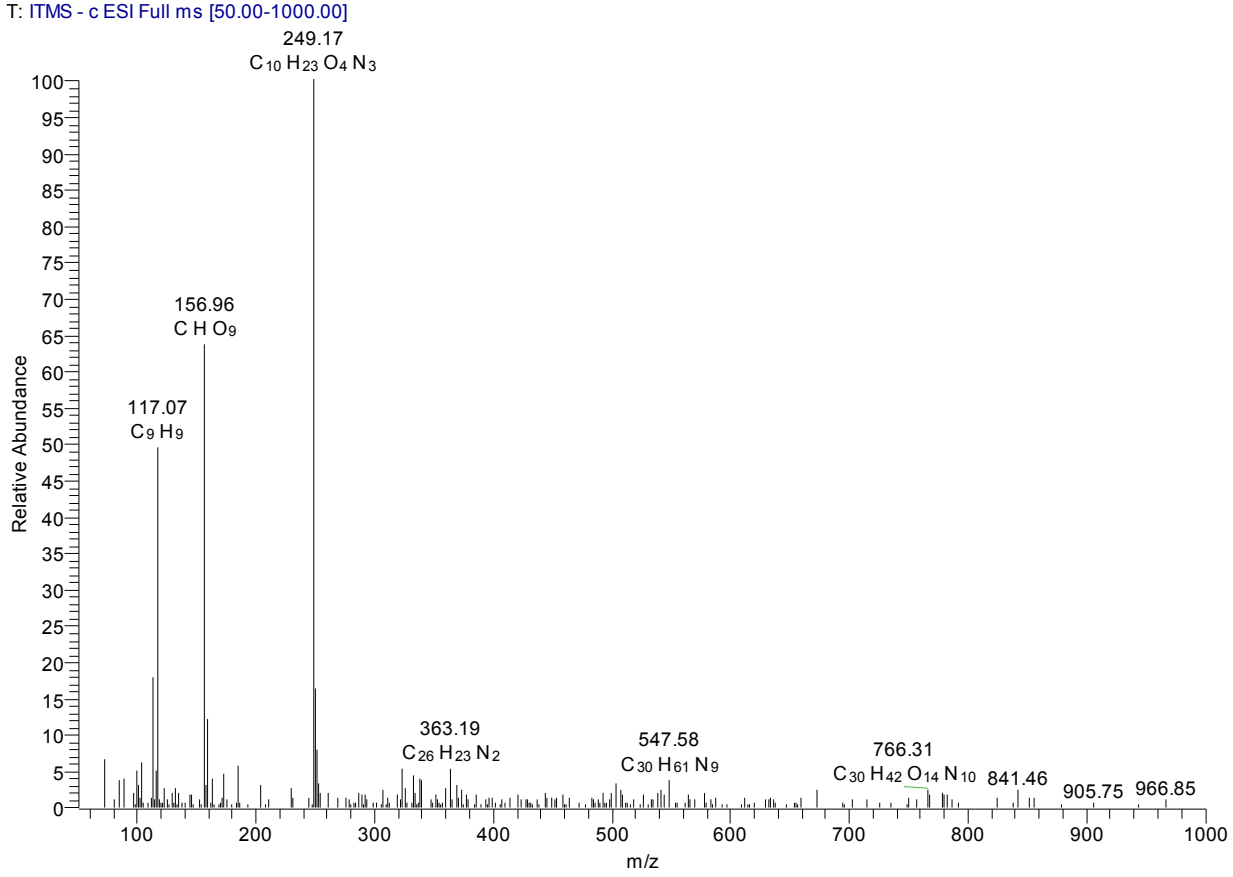

Figure 42: Background Corrected Mass Spectrum of the Effluent Collected for the 2G Resin Plate Cell 04 at a Retention Time of 6.37 Minutes, After 240 Hours of Single Cell Operation.

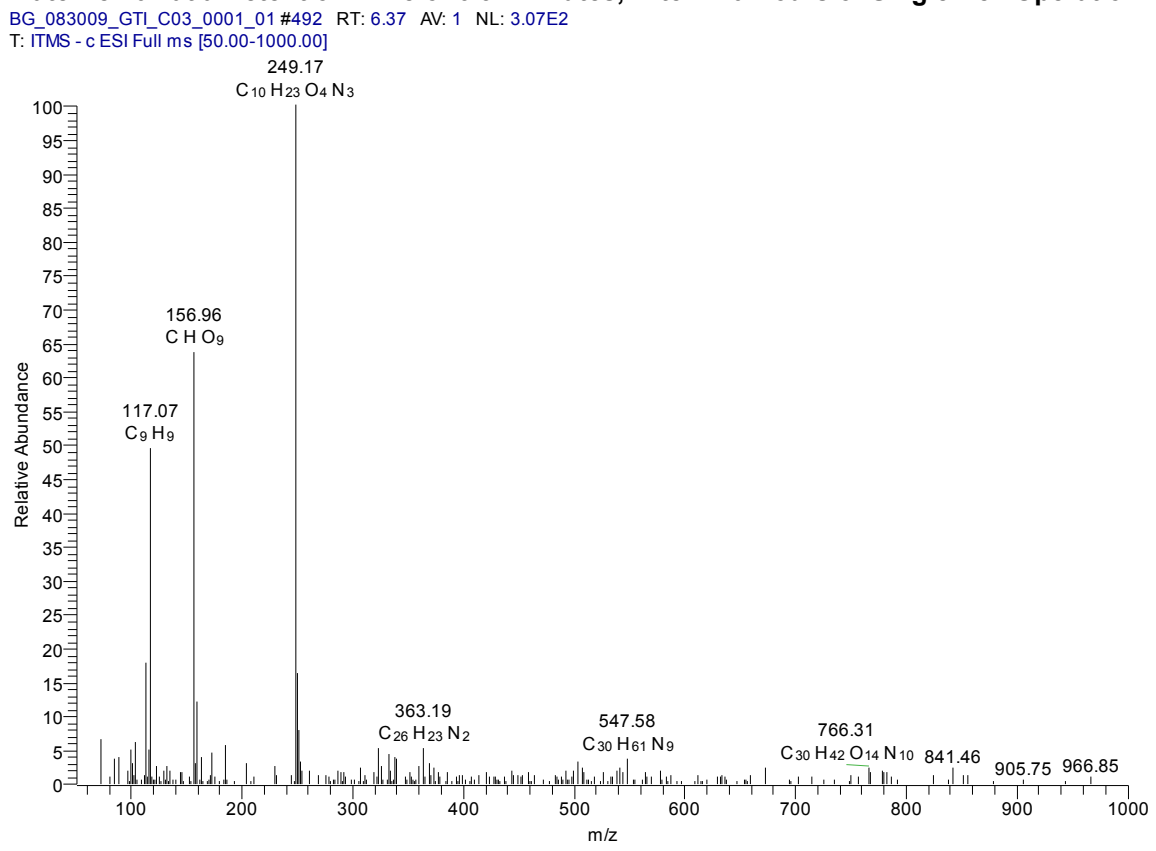

Table 63: Identified Compounds from the Effluent at a Retention Time of 6.37 Minutes for the 2G Resin Plate Cell 04 After 240 Hours of Single Cell Operation.

mass	status	name or formula
117.07	ident.	C9H9 (-)
156.96	unknown	CH2O6FSi
249.17	ident.	H10O11S2 (2-)
363.19	ident.	C16H33NO4SSi
547.58	unknown	C28H55O12N5F10Si9 (2-)
766.31	unknown	C24H58O7N10Si6

Figure 43: Background Subtracted Mass Spectrum of Effluent Collected from 2G Resin Plate Cell 04 at a Retention Time of 11.75 minute After 240 Hours of Single Cell Operation.

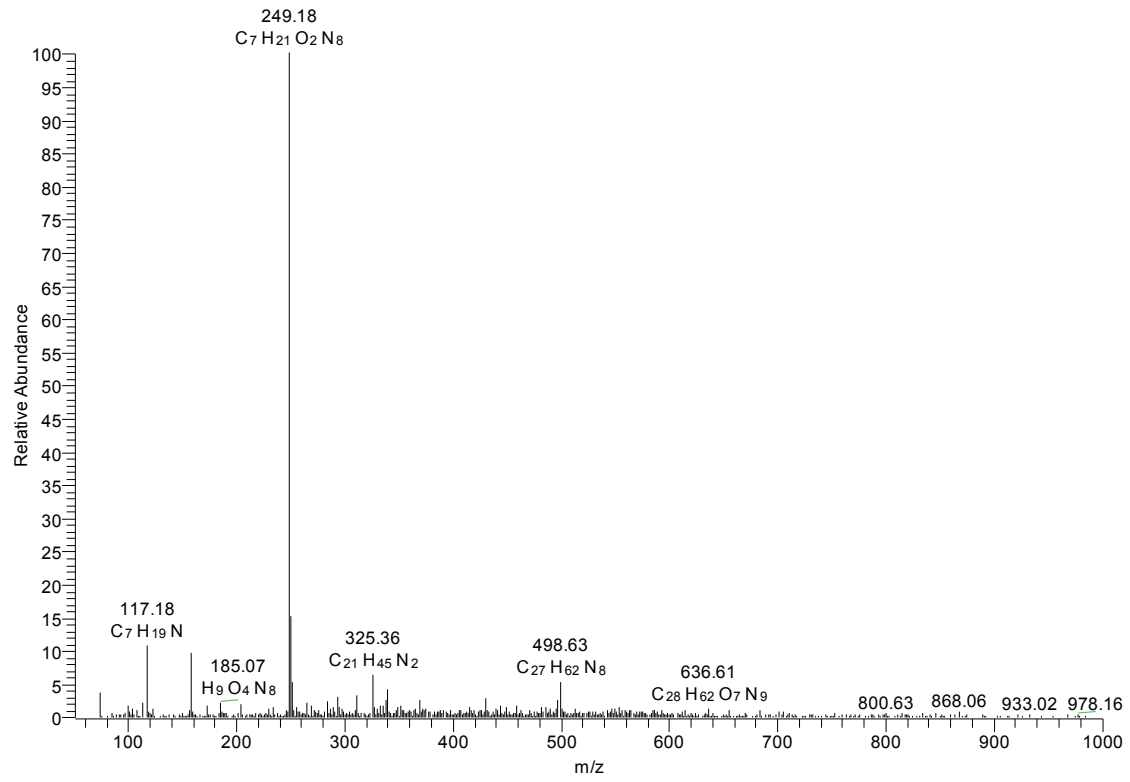

Table 64: Compounds Identified in the Effluent at a Retention Time of 11.75 Minutes for the 2G Resin Plate Cell 04 After 240 Hours of Single Cell Operation.

mass	status	name or formula
117.18	unknown	C10H30N6
185.07	ident.	inophenoxy)acetic acid hydrate or 3-butylamino-6-chloropyrid
249.18	unknown	C8H27N5Si2
325.36	unknown	C21H45N2
498.63	unknown	C29H60O4N10F7Si9 (2-)
636.61	ident.	C41H80O4, dioctadecyl gluatarate

Figure 44: Background Subtracted Mass Spectrum of the Effluent at a Retention Time of 25.11 Minutes from the 2G Resin Plate Cell 04 After 240 Hours of Single Cell Operation.

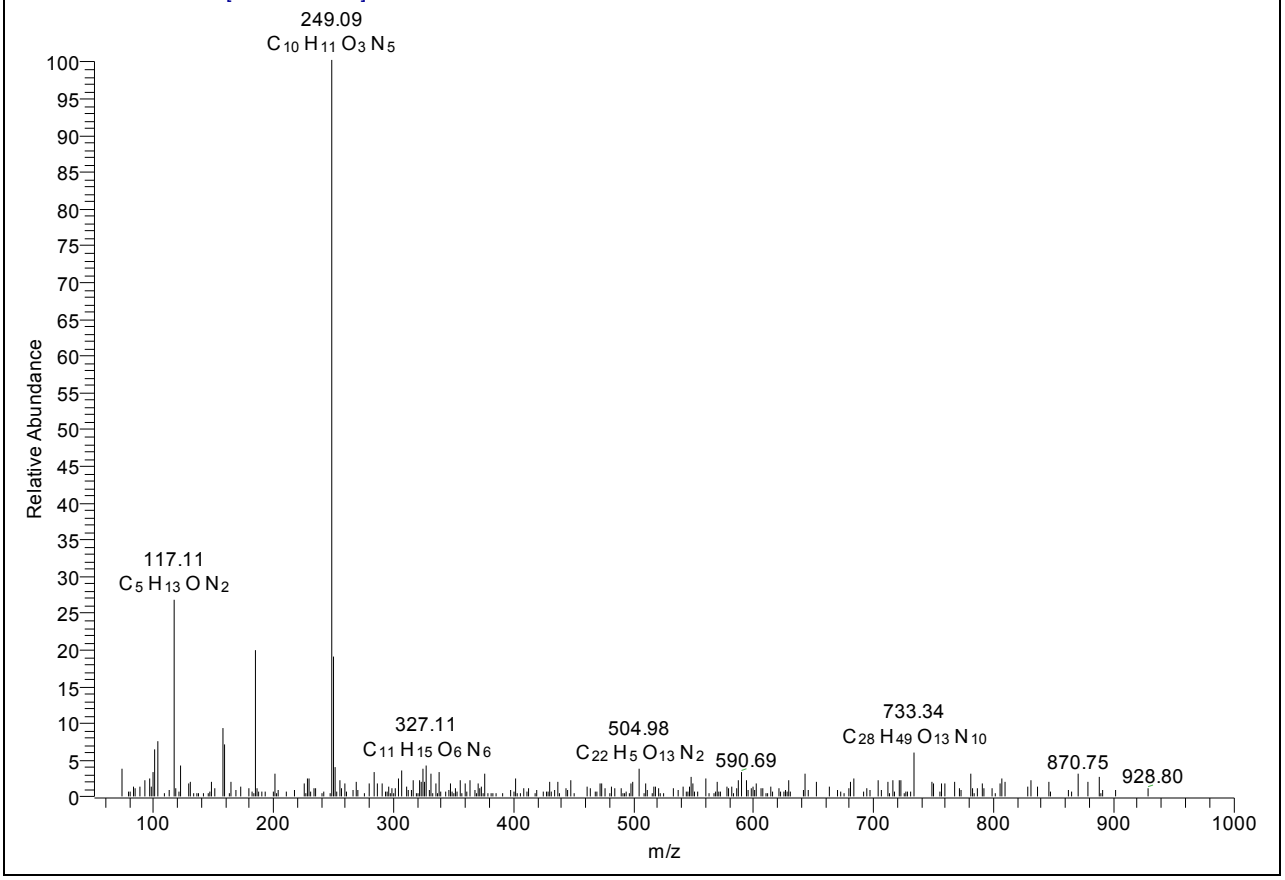

Table 65: Compounds Identified in the Effluent at a Retention Time of 25.11 Minutes for the 2G Resin Cell 04 After 240 Hours of Operation

mass	status	name or formula
117.11	ident.	C6H17Si (-)
249.09	ident.	C15H11N3O, daniquidone or 1-(2-pyridinylazo)-2-napthalenol
327.11	ident.	C18H18ClN3O or C21H17NOSi
504.98	unknown	C9H5O6N9F6Si2
733.34	unknown	C21H60O2N9F5Si6

HPLC – MS Results for 2G Resin Impregnated Plate after 1104 Hours of Single Cell Testing (Cell 08)

Figure 45: Background Subtracted HPLC-Mass Spectral Scan of the Effluent Collected from 2G Resin Plate Cell 08 After 1104 Hours of Single Cell Operation.

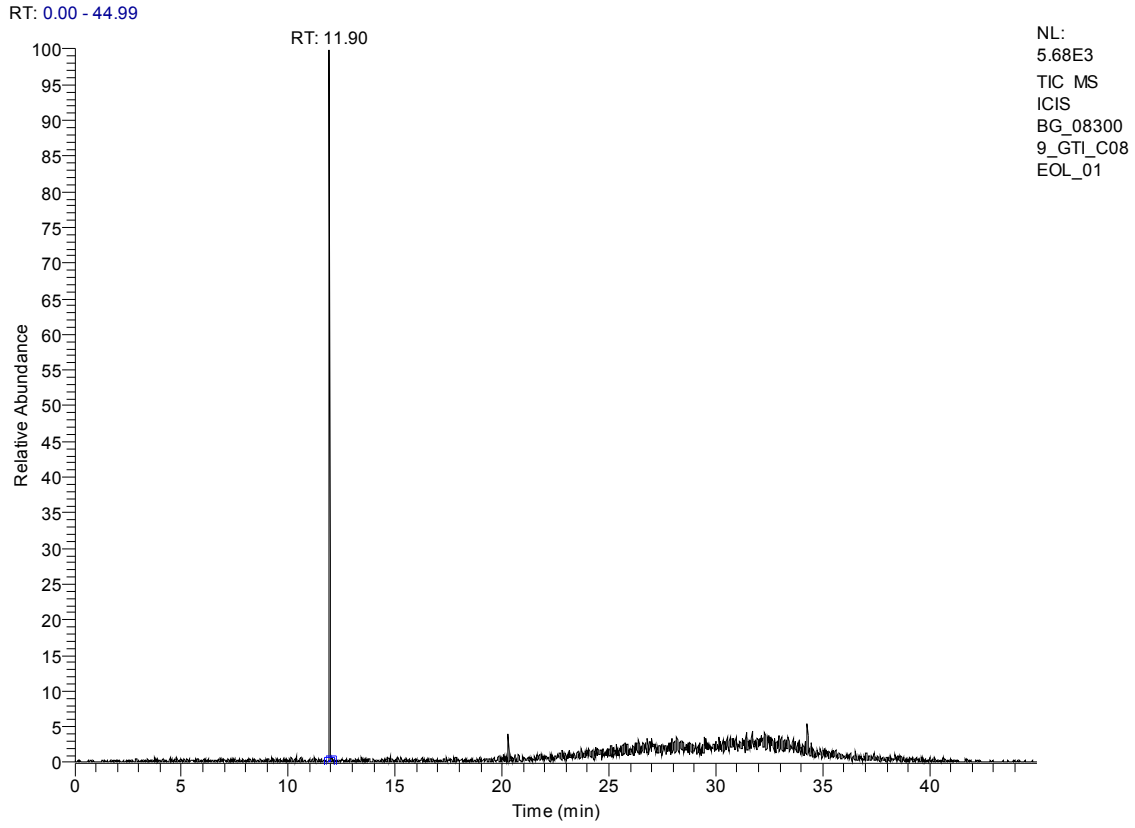

Figure 46: Background Subtracted Mass Spectrum of the Effluent Collected at a Retention Time of 11.90 Minutes for 2G Resin Plate Cell 08 After 1104 Hours of Single Cell Operation.

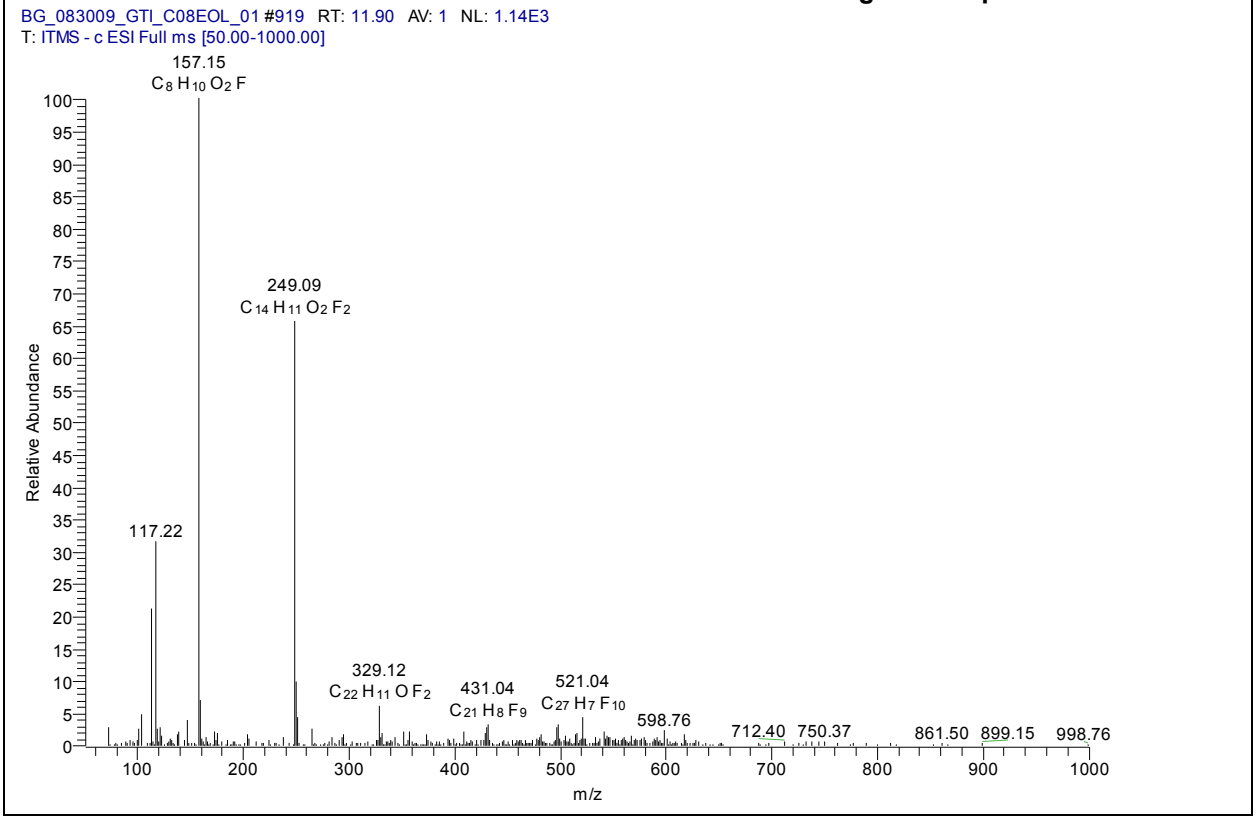

Table 66: Compounds Identified in the Effluent at a Retention Time of 11.90 Minutes for the 2G Resin Plate Cell 08 After 1104 hours of Operation.

mass	status	name or formula
117.22	unknown	C7H19N
157.15	ident.	C9H19NO, n-isobutyl pentanamide
249.09	ident.	C15H11N3O, daniquidone
329.12	ident.	C17H19N3O2S or C16H18F3NO3
431.04	unknown	C13H10ON7F5Si2
521.04	unknown	C14H13O9N10Si2

Figure 47: Background Subtracted Mass Spectrum of the Effluent at a Retention Time Between 11.55 and 21.64 Minutes from 2G Resin Plate Cell 08 Collected After 1104 Hours of Singe Cell Operation.

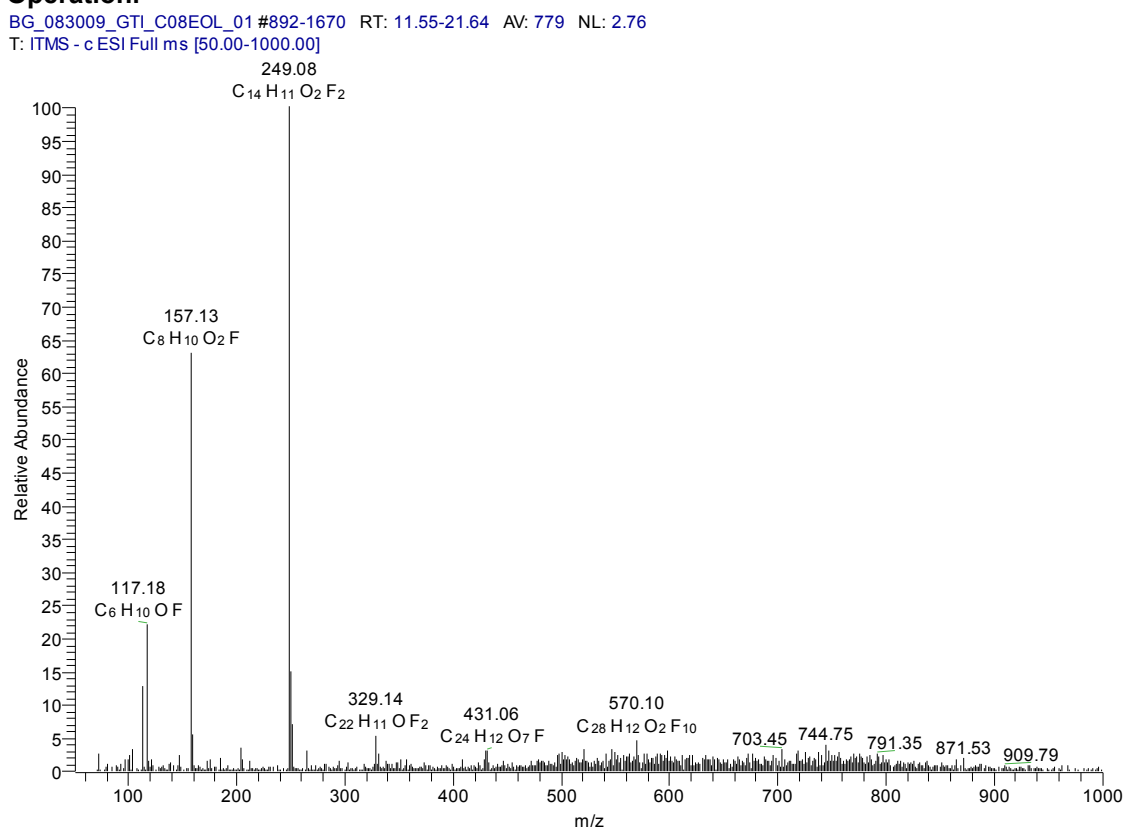

Table 67: Compounds Identified in Effluent at Retention Time Between 11.55 and 21.64 Minutes for 2G Resin Plate Cell 08 after 1104 Hours of Operation.

mass	status	name or formula
117.18	unknown	C10H30N6
157.13	ident.	C8H19NSi
249.08	ident.	C16H11NO2
329.14	ident.	C19H20FNO3
570.10	ident.	C15H33Cl2IrO2P2

20. LIST OF ABBREVIATIONS

Abbreviation	Meaning
AFGF	Advanced Flexible Graphite Facility
ANOVA	Analysis of Variance
ASTM	American Society for Testing and Materials
BPP	Bipolar Plate
CWRU	Case Western Reserve University
DMA	Dynamic Mechanical Analysis
DMSO	Dimethylsulfoxide
DoE	U. S. Department of Energy
DSC	Differential Scanning Calorimetry
DTI	Directed Technologies Inc.
FFP	Flow Field Plate
GLM	General Linear Model
GTI	GrafTech International Inc.
HPLC – MS	High Performance Liquid Chromatography - Mass Spectroscopy
MEA	Membrane Electrode Assemble
OCV	Open Circuit Voltage
ORR	Oxygen Reduction Reaction
PBI	Polybenzimidizol
PEM	Proton Exchange Membrane
Psig	Pounds per square gage
RHE	Reference Hydrogen Electrode
µg/L	Micrograms/liter
T_g	Glass Transition Temperature
TGA	Thermogravimetric Analysis
TMA	Thermomechanical Analysis

21. LIST OF FIGURES

22. LIST OF TABLES

23. REFERENCES

1. "Hydrogen, Fuel Cells and Infrastructure Technologies Multi-Year Research, Development and Demonstration Plan", U. S. Depart of Energy, Hydrogen, Fuel Cells & Infrastructure Technologies Program, DoE/GO-102003-1741, Oct 2007
2. "Hydrogen, Fuel Cells and Infrastructure Technologies Multi-Year Research, Development and Demonstration Plan", U. S. Depart of Energy, Hydrogen, Fuel Cells & Infrastructure Technologies Program, DoE/GO-102003-1741, Oct 2007
3. S. J. Lee, S. Mukerjee, E. A. Ticianelli and J. McBreen,; *Electrochimica Acta*, **44**, 3283 (1999).
4. C. Song, Y. Tang, J. L. Zhang, J. Zhang, H. Wang, J. Shen, S. McDermid, J. Li and P. Kozak; *Electrochimica Acta*, **52**, 2552 (2007).
5. A. J. Bard and L. R. Faulkner, "Electrochemical Methods, Fundamentals and Applications", Wiley, New York (1980).
6. J. Larminie and A. Dicks, "Fuel Cell Systems Explained", Wiley, West Sussex (2003).
7. J. Zhang, Z. Xie, J. Zhang, Y. Tang, C. Song, T. Navessin, Z. Shi, D. Song, H. Wang, D. P. Wilkinson, Z.-S. Liu and S. Holdcroft, *Journal of Power Sources*, **160**, 872 (2006).
8. N. Gourdoupi, K. Papadimitriou, S. Neophytides and J. K. Kallitsis, *Fuel Cells*, **8**, 200 (2008).
9. Compliant Terminal Technologies Summary Test Report ER04100, Autosplice Inc. September 2004, Pgs 3, 9, 10
10. "Physical Propriety Measurements of GRAFOIL® Sheet Materials Graphite Grades GTA, GTB, and GTC", Technical Memorandum, GrafTech International, TM-79-56.
11. R. Sidik, *Journal of Solid State Electrochemistry*, **13**, 1123 (2009).
12 . NIST Chemistry WebBook, in (2009).
13. J. P. Meyers and R. M. Darling, *Journal of The Electrochemical Society,* **153**, A1432 (2006).
14. L. Wang, B. L. Yi, H. M. Zhang, Y. H. Liu, D. M. Xing, Z.-G. Shao and Y. H. Cai, *Journal of Power Sources*, **164**, 80 (2007).
15. C. Zhou, "Chemical Durability Studies of Ionomers and Model Compounds for Fuel Cell Applications in Department of Macromolecular Science and Engineering", p. 243, Case Western Reserve University, Cleveland (2009)
16. C. Zhou, "Chemical Durability Studies of Ionomers and Model Compounds for Fuel Cell Applications in Department of Macromolecular Science and Engineering", p. 243, Case Western Reserve University, Cleveland (2008).

17. R. J. Wayne, O. L. Adrianowycz, J. Norley, J. Stuart and D. Flaherty, “Flexible Graphite Resin Composite Bipolar Plates for High Temperature High Energy Density PEM Fuel Cells”, Fuel Cell Seminar, Palm Sprigs, CA (2009).
18. A. Allouche, Y. Ferro, T. Angot, C. Thomas and J. M. Layet, *The Journal of Chemical Physics*, **123**, 124701 (2005)
19. A. D. Modestov, M. R. Tarasevich, V. Y. Filimonov and N. M. Zagudaeva, *Electrochimica Acta*, **54**, 7121 (2009).
20 . X. Cheng, J. Zhang, Y. Tang, C. Song, J. Shen, D. Song and J. Zhang, *Journal of Power Sources*, **167**, 25 (2007).
21. Ballard Internal Report and private communication.
22. James, Brian D. and Jeff A. Kalinoski, “Mass Production Cost Estimation for Direct H2 PEM Fuel Cell Systems for Automotive Applications: 2008 Update”, DoE Contract # GS-10F-0099J, 26 March 2009.